Helsinki University of Technology Publications in Materials Science and Engineering
Teknillisen korkeakoulun materiaalitekniikan julkaisuja
Espoo 2007 TKK-MT-195

STUDY ON THE LAYERS IN THE FILM ORIGINATING FROM THE CASTING POWDER BETWEEN STEEL SHELL AND MOULD AND ASSOCIATED PHENOMENA IN CONTINUOUS CASTING OF STAINLESS STEEL

Doctoral Thesis

Paavo Hooli

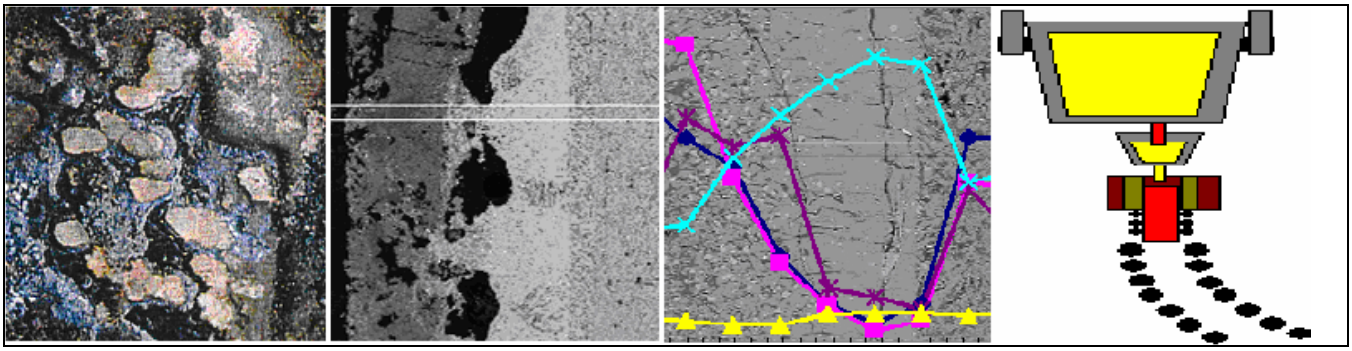

TEKNILLINEN KORKEAKOULU
TEKNISKA HÖGSKOLAN
HELSINKI UNIVERSITY OF TECHNOLOGY
TECHNISCHE UNIVERSITÄT HELSINKI
UNIVERSITE DE TECHNOLOGIE D'HELSINKI

Helsinki University of Technology Publications in Materials Science and Engineering
Teknillisen korkeakoulun materiaalitekniikan julkaisuja
Espoo 2007 TKK-MT-195

STUDY ON THE LAYERS IN THE FILM ORIGINATING FROM THE CASTING POWDER BETWEEN STEEL SHELL AND MOULD AND ASSOCIATED PHENOMENA IN CONTINUOUS CASTING OF STAINLESS STEEL

Doctoral Thesis

Paavo Hooli

Dissertation for the degree of Doctor of Science in Technology to be presented with due permission of the Department of Materials Science and Engineering, Helsinki University of Technology for public examination and debate at Helsinki University of Technology (Espoo, Finland) on the 16th of November, 2007, at 12 o'clock noon.

Helsinki University of Technology
Department of Materials Science and Engineering
Laboratory of Metallurgy

Teknillinen korkeakoulu
Materiaalitekniikan osasto
Metallurgian laboratorio

Available in pdf-format at http://lib.tkk.fi/Diss

Distribution:

Helsinki University of Technology
Laboratory of Metallurgy
P.O. Box 6200
FI-02015 TKK, Finland
Tel. +358 9 451 2756
Fax. +358 9 451 2798
email: lea.selin@tkk.fi

Outokumpu Tornio Works Oy
TRC / Melt Metallurgy

FI-95400 Tornio, Finland
+358 16 452 576, +358 40 744 5936
+358 16 453 295
paavo.hooli@outokumpu.com

Cover: Fig. 1: Mould side surface of a film, Fig. 2: A cross cut of a film, Fig. 3: Curves showing contents of elements in a film, Fig. 4: A sketch of a part of a casting machine

ISBN 978-951-22-9030-7
ISBN 978-951-22-9031-4 (electronic)
ISSN 1455-2329

Multiprint Oy
Espoo 2007

ABSTRACT

Studies were conducted at Outokumpu Tornio Works in order to examine the properties of films between the mould and steel shell during the continuous casting of stainless steel. Film sampling was carried out in the tail-out phase at the end of the cast. The films were subjected to chemical analyses and respective compounds and phases were distinguished. Local heat fluxes were measured with thermocouples and the resulting data was subjected to analyses.

No previous study utilising equivalent sampling and analysis has been reported. Several massive samples were collected, a number of which were several millimetres in thickness and covered virtually the entire width of the mould, descending 40cm below the meniscus. Analysis showed that the flux films could explain some of the very low, local heat fluxes that were observed.

The most typical feature in the sampled films was the layer dominated by a cuspidine phase. The crystalline structure of these films had either formed during solidification, or via the devitrification process. Following a high cooling rate and short residence time prior to sampling, glassy structures were found. Most of these findings accord well with the literature. Such crystalline structures are to be expected in these conditions, via either direct formation or devitrification. Evidence from the literature confirms that the layers in the films were formed during the longer period of the casting process and not during tail-out.

The most unexpected feature was the formation of a separate NaF layer, and the formation of elemental sodium (Na), and probably sometimes potassium (K), against the mould wall. The study found that the films can have residence times of as much as several hours on the mould wall, and complex structures containing several sub layers, voids and pores can develop. With the aid of temperature recordings, evidence of fracturing was found in the sampled films. Variation was seen in the appearance of surfaces on the mould side. There were variations between samples from different heats, and local variations in centimetre scale.

This method can be used when evaluating the functioning of different casting powders.

Key words: mould powders, continuous casting, flux film, gap, slag phases, cuspidine

PREFACE

These studies were originally started as a part of normal research and development work in the Tornio research centre of Outokumpu Stainless. The topic in these studies belongs as a natural part in these research activities, but in this deeper phase, studies have taken a lot of the author´s own time in addition to a countless number of extra working hours. Outokumpu Stainless Oy have accepted this and encouraged me with this study. I would like to thank my employer for this approach, and particularly Eero Rättyä, the R&D Director.

I express my gratitude to Professor Lauri Holappa for his support and for "pushing" me forward. His guidance was of prime importance for this study to be realised.

Thanks to Dr. Seppo Louhenkilpi for his encouragement, comments and guidance, especially concerning problems with the heat flux phenomena.

Thanks to Kimmo Pesonen and Juha Jokisaari for their contribution to this study.

Thanks to Leeni for her patience and carrying extra housework, and to my daughters, Ilona and Liisa, for their encouragement.

Tornio, 19th October, 2007

Paavo Hooli

CONTENTS

1 INTRODUCTION

1.1 Continuous casting of steel

Since its industrial breakthrough in the 1960s, the continuous casting process has undergone extensive development. This well-established technique is now applied to the majority of steel grades by most steel manufacturers and has a ratio currently exceeding 90%. Continuous casting has thus largely replaced ingot casting in developed countries; only some special products, including very large forgings or extremely crack-sensitive grades are still produced via the ingot route.

Stainless steel production began in Outokumpu Tornio Works in 1976, during which time alternatives for the casting process were still under discussion. The continuous casting process was finally chosen, and current discussion chiefly concerns finer details of the process itself. The second melting shop, commissioned in Tornio in 2002, continued to discuss processing details, as the casting process has a significant influence on the capacity, costing and quality of steel.

The main parts of the continuous casting machine are as follows:

- ladle turret
- tundish
- water cooled copper mould
- secondary cooling with support rolls
- driving units
- slab cutter

Steel flows from the ladle to the tundish, then to the water-cooled mould where solidification begins with the formation of a solid steel shell along the surfaces of the mould. The mould oscillates constantly so that the shell does not stick to its surface. The mould is thus a key element in the casting process and disturbances in this part of the process can lead to serious problems. Good understanding and control of phenomena in the mould are therefore essential to the success of the casting process.

1.2 The role of casting powder

The presence of a lubricating medium or layer between the oscillating mould and the solidifying steel shell is essential. This layer must, however, permit heat transfer from the liquid steel to the cooling water in the mould. The use of casting powder, which forms a liquid slag film in the gap between the shell and the mould, is currently standard practice for both slab and bloom casters as well as for billet casting of demanding steel grades.

The role of casting powder is multitudinous. Figures 1 (a – c) show three views of the state of the mould in relation to the function of the casting powder. Mills et al. (2003) gave an excellent description of the behaviour and functions of powder, which is reproduced as follows. Mould fluxes are added to the top of the mould. The carbon in the mould flux reacts with oxygen to form CO (gas) which creates a reducing atmosphere. The sintering and melting of oxide powders are controlled by adding carbon particles to separate the oxide particles, thus preventing them from joining together. Agglomeration proceeds when the carbon is burnt off and a pool of molten slag is formed on the steel surface in the mould.

During casting, molten slag infiltrates into the channel between the mould and the strand, assisted by the oscillation of the mould. Most of the infiltrated slag solidifies as a glassy, solid layer ca. 2mm thick, but a thin liquid slag of ca 0.1mm thick remains in contact with the steel strand. In time, the hotter parts of the solid, glassy layer crystallize. If the slag film remains in the mould for a long time, crystallization can extend to the colder mould side (O'Malley & Neal, 1999).

The mould flux has several different functions:

1. Provide the steel surface with protection from oxidation
2. Provision of sufficient thermal insulation to prevent the steel from freezing
3. Absorption of any inclusions that may float up from the metal
4. Provision of adequate lubrication of the strand
5. Provision of homogeneous heat transfer between the shell and the mould

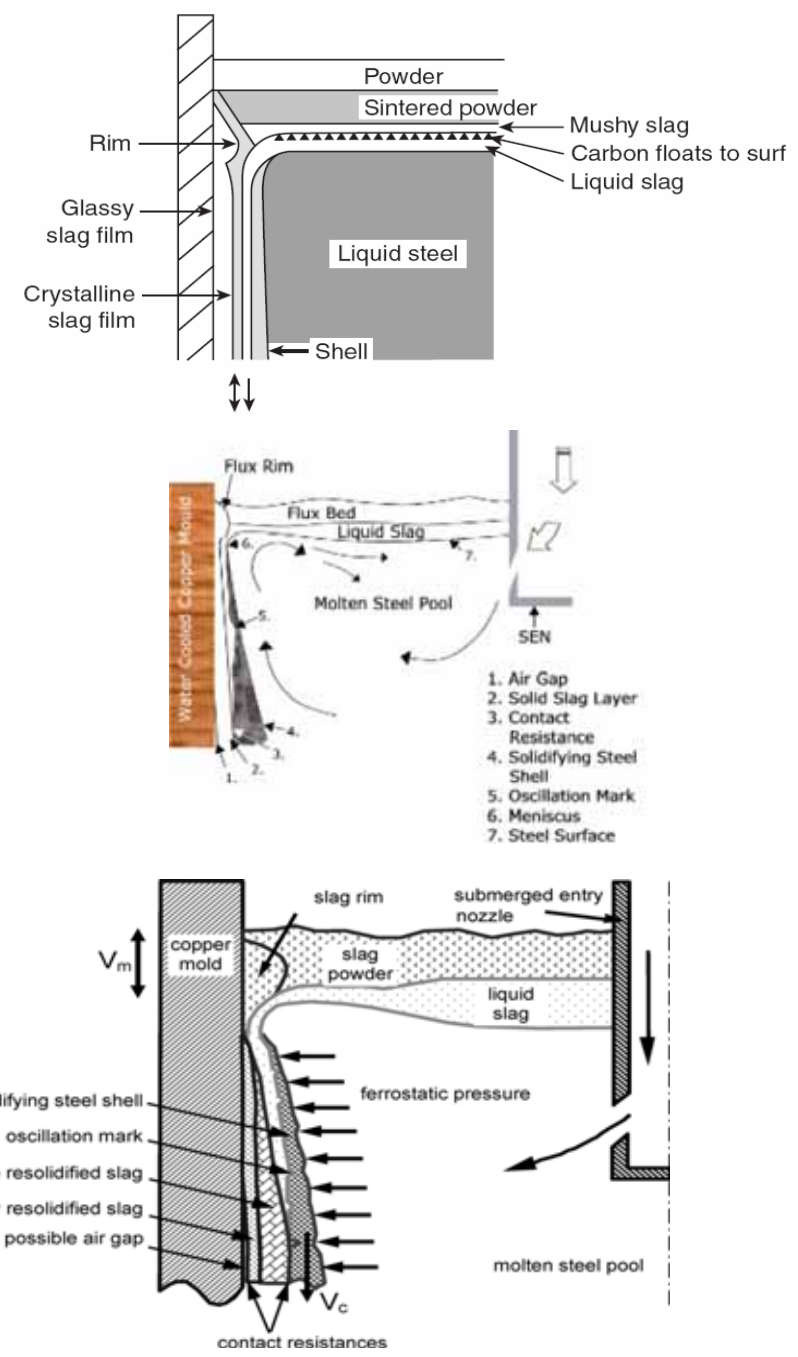

Figure 1. *Schematic representation of the various slag layers formed in the mould, steel flows and associated parameters a) (Mills, 2003), b) (Mills et al. 2003) and c) (Meng & Thomas, 2006).*

Mould powder compositions are carefully designed with these aspects in mind and important properties such as viscosity can be tuned to accommodate different steel chemistries, which can then be cast in different section sizes and at different casting speeds (Mills et al. 2003).

Steel flows in the mould are designed, as one of the most important factor, to favour the functioning of the casting powder and lubrication. In the slab, casting flows are usually directed with the aid of the design of the Submerged Entry Nozzle (SEN). Figure 1 b) shows the principle of the flow pattern, the main purpose of which is to move hot steel to the upper surface in connection with the powder slag, which favours the melting of the powder and keeps the temperature of the liquid flux uniform around the perimeter, where liquid flux starts to infiltrate into the cap between the steel shell and the mould.

The flow also causes some non-uniform phenomena to take place. These include wave formation near the narrow faces. The liquid flux layer is thinner in this area and thicker near the SEN (Figure 1c). The flow pattern thus has different effects on the lubrication in different parts of the mould perimeter.

Behaviour of casting powder in the conditions of the mould gap

This chapter presents examples of flux films reported in the literature. One of the concerns of the present work is the type of phases expected to occur during solidification and cooling of powder flux slag between the shell and the mould. Laboratory simulations enable the prediction of phases via mathematical formulae during the solidification and cooling of liquid slag.

Because the casting powders contain fluorides, cuspidine ($3CaO \cdot 2SiO_2 \cdot CaF_2$), a crystalline silicate-fluoride phase is commonly observed in solidified casting flux. Crystallization of cuspidine plays an important role during casting, because it affects heat transfer (Watanabe et al. 2000). Good casting results depend on the ratio of crystallization of cuspidine in each layer, for which there is an optimum distribution.

The melting point of cuspidine has been determined as 1680 ± 2 ºK by extrapolating to the cooling rate value at 0 K/min (Watanabe et al. 2000). Because the melting point of cuspidine is so high, there is potential for it to form between the shell and the mould at very early stages in the process, in the area below the meniscus.

Li, Thackray and Mills (2004) developed a model to predict the proper flux composition in terms of the optimum lubrication, powder consumption, and horizontal heat transfer for different casting conditions and steel grades, which is of interest to the scope of the present work. However, at the present time, heat transfer is calculated solely from the thickness of the slag film (which is represented by the break or solidification temperature). In order to incorporate the effect of the % crystallinity in the slag film, it is first necessary to derive a relation between % crystallinity (% crystallinity + % glass = 100%) and chemical composition.

Consequently, the objectives of the study were chosen (Li et al. 2004):

- To develop a test that provides a reasonable measure of the % crystallinity in slag films sampled from the mould
- To use the samples derived in the test to obtain a relation between chemical composition and % crystallinity.

Li et al. (2004) found it extremely difficult, however, to obtain sufficient slag films for the establishment of meaningful results. This provided the present study with further motivation for an attempt at corresponding measurements.

In order to obtain an enhanced estimation method for crystallinity of flux slag, Li et al. (2004) developed a modified test to simulate conditions in the cap between the mould and the shell. They found greater crystalline phases than had been detected with other methods. Their results were also in better accordance with slag samples from industrial castings.

They also tested different formulae for the prediction of the tendency of powders with different compositions to form a crystalline phase when cooling. The best correlation was obtained by the formula given below, and represents the NBO/T ratio or basicity index. This is the number of non-bridging oxygens per tetrahedrally-coordinated atom, and represents the degree of depolymerization of silicate slags (Li et al. 2004).

$$NBO/T = \frac{2x_{CaO} + 2x_{BaO} + 2x_{CaF_2} + 2x_{Na_2O} - 2x_{Al_2O_3} + 6x_{Fe_2O_3} + \left(2x_{MgO} + 2x_{MnO}\right)}{x_{SiO_2} + 2x_{Al_2O_3} + x_{TiO_2} + 2x_{B_2O_3} + \left(x_{MgO} + x_{MnO}\right)} \quad [1]$$

where x = the mole fraction of the component in the mould flux. The bracket in the denominator/numerator means it will be included in the denominator if MgO is larger than 7.0% and/or MnO is larger than 4.0%, otherwise it will be included in the numerator. It was shown that:

- there was a good relationship between the % crystallinity and the modified NBO/T
- the critical point occurs at NBO/T=2.0. Below this critical point, the slag samples are completely glassy (very low % crystallinity), whilst above this point, the % crystallinity increases linearly with increasing the modified NBO/T
- the recommended equation to calculate the % crystallinity is:

% crystallinity = 141.1(NBO/T)-284.0 [2]

In the present work, use of these equations for the powders was carried out in the following way: NBO/T ratio was given the values 2.2-2.3, corresponding to a crystallinity of around 30-35 %. When freezing these powders, either glassy or crystalline phases form, depending on the cooling rate.

The addition of 2% BaO resulted in approximately 5% unit increase in crystallinity when calculated with this formula, which provides interesting data, because BaO was also used as a tracer in the present work. For sodium-free powder, the formula produces a higher percentage of crystallinity (approximately 55%). This is caused by the higher CaO content and the lower Al_2O_3 content.

According to the previous study, additions of ZrO_2 and TiO_2 (3-6 %) did not result in any significant increase in crystallinity. In the present study, some of the powder lots were doped with ZrO_2 tracer for trials. With Ti stabilized steels, the TiO_2 concentration in the mould slag went go up to 10 %.

Figure 2 (Li et al. 2004) shows the effects of annealing temperature for a fixed duration of 20 minutes. It can be seen that % crystallinity increases steadily with increasing annealing temperature. The % crystallinity of the tested mould flux sample CA at the temperature of

600°C to 650°C is similar to that for the CA slag film (in the powder CA basicity index C/S is 1.25). The % crystallinity was not affected by an annealing time of 10 minutes to 40 minutes.

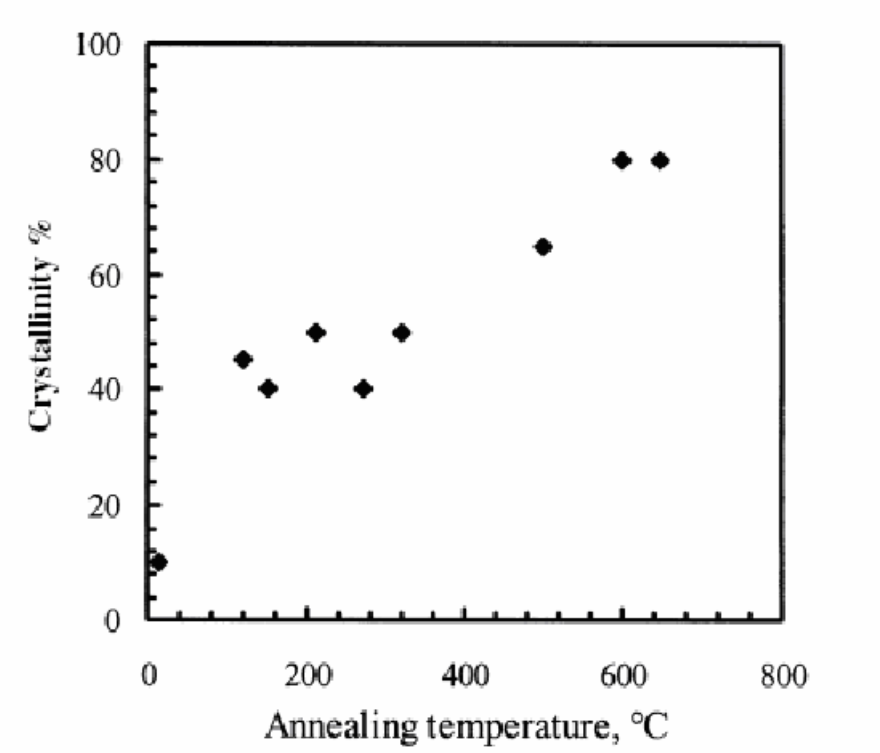

Figure 2. *Percentage of crystallinity vs. annealing temperature with holding time of 20 minutes (Li et al. 2004).*

These results show that even a temperature as low as 100 ºC, with a holding time of 10 – 20 minutes is enough to clearly influence crystallinity percentage, and is, again, of interest regarding the layers found in the present study.

Grieveson et al (1988) melted powders, cast them and formed glassy phases which were then transformed to crystalline by keeping them at 800ºC for 24 hours. They tested twenty-six pieces, and some of the powders had similar compositions to those in the present study (C/S about 1.1), with most containing the same basic compounds. By focusing on powders most closely resembling those used in the present study, the properties of the latter can be evaluated, and the following assumptions made:

- a strong tendency to form cuspidine ($3CaO{\cdot}2SiO_2{\cdot}CaF_2$)
- a medium tendency to form combeite ($Na_2O{\cdot}2CaO{\cdot}3SiO_2$)
- a weak tendency to form gehlenite ($2CaO{\cdot}Al_2O_3{\cdot}SiO_2$)
- a weak or negligible tendency to form pseudowollastonite ($CaO{\cdot}SiO_2$)
- a weak tendency to form nepheline ($Na_3K(AlSiO_4)_4$)
- a medium tendency to form a phase $2Na_2O{\cdot}Al_2O_3{\cdot}2SiO_2$
- a weak tendency to form NaF

NaF was found in only one of the samples heated to 800ºC, but not at all in melted, cast and crystallized samples (Grieveson et al. 1988). The formation of NaF, which was found in the present work in certain layers, is one of the most difficult findings to explain.

Courtney et al. (2001) tested different methods to measure the distribution of glassy and crystalline phases in slag samples. Their micrograph of slag film shows the following layers:

glassy, glass and crystalline, crystalline and a layer assumed to be liquid during casting. Among other results, they found that data obtained by micrographic examination were in good agreement with the results obtained by DTA, which involved observation of the shares of glassy and crystalline phases.

Brandalese et al. (2004), using similar powder to that in the present study, found that cooling DTA ran an exothermic peak at 1153ºC and a weaker one at 946ºC. These peaks evidently indicate the formation of new compounds.

There are increased levels of the crystalline phase in plant samples when compared to those in the laboratory. Carli et al. (2004) showed that this could be explained by devitrification. In the case of plant samples, sampled slag pieces have undergone the actual process, during which devitrification takes place more readily than in laboratory samples, and as a consequence, they contain increased levels of the crystalline phase. During the actual processes, factors other than time and temperature are at work, including altering mechanical deformation (for example oscillation) and pressure.

Hayashi et al. found that Na_2O decreases the glass transformation temperature and the crystallization temperature of cuspidine, and also that the incubation period is shorter with higher Na_2O content (Hayashi et al. 2006). Most of the casting powders used in this work have high Na_2O, which should favour the crystallization of cuspidine. Some trials in the present study were made with a powder that did not include Na_2O.

Nakada et. al. (2006) investigated the effect of the addition of NaF to the mould flux on cuspidine primary field. They also annealed the mixture of cuspidine, $Na_2O{\cdot}2SiO_2{\cdot}2CaO$, CaF_2, at 734ºC for 288 hours, and found that the equilibrium phase relation was mainly cuspidine + NaF. In these mixtures, the Na and F concentrations were higher than in the casting powder used in the present study.

Ogibayashi et al. (1987) also took samples from the layer located 360-400mm below the meniscus. The preceding steps of sampling were not explained. With tracer tests, they found that there had been a layer of 0.25mm thick on the mould wall at least 1 hour 12 minutes before the end of the casting, and a 0.6 mm thick layer 20 minutes before the end of the same casting. They showed a layer with a thickness of up to 2mm in the samples taken after the end of casting from the mould wall, but in the samples taken below the mould during casting, the thickness was predominantly well below 0.5mm, with an occasional maximum of 1mm. Evidently, part of the layer taken after the end of casting had formed during tail-out (as it did in the present study).

They presented two black and white photographs of the layers, and the appearance of the mould and shell side are very similar to the layers in the present study. They also found that when casting speed was briefly decreased to a very low level, the thickness in film samples taken below the mould increased. When casting speed was returned to the previous value, the film remained thicker than before the low speed casting period, and as a result, heat flux remained lower.

The results of the present work reflect those reported by Ogibayashi et al., who also found that the flux film on the shell side appeared smooth. This meant that the powder was in a molten state, whereas on the mould side the powder film surface was markedly irregular. They did not, however, give any further comment concerning the latter observation. An explanation is suggested in the present study.

O'Malley and Neal (1999) reported interesting results in relation to the present study. They took flux films at "cap off" (tail-out) in a casting of AISI 430 stainless steel with a medium-thin slab caster. Unfortunately, they did not describe their sampling methodology, or report the distances of samples from the meniscus. According to all their observations, the flux films that contained crystalline structures also possessed a crystalline layer on the mould wall side of the flux film, which, as they acknowledge, contradicts the traditional flux film structure models.

When tracer was placed in the mould flux, they found that the crystalline layer against the mould was formed from the working flux and not from the starter flux. In the area closest to the mould wall, the crystal structure was non-dendritic in appearance, and had a structure characteristic of devitrified glass, whereas the structure further away from the mould wall was dendritic. This is characteristic of growth from the liquid. The stationary glassy layer could devitrify to form a crystalline layer on or near the mould wall because of the extended duration of time that it spent in this lower temperature region.

In this study, heat transfer was also studied by installing thermocouples in the mould (O'Malley and Neal, 1999). The behaviour of the heat flux is associated with the behaviour of flux film. A very slow drop in the broad face heat removal suggests sluggish growth of the crystalline layer within the mould gap lower in the mould. This took place over several hours of caster operation and strong resistance to film fracture, because the crystalline film adheres well to the mould wall. The drop in the broad face heat removal in the lower part of the mould (500-700mm) suggests that the flux film increased in thickness and/or changed its structure in a manner that decreased heat removal to the mould very slowly with time. This conclusion is in agreement with the present study, which shows how the structure can change.

Temperature fluctuations with a saw-toothed appearance occurring low in the mould have been associated with fracture and sheeting of the crystalline mould flux layer. The longitudinal temperature profiles measured with the instrumented mould indicate that the changes in heat removal are directly associated with temperature profile changes low in the mould.

O'Malley and Neal (1999) also found that disturbances in heat removal, caused by fractures in the flux film and occurring low in the mould can propagate disturbances to the upper part of the mould and ultimately cause the shell to stick to the mould. This was not commented upon in their report, but when looking at photographs of the flux films in the article, the surfaces of the films on the mould side are noticeably uneven, whereas the surfaces on the shell side appear even. Despite being uninformed of the sampling methodology of this study, the present study is able to explain these surface observations.

O'Malley and Neal (1999) concluded that if the flux film has a good ability to remain adherent to the mould wall, it is also likely to have a strong effect on the heat flux, especially in long sequential castings.

Their results can be summarised as follows:

- decrease in heat flux during casting takes place low in the mould
- decrease in heat flux is caused by the increase in thickness and/or structure of the flux film
- fracturing takes place in the flux film
- fractures in the flux film low in the mould can propagate disturbances in the area near the meniscus and cause sticking of shell onto the mould

- because of long residence times, the glassy layer formed against the mould in the early stages of casting can crystallize in the gap between the mould and the shell despite low temperatures
- the film layer close to the mould is crystalline when sampling at cap-off
- the structure of the devitrified flux film layer is not dendritic, whereas the structure of phases formed with lower cooling rate is dendritic

Terauchi and Nakata (2002) have investigated the thermal characteristics of various kinds of mould powders using a pilot plant continuous caster and a chill block test. They found that the heat transfer coefficient tended to decrease with the decrease of glassification ratio. An interesting finding was presented on their photograph of a cross-sectional microstructure of the powder film 6 cm below the meniscus.

On the mould side, there is a "solid film during casting" and a "dendritic structure which grew after sampling". This represents a layer which formed during casting and another which formed later, but evidently not after sampling. To confirm solid powder thickness below the meniscus, two types of powders, with different chemical compositions, were used and changed from one to the other during the casting.

Chemical composition on the mould side was the same as that of the initial powder, and that in the "dendritic structure" (on the shell side) was an average of both powders. The first part, therefore, was considered to be the solid powder film during casting. The thickness of the solid film during casting was, as measured in the photo, about 250μm. The authors did not describe their sampling methods or provide additional information on the casting data, but they were able to separate out two main layers in the film sample: one film layer formed during casting, and another layer formed later.

Ludlow et al. (2004) used the following methods for their sampling during casting: slag films were collected at Scunthorpe by removing the slag rim, which had attached to the slag film up to 150mm (thus the slag film sample down to a 150 mm below meniscus was possible to get). At Teesside, slag films were collected using three methods: a wire mesh basket at the mould exit, collection from the cooling grids at the end of a cast or sequence, or from breakouts. The collection of samples at the mould exit meant that there were no data on their exact location within the mould. The composition of these powders is shown in Table 1.

Table 1. Mould powder designation, usage and chemistry (Ludlow et al. 2004).

Powder	Powder Usage	Powder Analysis (wt%)							Calculated Viscosity
		CaO	SiO_2	Al_2O_3	MnO	K_2O	Na_2O	CaF_2	at 1300°C
SB	Standard <0.17%C Steels	32.30	40.69	8.38	0.12	0.12	5.378	11.69	7.351
SD	Trial Peritectic Carbon Steels	33.76	34.45	5.44	0.13	0.35	6.59	12.65	2.340
SH	Trial Peritectic Carbon Steels	32.00	38.95	6.20	0.16	0.44	7.43	14.23	2.840
TA	<0.085% C Steels	23.90	41.71	5.74	0.06	0.70	9.98	15.53	3.724
TB	>0.145% C Steels	29.98	41.75	4.82	0.06	0.66	8.13	13.62	3.430
TC	Peritectic Carbon Steels	33.19	38.4	8.60	0.04	0.12	5.23	11.33	6.767
TG	>0.15% C Steels	23.26	40.93	5.31	0.09	0.66	10.24	15.93	3.22
TH	Peritectic Carbon Steels	34.96	38.61	5.36	3.79	0.18	5.19	9.76	10.090

Figure 3 shows that scatter of the slag film thickness for powder SB was low, reflecting the good long-term performance of this powder. For powder TA (for both peritectic carbon steels and > 0.15% C steels) there is considerable variability in thickness. The variability in slag film thickness for peritectic steel reduced in the order TA > TC > TH. It is interesting to note that the mean film thickness for the powders was different. The performance of powder TH is far superior with respect to longitudinal cracking.

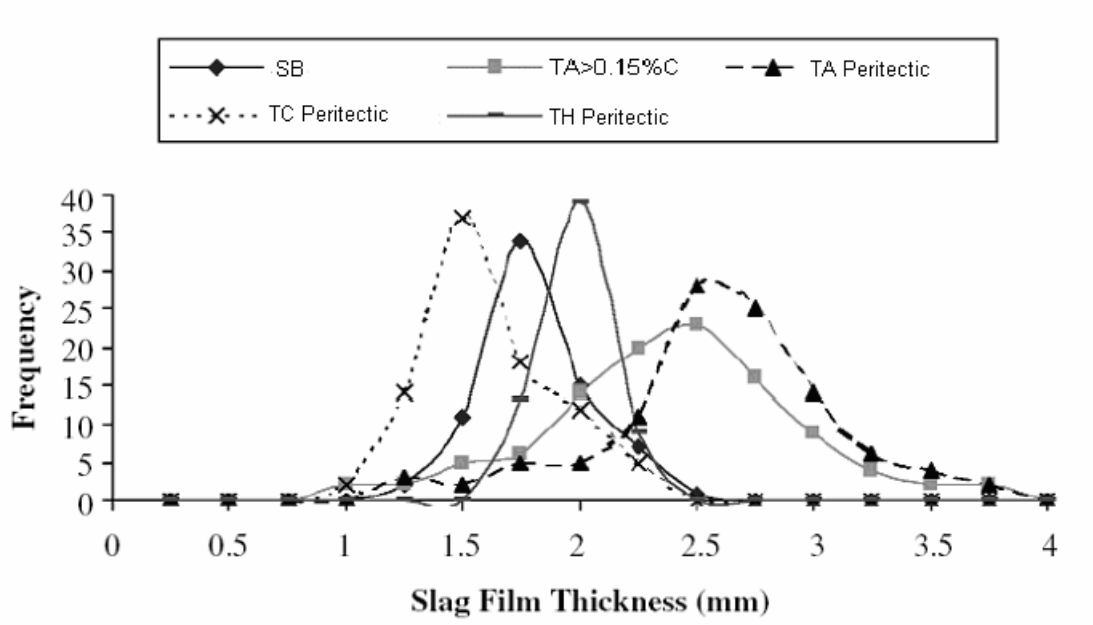

Figure 3. *Frequency distribution for thickness of slag films from mould-strand gap for powders SB, TA, TC, and TH (Ludlow et al. 2004).*

The slag film thicknesses found by Ludlow et al. (2004) were larger than those found in the present study. Part of the scatter in thickness could be explained by the fact that the films came from various distances below the meniscus. The films lower down on the mould were probably thicker than the films in the upper part of the mould.

The observations shown on photographs of slag films, and the microscopic examination of slag film structures, were summarized as follows:

Porosity varied across the thickness of the sample

- Porosity was often associated with bands between the glassy and crystalline phases
- Pore size was generally between 2 and 20 microns but some pores were greater than 50 microns
- Crystallization appeared to have nucleated on some pores
- Multiple bands of crystallized and glassy phases were observed
- The bands of crystallized/glassy phases in many combinations between the mould and shell were observed, i.e. glassy/crystalline, crystalline/glassy/crystalline etc
- Numerous randomly distributed metal droplets were detected in the slag film
- Voids were associated with solidification shrinkage

Chilov (2005) together with Shilov and Holappa (2006) made mass spectrometric studies of volatile components in mould powders. They found that following carbon oxidation, fluorides (including NaF) dominate in the gas phase. They also explained the existence of sodium vapour (Na(g)). In the present study, the behaviour of NaF and Na are of most interest, and formation of these gases might provide an explanation for the presence of the NaF layer and elemental Na. Chilov also found the gases SiF_4 and KF, although potassium (K) content was very low in the casting powders.

Kallio et al. (2004) carried out a study of flux films using similar sampling methods to those in the present study. The formation of cuspidine was a common feature in the films following the use of certain powders.

During laboratory trials, Petäjäjärvi (*in press*) poured liquid slag on a copper plate which was cooled with water and coated with nickel. He found that when the liquid slag was poured on the Ni surface, droplets formed. These droplets were virtually spherical, and the phenomenon indicated that there was very poor wetting of liquid casting flux on the cold Ni surface. This point should be noted when the first layer forms at the beginning of casting, and also later, during direct contact through fractures. Liquid flux slag does not readily spread on a Ni surface; rather, the lubrication process appears to be almost a forced procedure. It is possible that this causes irregularity on the surface of solid slag film on the mould side, and also increases contact resistance between the mould and the solid slag flux film.

Scheller (2005) studied interfacial phenomena between flux and liquid steel in stainless steels. The steel grades and casting powder used in this study were very similar to those in the present work. He found, that in the slag phase near the interface (10 μm) it could be found high amounts of several picked-up elements, among others Mn, Ti, Mg and Na. He pointed out that in the vicinity of the slag/steel interface, the Na concentration could increase up to 35% with an average concentration of around 8% Na_2O in the slag.

Thus, in this very thin layer of slag next to the surface of steel, besides Na, high concentrations of Mn (8.9%) and Mg (2.5%) can form. It is possible that this layer is the first to infiltrate into the gap between the steel shell and the mould. Through flows and diffusion in both fluids (slag and steel), the concentration of elements varies. The pick-up of elements in the slag layer might be the first step to consider when looking for explanations for the observations made in the present study.

Meng et al. (2006(2)) made measurements concerning mould slag properties in order to characterize phenomena in the gap between the mould and the shell, and in their study there are several interesting observations concerning the present work. They carried out several tests on the mould powders, including friction measurement for liquid flux (which is very seldom carried out), CCT (Continuous-Cooling-Transformation) and TTT (Time-Temperature-Transformation) curves, DSC/TG (Differential Scanning Calorimetry / Thermogravimetric) analysis, thermocouple dip tests, atomization (glass formation) and devitrification tests (furnace holding).

They also analyzed a sample of a slag film from an interfacial steel shell/mould gap. It was caught as it folded off the mould wall during tail-out after a continuous casting sequence. The compositions of the powders used in the study are shown in Figure 4 (asterisks). The composition of the powders A and B used in the present study are also shown (circle). The figure ignores the other components. Their report noted that the actual phases in the mould slag film are more complex because in addition to being affected by about ten minor constituents, all these components may react together to form new phases and change the eutectic point.

After the atomization experiments, they observed a thin film of black deposit on the furnace walls, which indicated selective volatilization of small amounts of mould powder compound(s), most probably CaF_2. Those atomized slag droplets with a fully glassy state were then subjected to reheating and furnace holding to investigate devitrification.

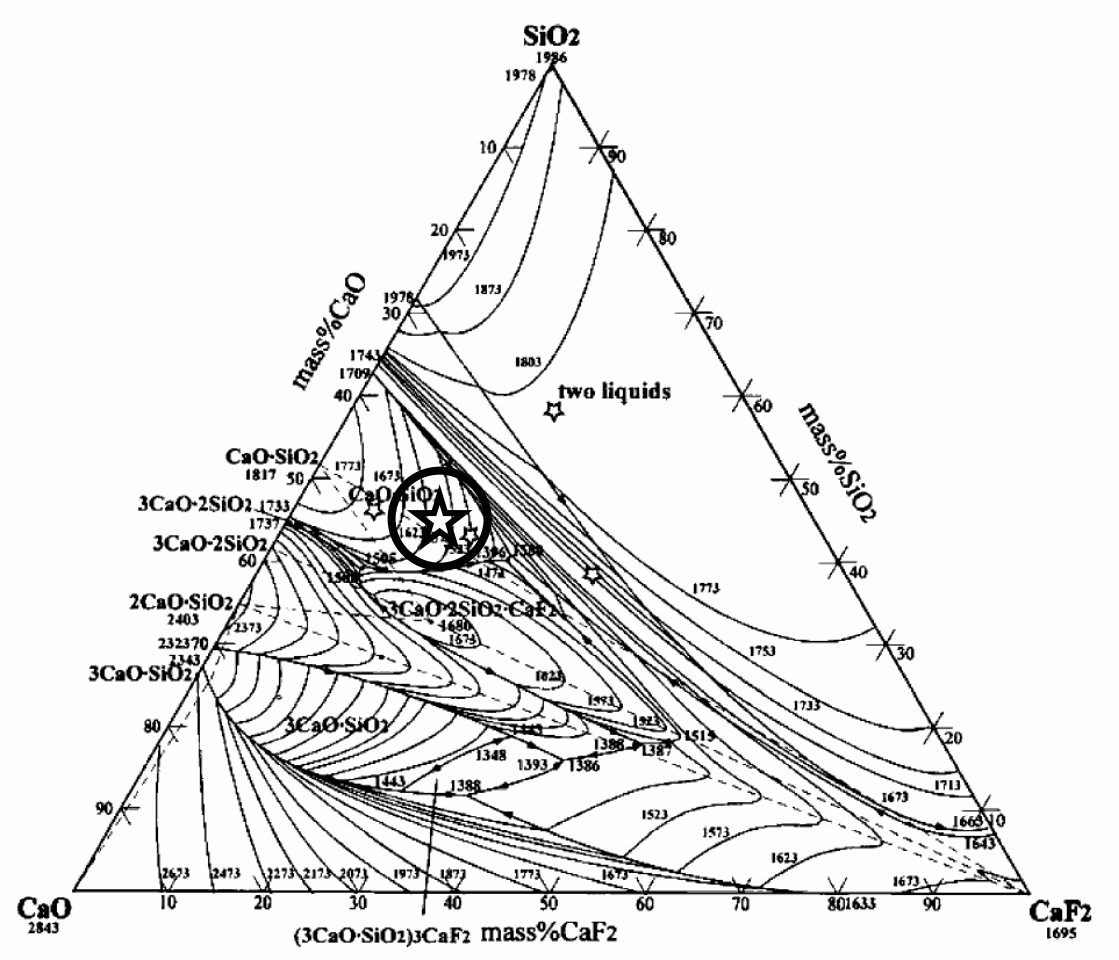

Figure 4. *Ternary phase diagram showing liquidus temperature contours (Meng et al. 2006(2)).*

One of the powders in that study (large asterisk) had a composition relating to those three compounds shown in Figure 4 near the composition of powders A and B in the present work. In that slag, the first, and easiest phase to form is cuspidine, which first appears when the temperature is kept at 700ºC for 30 minutes. With increasing furnace temperature, different phases (together with cuspidine) formed. These were calcium silicon oxide fluoride, nepheline and finally gehlenite at 1100ºC within 60 minutes holding time. The results of this study are shown in Table 2. The composition of the powder S1 was as follows: SiO_2 33.3%, CaO 39.9%, Al_2O_3 5.55%, F 7.52%, Na_2O 4.61% and MgO 2.96%. This powder had a different composition to that in the present study, but contained all the typical components in the typical range, making the results comparable.

Table 2. Phases present in slag S1 after devitrification test (Meng et al. 2006(2)).

Phases \ Test	700 °C 1 min	700 °C 30 min	700 °C 60 min	900 °C 1 min	900 °C 120 min	1100 °C 1 min	1100 °C 60 min
Glass	X	X					
Cuspidine ($3CaO•2SiO_2•CaF_2$)		X	X	X	X	X	X
Calcium silicon oxide fluoride ($SiO_2•2CaF_2$)				X	X	X	X
Nepheline ($Na_2O•Al_2O_3•2SiO_2$)				X	X	X	
Gehlenite ($2CaO•2Al_2O_3•SiO_2$)							X

Meng et al. (2006(2)) also investigated a slag film removed from the continuous casting machine while in operation. The composition of the powder was: SiO_2 35.8%, CaO 40.4%, Al_2O_3 4.6%, F 3.3% and Na_2O 6%, which is slightly different compared to those in the present study. Nevertheless, it is interesting to make observations of most of the films taken from the caster. BSE images of the tail-out slag film are shown in Figure 5.

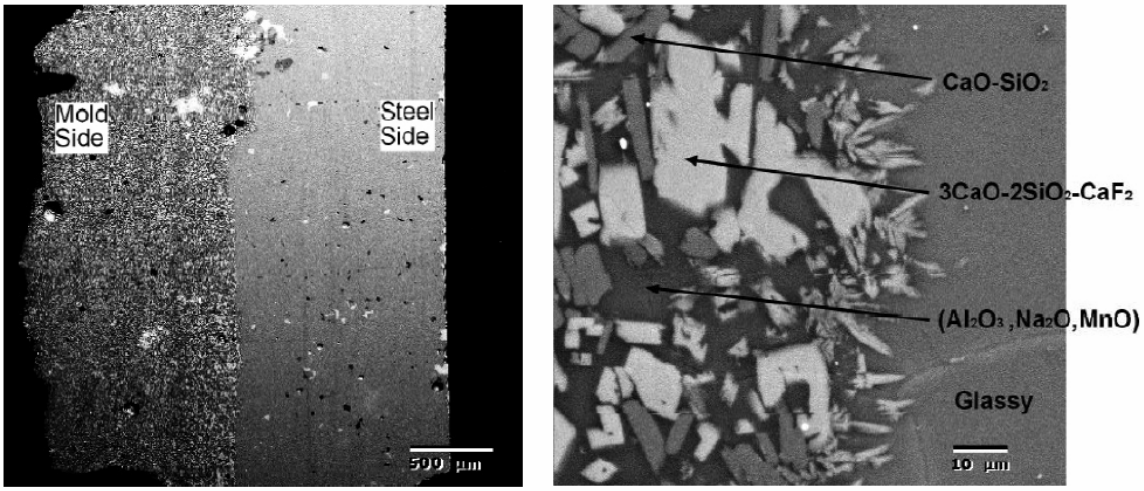

Figure 5. *BSE image of slag H1 film (Meng et al. 2006(2)).*

In this film, there are crystalline and glassy layers but no severe macro-segregation. It is evident from Figure 5 that crystals are growing into the glassy layer on the right. It is possible to see that the surface of the mould side is uneven, while that of the shell side is very straight, although these points are not commented upon in the paper. The boundary line between crystalline and glassy layers is also somewhat uneven. Based on EDX analyses, all elements on the steel side are distributed homogenously which again, along with the other observations, confirms that the microstructure of the steel side is glassy.

The crystalline mould side is composed mainly of high calcium-bearing grains in a silicon-rich background. These grains are likely to represent crystals of cuspidine that precipitated first, followed by the crystallization of other compounds, finally leaving a glassy portion in the remaining background. Similar phenomena are also found in the present study. The average composition of this area was found to be virtually the same throughout the film, which indicates that there were no macro-segregations. It is important to point out that noteworthy MnO concentrations were also found. The behaviour of manganese is just one of the items to be explained in the present work.

Susa et al. (1994) have investigated the thermal properties of slag films taken from continuous casting mould at several steel works, but they do not explain their sampling methodology. They presented a photograph showing crystalline and glassy layers in part of the slag film. They compared chemical analyses of the powders and the slag films, and noticed pick-up of Al_2O_3, which probably originated from Al deoxidized carbon steel. They also found pick-up of 2%MnO. The latter observation is of more interest to the present study.

There are many references from papers by Kashiwaya et al. (1998), because these researchers conducted trials with a powder that had almost the same chemistry as the powders used in the present study. Of no less importance is the fact that they conducted their trials with a technique simulating the conditions in the gap between the mould and the shell, and these results are very useful when analysing the films found in the present study.

Kashiwaya et al. (1998) developed a hot thermocouple technique to observe and measure the mould slag crystallization. The Double Hot Thermocouple Technique (DHTT) allows a simulation of the transient conditions, which occur in the infiltrated slag film. With this method, it is possible to generate the various thermal gradient conditions that may be experienced in the mould of a continuous caster.

Bubble evolution was also observed in the melting of industrial mould slags, although the powder was already decarburized. The authors did not make any assumptions about what the gases might be, but this bubble formation takes place in the mould. The crystals were coarser in the higher temperature enhanced by diffusion. The morphology of the crystals varied from dendritic at high cooling rates to blocky faceted crystals at lower cooling rates.

In order to determine the crystallization behaviour of an industrial mould slag used in the continuous casting of austenitic stainless steels, the authors conducted an isothermal experiment with SHTT (Single Hot Thermocouple Technique). The chemical composition of the slag was 37.8 mass% SiO_2, 33.3 mass% CaO, 7.9 mass% Al_2O_3, 8.2 mass% Na_2O and 8.4 mass% F. (CaO/ SiO_2 was 0.9, thus clearly lower than in the powders in the present work). They found that crystallization initiated within 10 to 400 seconds of isothermal holding (depending on the temperature) and the crystals grew for up to 45 min after the initiation of crystallization. (This may have been a coincidence, but stabilization of the temperatures shown in Figure 43 took about 40 - 50min.)

In a later paper, Kashiwaya et al. (1998) investigated the crystallization of a continuous casting mould slag. A TTT diagram was constructed for the powder, with a composition as shown in Table 3. This composition is fairly similar to that used in the present work, as it is a commercial mould powder employed in the continuous casting of stainless steels. It is of interest to note that the powder also contains Fe_2O_3 as does the powder in the present study.

Table 3. Chemical composition (wt%) (Kashiwaya et al. 1998).

T.CaO	SiO_2	Al_2O_3	Na_2O	T.F	MgO	K_2O	Fe_2O_3	CaO/SiO_2	Viscosity at 1300ºC (Pa·s)
37.8	33.3	7.9	8.2	8.2	0.6	0.6	1.7	1.14	0.2

The TTT diagram shown in Figure 6 was divided into two separate regions, which corresponded to the precipitation of dicalcium silicate at temperatures over 1050ºC and of cuspidine at temperatures below 1050ºC. The numbers 0.005 and 0.5 indicates the shares of the crystalline structure.

This work indicates that industrial mould slags are easily under-cooled, crystallization occurs throughout the melt, crystals grow initially as equiaxed dendrites and the onset of crystallization is a function of cooling rate and must be described by TTT or CCT curves.

The liquid slag in the gap is exposed to different cooling paths, which can promote or prevent crystallization. With this powder, bubble formation was observed during the melting process. Trials with an industrial mould slag revealed an image that was translucent (liquid slag was not transparent, probably due to the iron oxide content of the flux) and more difficult to analyze.

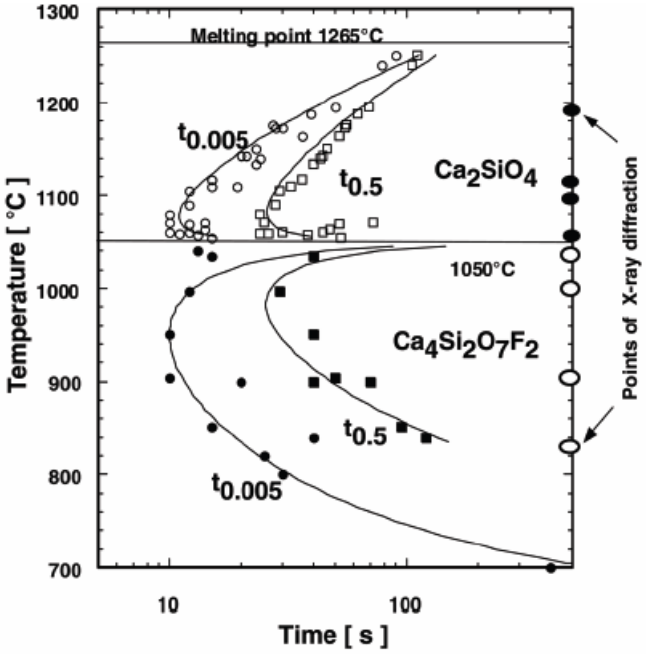

Figure 6. *TTT diagram of industrial mould slag obtained (Kashiwaya et al. 1998; Cramb 2007)*

Based on these trials, crystallization in the industrial slag can be seen to occur by nucleation and growth of individual crystals in an under-cooled liquid rather than by plane front solidification. This phenomenon must, therefore, be doped using the technique developed for classical nucleation theory. This industrial mould slag can be under-cooled significantly below its equilibrium liquidus temperature and the phase diagram (if one existed) would not be useful in the determination of the conditions under which crystallization will occur. Additionally, these results suggest that nucleants could be used to modify the crystallization behaviour of fluxes.

When analysing crystal growth during the experiment in an industrial mould slag, researchers state that the rate of reaction is quite fast and a non-diffusional transport mechanism is dominant. This transport mechanism is probably due to convection. In the present study, the phases found indicate that convection might have a role.

Cramb (2007) made comments on the previous paper, in which he was also involved. He noted that cuspidine is the most stable phase, and therefore expected from thermodynamic considerations, especially if mould slags are reheated. During solidification, however, another transient phase (dicalcium silicate, see Figure 6) is found if one quenches the sample from a high temperature. The solidification phenomena can thus be quite complex, with precipitated phases varying with the details of the process and with process time.

Cramb further proposed that a phenomenon of solidification can also be observed in Figure 6. When the chemistry of the precipitated crystal is compared with that of the original liquid, in the case of both precipitated crystals, the precipitated crystal has a different chemistry from the initial liquid. Thus, during solidification, the remaining liquid must change its chemistry to ensure mass balance in the liquid. This is, of course, the phenomenon of segregation. As solidification proceeds, the liquid from which the solid precipitates changes its chemistry. His final comments pointed out that to understand the nucleation of a solid from a liquid, one must first recognize that there are two mechanisms for producing solid from a liquid.

The first clause of the paper by Kashiwaya et al. (1998) mentions the interesting fact that the conditions under which crystallization develops in a mould slag must be understood in order to select or design a mould flux for use in the continuous casting of steels. Hopefully, the

present study will provide some supplementary information concerning the conditions under which crystallization takes place in the gap between the mould and the steel shell.

Cho et al. (2005) investigated the effect of hydrogen on the behaviour of the mould flux using a Hot Thermocouple Test (HTT) and breakout frequency in the caster. The casting powder information was as follows: basicity (CaO/SiO_2) was 1.32 and viscosity at 1300 ºC was 0.3 poise. They found that crystallization was accelerated in a wet atmosphere because nucleation of cuspidine was seriously accelerated by the increase of hydroxyl in the mould slag. They noted that natural cuspidine contains hydroxyl ($3CaO{\cdot}2SiO_2{\cdot}Ca(F+OH)_2$).

They also performed trials in the caster, and found that higher hydrogen content in steel produced a higher hydrogen content in the molten slag.

They concluded that hydrogen induces breakouts in two ways:

1. the entrapment of bubbles into the molten flux film interrupt the infiltration
2. the increase of hydroxyl in the molten slag accelerate the crystallization of cuspidine

As a measure to prevent hydrogen induced breakouts caused by cuspidine, they suggest a fluorine free casting powder, which crystallizes as phases other than cuspidine.

1.4 Heat transfer between shell and mould

Li et al. (2004) studied the influence of the crystalline phase on heat transfer. There are two mechanisms involved in the heat transfer process, namely lattice and radiation conduction. The latter is a process of absorption of radiant energy and its subsequent re-emission. In molten glasses, over 90% of the total energy comes from radiation conductivity (k_R) but it is decreased by (i) the presence of transition metal oxides e.g. FeO and (ii) by crystallites in solids, which scatter the photons. It has been reported that for the heat transfer in slab casting, only 10-30% of the total conductivity arises from radiation conductivity. The overall thermal resistance between the shell and the mould (R_{eff}) can be represented as a series of resistances (Mills et al. 2003).

$$R_{eff} = R_{Cu/sl} + (d/k)_{gl} + (d/k)_{crys} + (d/k)_{liq} \quad [3]$$

where $R_{Cu/sl}$ is the thermal resistance at the Cu/slag interface, d is thickness and k thermal conductivity. Subscripts gl, crys and liq refer to glassy, crystalline and liquid phases respectively, and Cu to the copper mould. The radiation conductivity (k_R) can be represented in Equation [3] as a parallel resistance (Yamauchi 2001). Recent work has shown that the two important terms are $R_{Cu/sl}$ and the resistance of the solid layer $\{(d/k)_{gl} + (d/k)_{crys}\}$. Furthermore, it has been shown that $R_{Cu/sl}$ increases as (i) the thickness of solid layer increases and (ii) the amount of crystalline phase in the slag film increases.

The above findings are of interest to the present study containing measured thicknesses of the flux film between the shell and the mould and also measured temperatures of thermocouples in the mould (correlating with the heat flux). It may thus be possibility to make these parameters fit together, i.e., to obtain accordance between the layers and the measured and calculated temperatures.

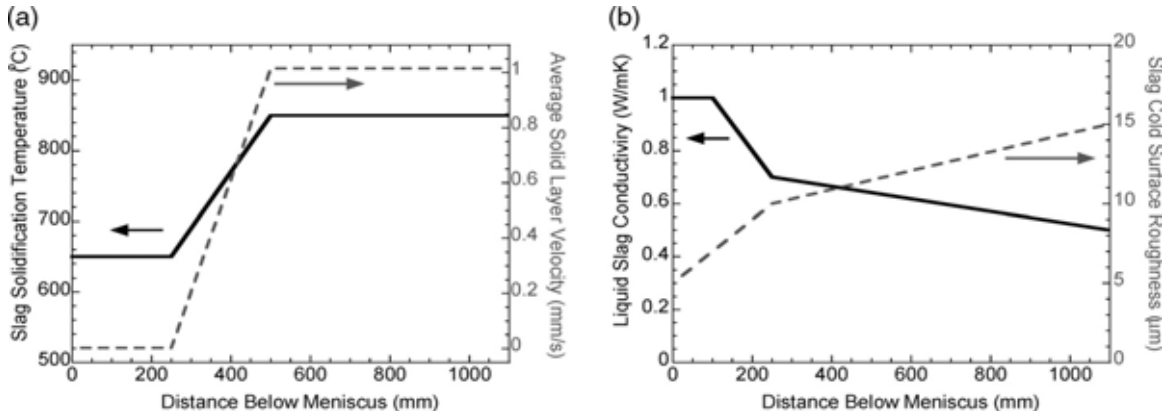

Figure 7. *Some of the properties of slag used in calculations by Meng and Thomas (2006) as a function of distance below meniscus. Input slag properties: (a) slag solidification temperature, T_{fsol}, and average solid layer velocity, f_v and (b) liquid slag conductivity, k_{liquid}, and slag cold surface roughness, for $r_{contact}$.*

Figure 7 shows some of the parameters which Meng and Thomas (2006) used in their model. The average solid layer velocity was assumed to be 0 down to the distance of 250mm below the meniscus, and below that, to have a linear increase with slag solidification temperature. Liquid slag conductivity decreased and slag cold surface roughness increased as a function of distance from the meniscus. (An increase in roughness means that the contact resistance between the mould and the solid slag is increasing). It is worth noting that they assumed a solidification temperature as low as 650ºC for slag in the gap near the meniscus.

Nakada et al. (2006) found from several sources (Susa et al. 1994; Susa et al. 1993; Yamauchi et al. 1993; Kawamoto et al. 1997; Taylor et al. 1988), that the most effective way to decrease heat flux is the crystallization of cuspidine ($3CaO{\cdot}2SiO_2{\cdot}CaF_2$) from mould flux. The reasons for the ability of cuspidine crystallization to control heat transfer can be classified into two views. One is that the radiation heat flux in the liquid layer is scattered at the front of the crystalline layer of cuspidine. The other is that the solidification shrinkage of mould forms the surface roughness on the mould interface and the large thermal resistance on the mould interface decreases the heat flux (Bagha et al. 1988; Cho et al. 1998; Cho et al. 1998(2); Yamauchi et al. 2002; Tsutsumi et al. 1999).

Based on their investigations on the thermal properties of slag films taken from mould, Susa et al. (1994) came to the following conclusions regarding the heat transfer between the strand (shell) and the mould:

- Thermal (´lattice´) conduction is the principal mechanism affecting heat transfer
- The contribution from radiation conduction does not exceed 10% of that originating from lattice conduction for the five slag films studied
- The crystallization of the slag is the primary factor affecting heat transfer via radiation conduction.

1.5 Influence of the casting powder on casting results

The casting powder is one of the key elements in the casting process when considering casting results, for example, the quality of the slabs and ‘sticking severity’ (O’Malley and Neal, 1999). These ultimately have an influence on the capacity of the caster, or “how fast you can cast with a good quality and without breakouts caused by sticking”.

Wang et al. (2004) concluded that longitudinal and micro cracks on the slab surface are the typical defects for continuous casting of medium and high strength low alloy steels. The crystallizing characteristics of mould fluxes play a key role in preventing such defects.

Ludlow et al. (2004) tested several casting powders as discussed in Chapter 1.3. According to their results, the performance of powder TH was far superior with respect to longitudinal cracking. They did not comment on the reasons for the superiority of powder TH. It is worth noting that the calculated crystallinity % with NBO/T index was positive only for powder TH.

In the Tornio works, it has been found that the casting powder has a major role, especially when trying to avoid the necessity of grinding slabs (Hautamaki et al. 1992). Even minor changes in composition can give a result, so that oscillation marks become shallow enough, and slabs can be further processed without grinding. An important finding was that the powder with which good surface quality is obtained tends to give lower total heat flux (Hautamaki et al. 1992).

1.6 Summary from the literature

The following observations were found in the literature concerning the flux film between the mould and the steel shell, and are of interest to the current study:

- the slag film sample can be expected to consist of a layer formed during casting and a layer formed later
- cuspidine will be a dominating phase in the flux film
- the share of cuspidine depends on the cooling rate of the slag
- the glassy and crystalline structures will be formed, but if the residence time in the gap is longer than approximately 20 minutes, only the crystalline phase will be found, due to devitrification on the mould side. The surface of the film will be irregular and the shell side surface will be straight
- the film structure has an influence on the heat flux
- film with crystalline structure has a good adherence to the mould wall, and long residence times can be expected
- evidence of film fracturing should be found
- due to devitrification, the structure of the layer in the film next to the mould wall is not dendritic
- voids and/or pores should be found due to the shrinkage of slag or gas formation
- most of the trials and experiments were made for the powders/fluxes for carbon steels

The behaviour of the mould slag had been a topic of many investigations because it is one of the most important and complicated slags of all in the melting shop.

2 EXPERIMENTAL CONDITIONS AND METHODS

2.1 Casting of stainless steels at Tornio Works

The experimental part of the work was performed at Outokumpu Tornio Works. There will therefore be a brief description of the steelmaking facilities in the plant, followed by a more detailed discussion of the characteristics of casting, and the experimental arrangements of the study.

The process in the melting shop of Tornio works involves melting in an electric arc furnace (EAF), refining in an AOD converter, treatment in a ladle furnace (LF) and casting with a continuous casting machine.

The experiments were performed on casting machine No. 1. Details of this machine are as follows:

- bending caster with straight part 1.5m and bow radius 8m
- metallurgical length 14m
- mould dimensions 175 x 1000-1600mm, length 715mm
- casting speeds 0.9 – 1.17m/min
- sequence lengths: average about 4, max 10 heats (1 heat~1 hour)

Nominal compositions of steel grades (main elements) are shown in Table 4.

Table 4. Compositions of steel grades (wt%).

Grade	C	Si	Mn	S	Cr	Ni	Ti
AISI304	0.03	0.5	1.2	0.003	17	8	0
AISI316	0.03	0.5	1.3	0.003	17	10	0
AISI321	0.03	0.5	1.2	0.003	17	8	0.4
AISI316Ti	0.03	0.5	1.3	0.003	17	10	0.4

The metallurgical length limits the casting speed in this machine, which made it possible to focus on specific features of the casting process.

2.2 Casting powders

Compositions of the casting powders used in the present study are given in Table 5. The principal powder used in the present study was powder B. Powder A was used in the casts of Ti stabilized steel grades. Some trials were made with powder C.

The choice of casting powder is vital in the achievement of a successful result. It is a difficult task because of the complicated nature of the powder composition, and because the powder has many important functions. The choice is based on experience, recommendations from manufacturers, and most importantly, trials in the caster, investigations on the quality of the slabs and observations of casting results. For example, before powder B was chosen, over 20 different compositions were tested, all of which had reasonably small differences. This represented a “tuning period”. Finally, the main part of the slabs with standard steel grades could be left without grinding. For Ti stabilized grades, several powders were tested but powder A was still chosen.

The desired goal was a granulated powder, because it is easier to feed automatically, which keeps conditions in the mould constant, and also because dusting is minor. With the aid of casting powder, the main objective is to achieve an equal thickness of the solidified shell around the perimeter of the mould, thus avoiding areas where shell thickness is less than in the surrounding areas. Deformation of the shell tends to occur chiefly on the thinnest areas and is caused by shell shrinkage, ferrostatic pressure and bending. It can result in cracks and other consequences.

Table 5. Composition of the casting powders used in Outokumpu Stainless based on information by suppliers.

Compound	Powder A w%	Powder B w%	Powder C w%	Start powder w%
SiO_2	32.00	30.8	31.8	42.0
CaO	37.40	34.3	32.50	34.4
MgO	0.67	0.87	0.90	0.51
Al_2O_3	6.80	6.39	5.30	3.15
TiO_2	0.13	0.15	0.10	0.02
Fe_2O_3	1.38	1.88	0.60	15.4
MnO_2	0.07	0.04	<0.10	0.14
Na_2O	7.00	8.02	9.50	8.92
K_2O	0.42	0.58	0.70	0.06
C_{tot}	4.30	4.32	4.10	4.32
CO_2	4.40	7.0	-	3.5
Cfree	3.10	2.4	-	0.2
F	7.50	7.24	6.30	11.1
P_2O_5	0.02		0.6	
B_2O_3		0.69	-	-
Li_2O	1.00	0.72	0.7	-
viscosity(1300 C)	0.16 Pa*s	1.3 dPa*s		1.0 dPa*s
H_2O_{tot}	0.50	0.75		0.48
H_2O	0.10			
CaO/SiO_2	1.17	1.14	1.02	0.83

C_{tot} is total carbon content, CO_2 is carbon dioxide in carbonates, C_{free} is content of free carbon and H_2O_{tot} is the crystal water content distinguished when heating at 600 °C, H_2O is "loose" water content (removed when heating at 105 °C).

Note: start powder contains metallic Si, which should react with iron oxide, generating heat to accelerate the melting of the powder. (Metallic Si was included in SiO_2 content).

For starting powder: softening point 920°C, melting point 1110°C and flowing point 1150°C. For powder A: 1100°C, 1120°C, 1150°C. For B: 1010°C, 1090°C, 1120°C, respectively.

Powders A, C and start powder had a powdery consistency. B was granulated by spray drying.

Contents of elements (mass%) in powder B when carbon is removed (to compare later with the contents in the films): Si 15%, Ca 26%, Mg 0.5%, Al 3.6%, Ti 0.1%, Fe 1.5%, Mn 0.03%, Na 6.3%, K 0.5%, F 7.2%.

2.3 Mould with several thermocouples

One of the moulds was also equipped with thermocouples in the lower part of the copper faces. Thermocouple temperatures were used to observe local heat fluxes on different areas of the mould. The locations of the thermocouples are shown in Figure 8.

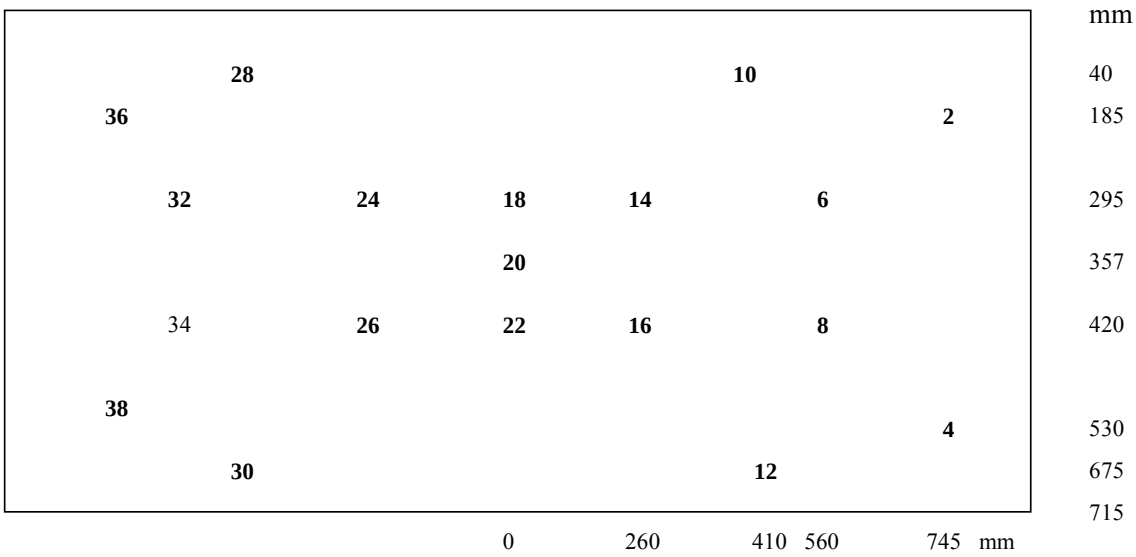

Figure 8. *Location and numbers of thermocouples on the inner (loose) bow side.*

In Figure 8, numbers on the right side show distances from the upper edge of the mould (mm), and numbers below show distances from the middle of the mould. The numbers on the same location on the outer bow side are +50 (i.e., number 60 is opposite to number 10; numbers are even, because odd numbers were reserved for other purposes.) The total length of the mould is 715mm. The level of the meniscus was typically 10-20 mm above the first row of thermocouples, but occasionally slightly below this.

Because only one of the moulds was equipped with the thermocouples in the lower part of the mould walls, monitoring of local heat fluxes in the lower part was not available in all sampled casts. Thermocouples were installed through fixing bolts.

2.4 Sampling procedure and phenomena observed in sampling

Sampling in the present study was made from the real casting process during normal production. This caused certain difficulties, because sampling ought to be done without disturbing the process too severely. Furthermore, in a real process, there are variations from cast to cast. It is important to analyze and explain features relating to sampling procedure, because these need to be taken into account during analysis of the layers in sampled films.
When finishing the casting, the tail of the “last” slab shell must be closed with solid steel. This is to prevent the steel on the tail of the shell from being drawn from the mould to the secondary cooling zone in the liquid state, because liquid steel might get squeezed out from the tail between the rolls, which would cause it to freeze and stick to the rolls. Removing and cleaning would cause delays.

Normal practice involves removing casting powder and liquid powder slag, and cooling the liquid steel surface with water until it freezes and forms a cover. In this way, liquid steel remains inside the shell during tail-out through the casting bow. A new practice was developed in the Tornio Works to close the tail during tail-out. It involved setting a specially fitted steel plate into the shell without any de-slagging. With this tail-out practice, it was noted that flux slag films remained in the mould after the tail of the last slab was removed, as shown in Figure 9. A thicker layer was produced, which loosened from the mould wall during shrinkage. However, a thinner fraction of film remained on the mould walls, seen as white areas in Figure 9 on the right. This layer was stiff, and small samples had to be removed by scraping.

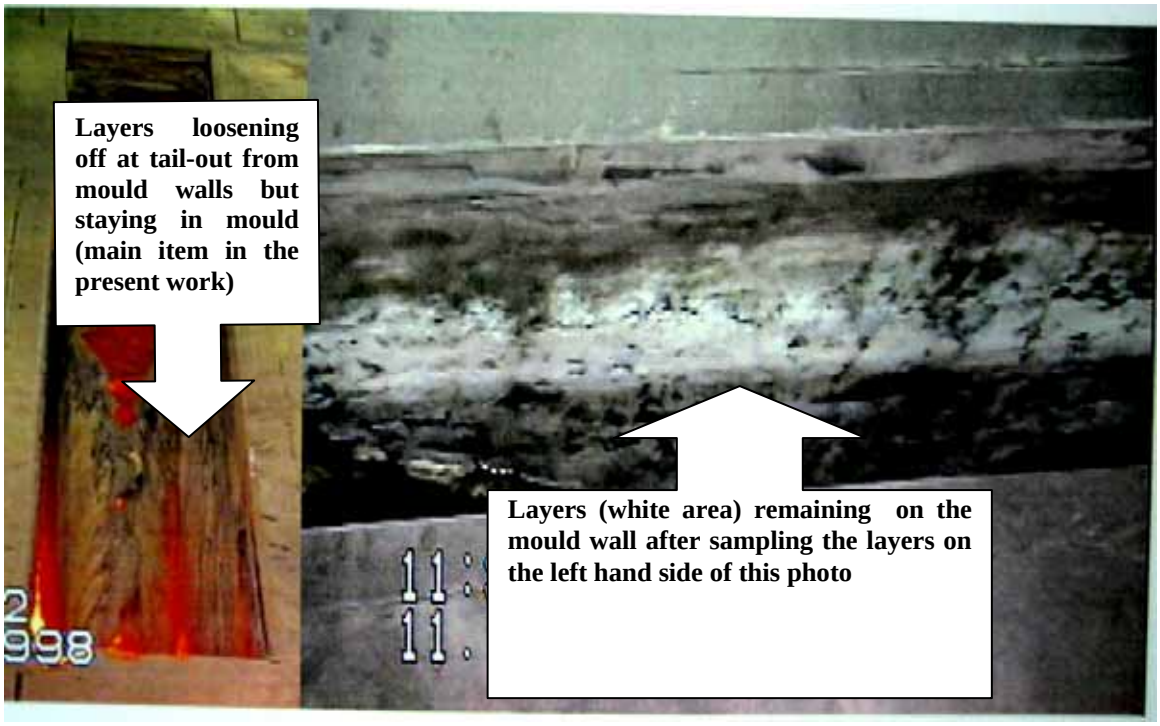

Figure 9. *These two photographs show conditions in the mould after tail-out, prior to taking a sample (photo on left side), and after (photo on right side) (Pesonen 1998). To scale: thickness of the mould is 176 mm.*

In Figure 9, slag layers remain in the mould, and although the tail of the steel shell has left the mould, it still has a red shine. The photograph on the right was taken after tail-out, and white areas on the mould surface are clearly visible. These flamed when sprayed with water.

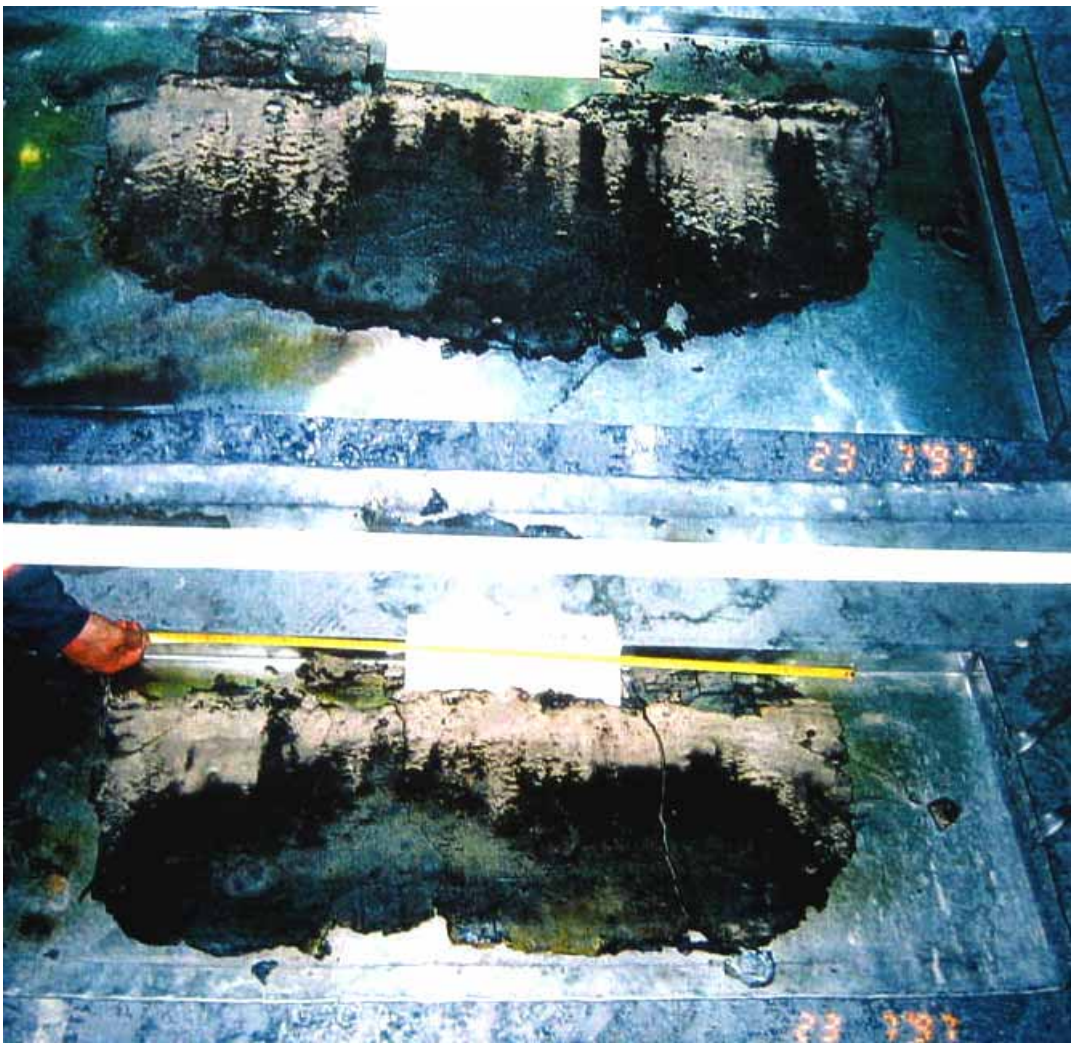

Figure 10. *Photographs show samples from outer and inner bow sides. The sampled pieces were lifted on a low tray immediately after sampling to maintain their correct placement following possible fracturing due to cooling. (Some fracturing always took place.)(Pesonen 1998). The width of this sample was about 1 m.*

As shown in Figure 10, the best samples traversed almost the whole width of the wide faces. The slag rim can be seen at the top. Some of the samples reached down to 40cm from the meniscus. A schematic illustration of the slag layers is shown in Figure 11 below.

Most of the analyzed films are from the middle part of the wide face.

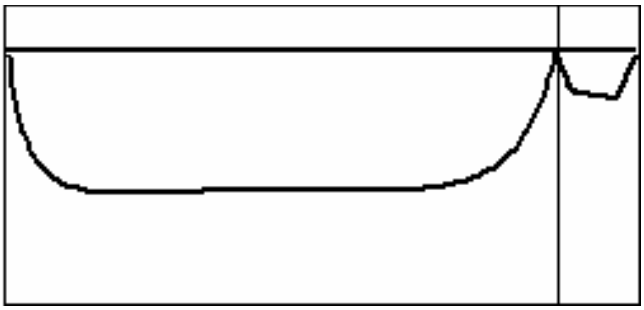

Figure 11. *Typical shape of the flux layer shown schematically on the wide and narrow faces of the mould.*

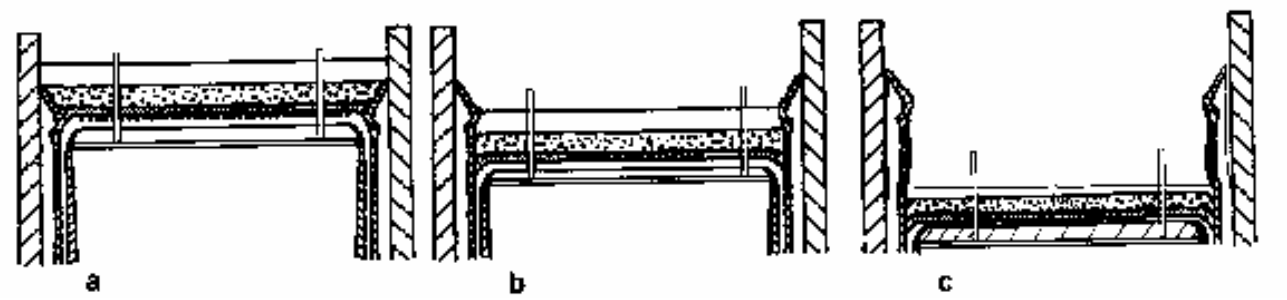

Figure 12. *The method of closing the tail of the last slab in the finishing procedure is shown schematically above: a) steel plate is placed into the shell, b) the shell is drawn down and c) the powder slag layer remains on the walls of the mould (Pesonen 1998).*

In this technique, the tail-out plate is immersed through all the powder layers into the tail of the shell. Powder layers remain on the top of the liquid steel (see Figure 12). The steel level has a tendency to rise due to the plate and steel shell shrinkage. Liquid flux slag rises over the edge of the steel shell, and when the shell is moving down at a speed of approximately 0.2m/min, a proportion of liquid slag from the top of the tail (and sometimes also liquid steel) adheres to the surfaces of existing solid slag layers, forming an extra layer.

This extra layer is usually clearly the thickest layer. This extra layer brings both problems and benefits. The disadvantages include problems in observing the difference between the extra tail-out layer and the "real" layer. Fortunately, the border between these layers is in most cases quite sharp. Benefits include bulking out the total thickness of the layer, and strengthening it mechanically. This makes it easier to catch the layers with clamps and samples remain in larger pieces while cooling. It also serves as a reference, as it has the same composition as the flux slag on the top of the liquid steel at the moment when the cast is finished.

2.5 Use of tracers

Powders doped with tracers were used to determine residence times of layers, and to make it easier to separate the layer formed during casting and that formed during tail-out. Doped powder was usually applied at a certain period at the end of the cast (20 to 60 minutes). In some of cases, two tracers were used; for example one tracer for a period of 20-60 minutes before the end of casting and the other tracer for the remaining 20 minutes. Doped powders were not used from the beginning of casting, because tracer can influence the properties of powders, which would make the evaluation of results more complex.

BaO and ZrO_2 were used as tracers in some of the trials. Concentrations of tracers were kept as low as possible, because even in low concentrations (about 1-2%) they can influence the phases which form, and they also tend to favour certain main or matrix phases, as shown later. They can also react with deoxidizers, and it is therefore possible to misinterpret data connected to tracers.

2.6 Methods used to analyze and study samples and associated phenomena

Samples were taken from over 50 casts. Much training was necessary in order to discover the correct sampling method, and some of the best samples were chosen for the more precise analyses. Steel grades were stainless grades AISI 304, 316, 321 and 316Ti.

Even without a microscope, different layers were visible. The thickness of layers from different locations in the mould was measured, but this turned out to be of less importance due to the fact that in most cases, the majority of the total thickness was formed during tail-out. The SEM/EDS analyzer was used to make more detailed analyses through cross-sections of sampled layers. BEI mapping images were also used.

Samples for microscopic examination were chosen on the basis of (i) different distances from the meniscus (ii) different horizontal positions and (iii) visually different layer types on the mould side surface. Some of the sampled layers were fragile, which made handling difficult. In some cases, layers moved more than usual, which made their initial locations difficult to estimate.

As a reference for analyses made with the SEM/EDS analyzer, some test layers were prepared. Liquid flux slag from the mould and slag melted in the laboratory were cast on a steel plate, and the resulting layers were analyzed in a similar way to the sampled flux slag layer films. The results were comparable to those of the layer films formed during tail-out.

Some studies were made using programs for thermodynamic calculations, which produced more data on the formation of the phases found in the flux films. Unfortunately, the calculations were only approximate due to missing data concerning these types of slag; the cuspidine phase was not included. Additionally, X-ray spectroscopy as well as chemical analyses (for Na and F) were used. The depth of the oscillation marks was measured with a tool equipped with a moving measuring head containing a laser detector.

3 RESULTS

3.1 Introduction

As discussed in Chapter 1, very little information was available on slag films between the solidifying shell and the mould. According to Li, Thackray and Mills (2004) it was exceedingly difficult to obtain sufficient representative slag films to establish a relation between the chemical composition and the percentage of crystallinity.

In the literature, few observations of flux films were presented. (Ogibayashi et al. 1987; O'Malley and Neal 1999; Terauchi & Nakata 2002; Ludlow et al. 2004; Kallio et al. 2004; Susa et al. 1994), made such observations, but in these, the exact location of the sampled film in the mould was unknown and/or the sampling method was not described. Very few of them presented flux film structures with layers formed during casting and layers obviously formed during tail-out (Ogibayashi et al. 1987). In one paper (Terauchi & Nakata 2002) it was clearly established that the slag film consisted of two sub-films.

3.2 Some features of the sampled flux film schematically

Characteristic geometric features of the films are shown in Figure 11. The film extends for longer in the middle of the wide face than near the narrow faces. This geometry is chiefly caused by the steel flows in the mould (see Figure 1).

When combining information from sampling and the analyses of transverse cuts of film layers, it is possible to describe the film layers as shown in Figure 13. These features are useful when considering the results presented later in the present study.

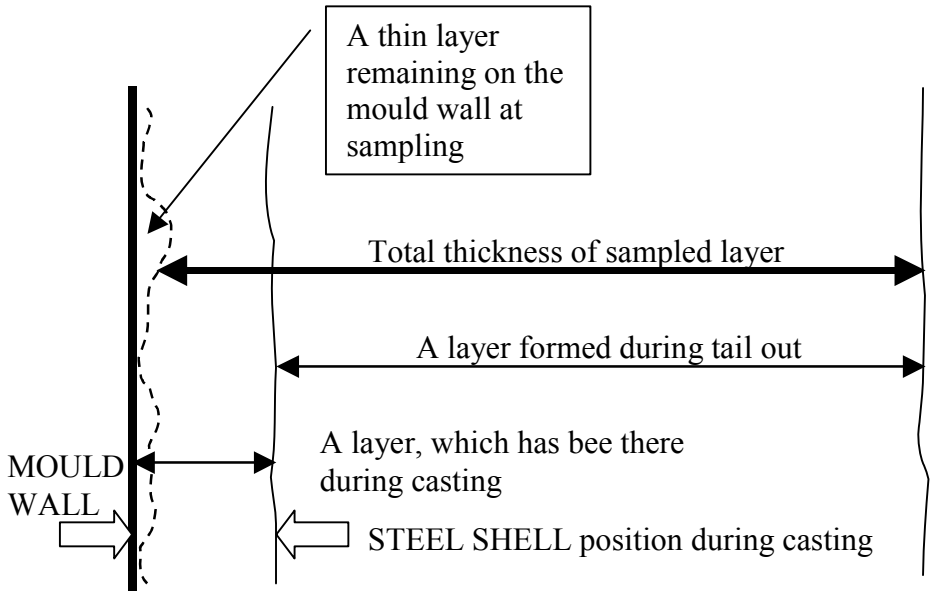

Figure 13. *Schematic picture showing different layers in the sampled film. (Hooli 2003).*

The followings features can be stated regarding the mould surface, beginning with the surface itself and working inwards:

- A thin “white” layer nearly always remained on the mould wall, which no longer existed in the sampled layers.
- With the exception of the white layer, residues of the “real mould slag film” sometimes remained adhered to the mould wall. This was dependent upon sampling success.
- In the sampled layer, there were layers formed during casting (except the above mentioned layers) and a layer formed during tail-out.
- The layer formed during casting often contained several sub-layers.

3.3 Macroscopic features of sampled layers

Photographs of surfaces of the flux films on the mould side are presented in Figures14-16. There was wide variability in the appearance of the surfaces. Surfaces of the flux films on the shell side are not presented, because these formed during tail-out. The photographs in the figures show sections of the flux films arranged systematically downwards from the meniscus.

On the slag surface shown in Figure 14 a), the dominating colour is black, with some bluish and brown areas. It appears that certain areas were formed later, after the cast started and began bleeding. On the surface shown in Figure 14 b), there are whitish areas which probably consist mainly of NaF. Some of the bleedings have a glassy appearance. The slag rim was included on the top, shell side up. On the surface shown in Figure 14 c), the mould side layer has quite a uniform colour. On this surface there are a lot of bleedings with a glassy appearance.

On the surface shown in Figure 14 d), one special feature is the presence of whitish, spherical spots. These probably contain a NaF phase. The appearance of sodium fluoride is either colourless, white crystalline powder, or crystals (data for sodium fluoride, n.d.). The films shown in Figures 14 a-c had broken into smaller pieces which was fairly typical, because the sampled films were often fragile.

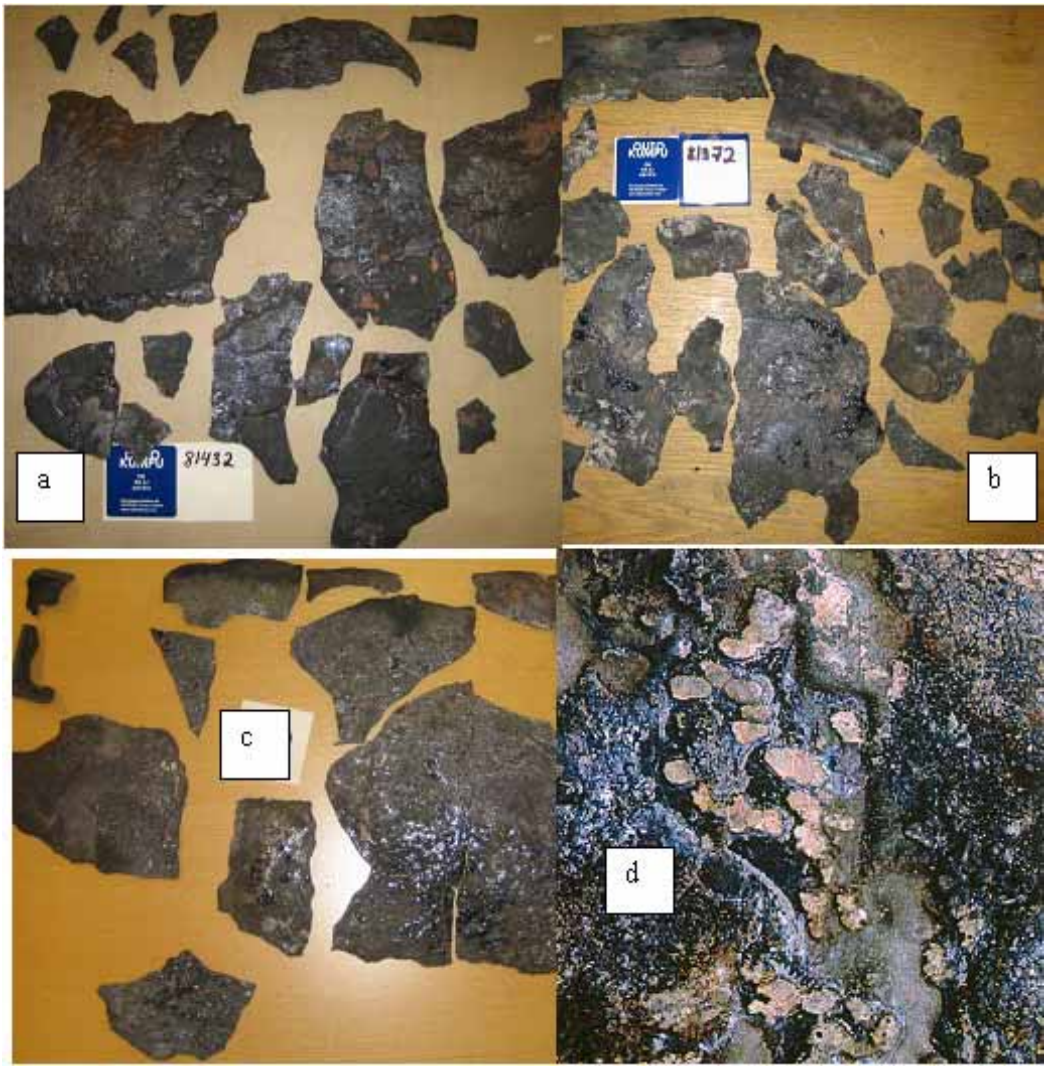

Figure 14 (a-d). *Appearance of mould side surfaces of selected films. Real width of Figures a, b and c is about 30 cm, and of Figure d about 5 cm.*

On the surface shown in Figure 15, there are a wide variety of colours. Different colours indicate different compositions; some areas contain shapes similar to oscillation marks, and others resemble volcanic craters. There were few areas of bleeding. The area marked with "x" in Figure 15 was examined with a magnification of 500, and different points (phases) were analyzed with SEM/EDS. This revealed that the matrix phase was NaF together with a cuspidine phase, which had a needle-like form (lengths about 20-30µm) and a multi-component compound containing O, Na, Cr, F, Si and Ca (in the order of concentrations). Separation of the phases had thus taken place on a small scale.

In this area, "overall" concentrations of fluorine and sodium were high (26 %F and 26 %Na) (composition 2: 16 %O, 26 %F,26 % Na, 6 %Si, 9 % Ca, 6 %Mn).

The film shown in Figure 16 was strong enough to remain in larger pieces. There are horizontal wavy shapes on the surfaces.

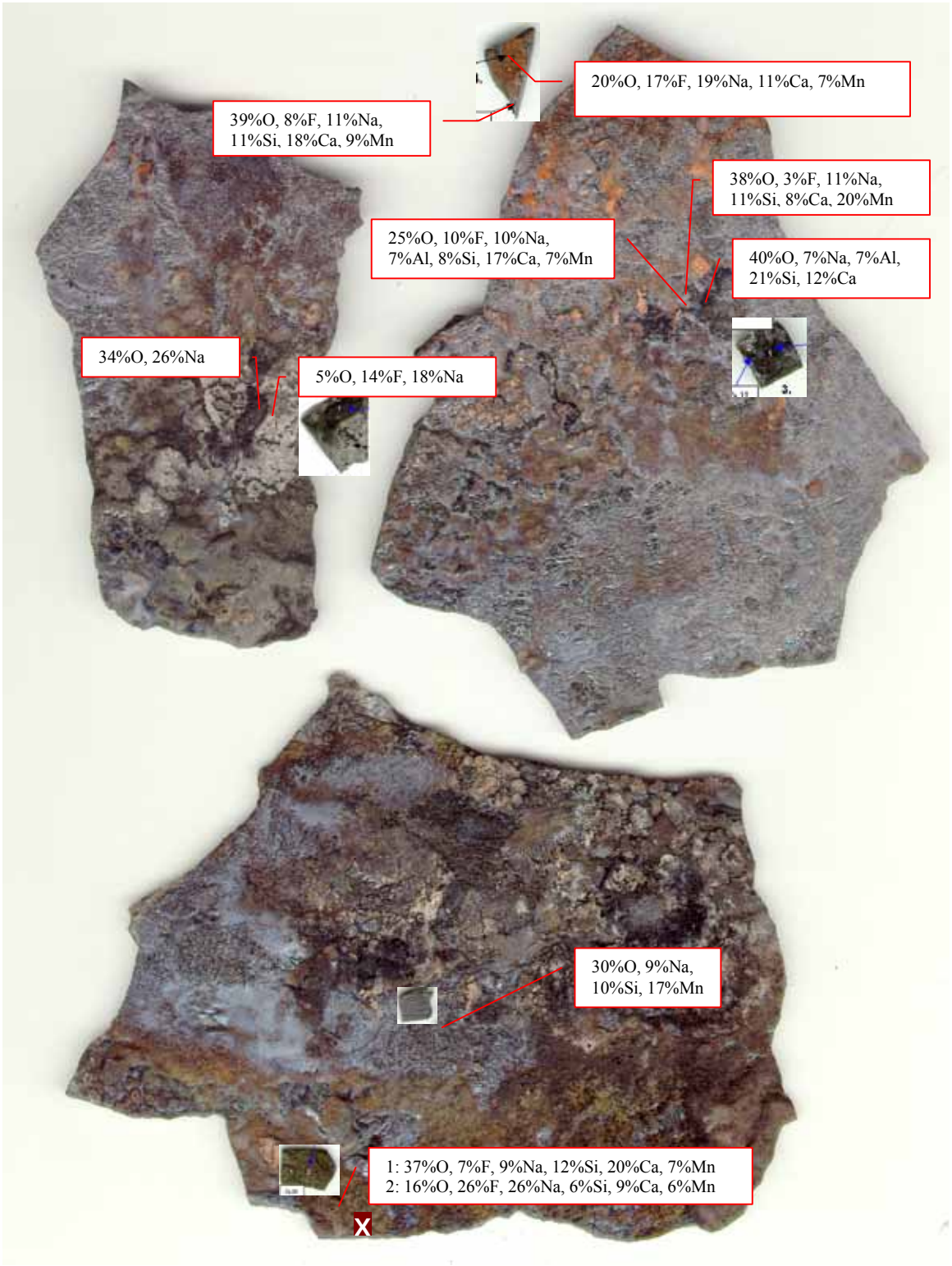

Figure 15. *The appearance of the surface of a sample on the mould side, with concentrations of elements in some spots and with magnifications from some of the spots. Real height of Figure is about 20 cm.*

Figure 16 . *An example of surfaces of slag layers on the mould side; cast number 80330. Height of sample is approximately 25cm and the upper edge is a few centimeters below the meniscus.*

3.3.1 Discussion concerning mould side surfaces of samples

The mould side surface of the sampled layer was in many cases quite confusing. As shown in Figures 14-16, there was a large variation in the appearance of the mould side surfaces. Some of them resembled the lunar surface or mountainous deserts, and some even contained craters. A wide spectrum of colours was observed.

Characteristic features of the mould side surfaces of the sampled films included:

- uneven surfaces
- colour variation
- variation of concentrations of different elements
- fractures and bleedings
- glassy bleedings
- wave lines resembling oscillation marks
- “craters”
- areas resembling netted patterns

Uneven surfaces
The surfaces of the films on the mould side were expected to be straight and even, but contrary to expectations, those surfaces against the steel shell were more even. The reasons for the uneven surfaces are discussed below.

Colours and compositions
A variety of colours were visible on the sampled surfaces. Where analyzed layers were very thin, the background may have had a strong influence on the result, and this is a factor that must be taken into account. Colour differences are caused by the presence of different compounds on the surface (Figure 15), which may occur during phase sorting. Another reason for this phenomenon was that in some areas, more layers remained stuck on the mould wall or became loosened during sampling.

Some surprising compositions were detected. In some areas, there were Mn concentrations of up to 17%, whereas the powder contained a maximum of only 0.5% MnO, and the content in the moulds flux slag was typically 2-3%. In all analyzed areas, Ca content was low or missing. In many areas, there was a higher concentration of Na than in the powder. The whitish area had a Na concentration of 14%, an F concentration of 18%, with low O content.

In the area 2 in Figure 15, "overall" concentrations of fluorine and sodium were high (26 % F and 26 % Na) (composition 2: O16,F26,Na26,Si6,Ca9,Mn6), which means that the area contained a NaF phase. The phases were on a small scale without dendritic structure, therefore the phases in this area were probably formed as a result of devitrification.

Bleedings
In areas where liquid slag appeared to have moved onto the mould surface through fractures in the solid film, phenomena resembling bleedings occurred. When solidified, these were round in shape, which indicates poor wetting of liquid flux slag on the nickel surface (copper mould was coated with nickel).

Figure 14c shows spot-like bleedings with a glassy appearance. These may have formed during the late period of casting before crystallization had time to occur. Figure 16 shows transverse bleedings in the layer, which indicates the presence of several fractures in the lower part of the film.

These bleedings appeared mostly in the lower areas of layer at 15-40cm from the meniscus. Fractures may have led to sticking of the shell near the meniscus with the mechanism, that when fractures occur on lower areas of the film, liquid flux runs out from the distance between the location of the fracture and the meniscus and this leads to poor lubrication also near the meniscus, and fractures in thin steel shells.

The bleedings in the flux films are analogous to so-called blind breakouts, or bleedings in the steel shell, which occurs when liquid steel enters via shell fractures and becomes frozen on the mould wall before emerging from the mould.

"Oscillation marks"
Surfaces exhibited wavy lines resembling oscillation marks. Although these were less organised than the marks on the steel shell, they were probably caused by the mould oscillation. These marks may have formed at the beginning of casting. When the liquid flux slag is very poorly wet on the Ni surface, slag attempts to avoid spreading, which is then a forced phenomenon. This can happen during downward motion of the mould. As a result, intermittent layers may form, which resemble oscillation marks. This explanation is only valid

for the first layer on the mould. It involves the claim that certain parts of the sampled surfaces were originally formed at the beginning of the casting.

Craters
Spots with the appearance of craters were also evident and resembled areas where escaping gas had pushed through. In a later chapter concerning the microscopic study of the layers, prominent porosity will be discussed.

Net patterns
In some samples, net patterns were evident, which might indicate that some areas solidified in a glassy phase, then crystallized later. As shown in Figure 14b, some of the samples exhibited a slag rim, which is unable to enter the gap between the shell and the mould, and acts as an "anchor". This means that if a solid layer were moving downwards during casting, at a speed lower than the casting speed, the solid layer may fracture occasionally.

In Figure 7 (from Meng & Thomas, 2006), they used different speeds for solid slag velocity, according to the distance from the meniscus. For the distance of 250mm, velocity was assumed to be zero, but increased from 250 to 500mm gradually to 1mm/s (0.06m/min). The findings in the present study are predominantly in accordance with those assumptions. They also conform to slag cold surface roughness, as shown in Figure 7 (b).

3.3.2 Wetting between the liquid casting slag and the nickel coated copper mould

Results presented in the literature (Petäjäjärvi, in *press*), indicate that on the Ni coated copper mould, wetting of liquid flux slag is poor. This could result in spherical, droplet-shaped forms, as shown in Figures 14-16. Figure 16 shows vertically oriented spherical forms with ridges. These probably formed when liquid flux bled through cracks. If the observed area had a glassy phase, it probably became frozen near the end of the casting, and did not have enough time to devitrificate at the relative low temperatures on the mould face.

Due to poor wetting, liquid flux slag was forced onto the Ni coated mould surface layer by layer. These layers are related to oscillation stroke. Wavy forms such as oscillation marks, are visible on some areas of the layer surface, as seen in the "blue" area in Figure 16. These first layer areas are likely to consist of a glassy phase, with devitrification taking place later. This hypothesis involves the claim that some of the areas were already formed at the beginning of the casting process; their lifetime spanned the entire casting time. More trials are needed in order to verify this hypothesis.

3.4 Microscopic features and layer structures in the samples

In order to study the structures of the films with optical and electron microscopy, cross-sectional cuts were prepared from several films of interesting appearance. The photo collage shown in Figure 17 presents a survey of the properties of the structures which were microscopically visible. Two series of photographs are shown. In the left series, photographs came from a cast with a total casting time of approximately 2 hours, which involved two heats. The right series represents a cast of approximately 5 hours, involving five heats. The photographs are presented in order of their distance from the meniscus.
More film photographs are presented in Appendices 1 and 2.

In Figure 17 (H), there is a short distance between the whitish cuspidine layer and the red line. In this sample, it was possible to separate what was probably the lubricating layer during casting, as discussed later. It was possible to visually separate different layers in the films, especially at longer distance from the meniscus. The layers farther of below the meniscus were typically thicker having had a longer cast, they had developed more complexity and more pores.

The next step was to analyze the concentrations of elements over the film cuts with the SEM/EDS analyzer. Figure 18 shows the film chosen as a representative layer, displaying the typical behaviour of the elements. It is again important to remember that on the mould side, part of the film is missing, because it remained adhered to the mould wall.

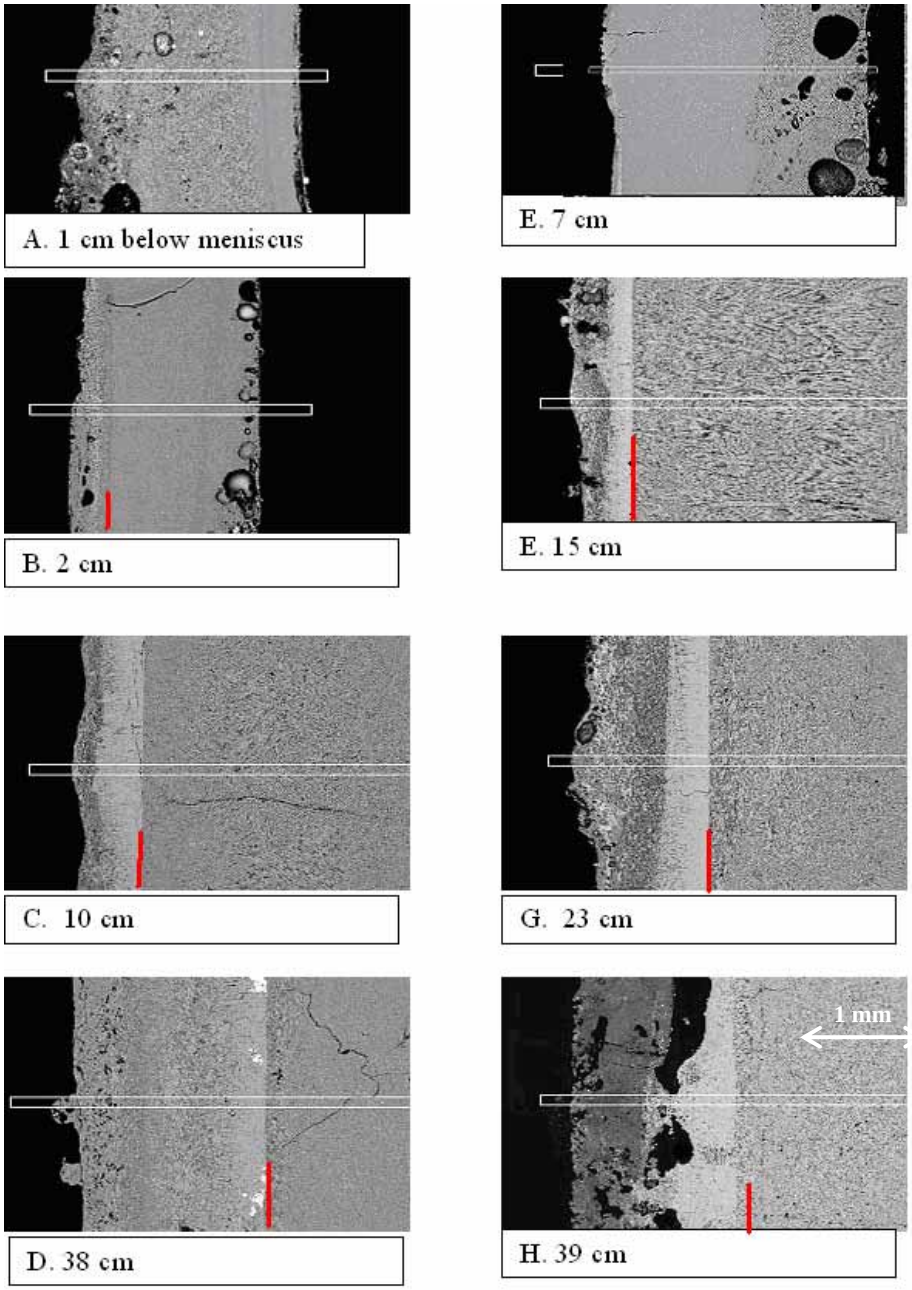

Figure 17. *Two series of the layer cuts of films from two casts with different distances from the meniscus. The series on the left is from a 2 hour cast; that on the right is from a 5 hour cast. Layers on the right of the short red lines are formed during tail-out (this is an assumption)(Hooli 2000).*

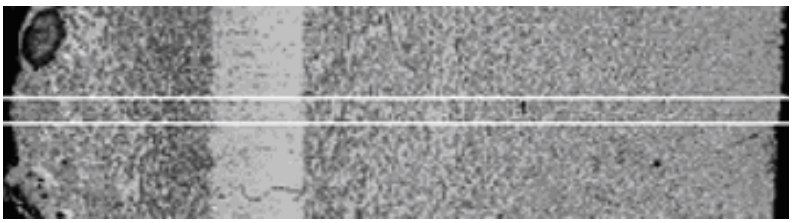

Figure 18. *A typical layer film structure (the layer in Figure 17 G). (The figure is scaled to fit with graphs in Figure 19).*

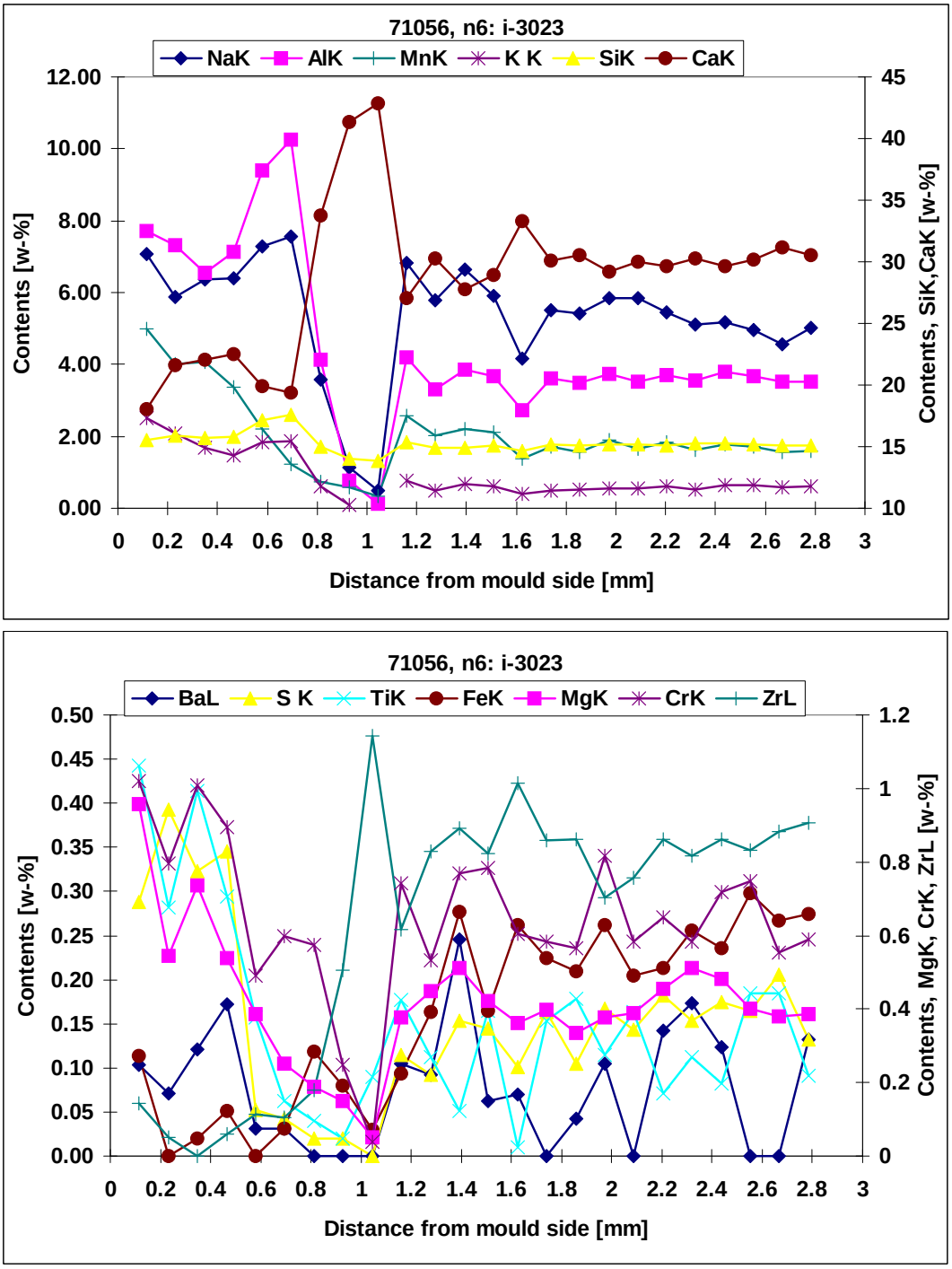

Figure 19. *The concentrations of elements in layers shown in Figure 18 (cast 71056). The elements with higher concentrations are in the upper graph.*

The most eye-catching feature in this film was the whitish layer containing over 40% Ca, which was about 10% units more than in the layer formed during tail-out. The latter layer served as a useful reference. The layer with over 40% Ca was composed of cuspidine (presented later), and also contained O, Si and F. The concentration of most elements was low, with some elements at zero concentration. Only zirconium (Zr) had a peak in the first point of the cuspidine layer.

The concentration of elements in the layer formed during tail-out were similar to those found in the casting powder. However, concentrations of some elements were higher than in the powder, for example Mn, Mg and S. The concentrations of several elements tended to increase on the mould side of the Ca rich layer, becoming higher than in the tail-out layer. Such elements included Na, Al, K, Mn. Ba and Zr and were used as tracers in the powder (as oxides). Concentrations of these depended both on when they were added and unfortunately, upon the matrix phase.

In the case of Figure 19, Zr-oxide doped powder was used during the last 30 minutes of casting and thus before sampling. The concentration of Zr in the tail-out layer was 0.9%; in the first point of the Ca-rich layer, the concentration was also high, but towards the mould side, it decreased down to almost zero. This suggests that only part of the Ca-rich layer formed during the last 30 minutes, whereas layers on the mould side formed earlier.

A steel film was sometimes observed in the flux films (see Appendices 1 and 2). This was located on the borderline between the layers formed during casting and those formed during tail-out. The steel film in the appendices was formed during tail-out. An overflow of steel had risen over the edge of the shell during tail-out, because the tail-out plate had been set into the tail of the slab. This overflow was confirmed when an extra box was mounted to the tail-out plate, and it removed more liquid steel from the tail than usual. In cases like these, steel films were obviously present in the flux films more frequently.

The effects of the formation of cuspidine are considered in Figure 20.

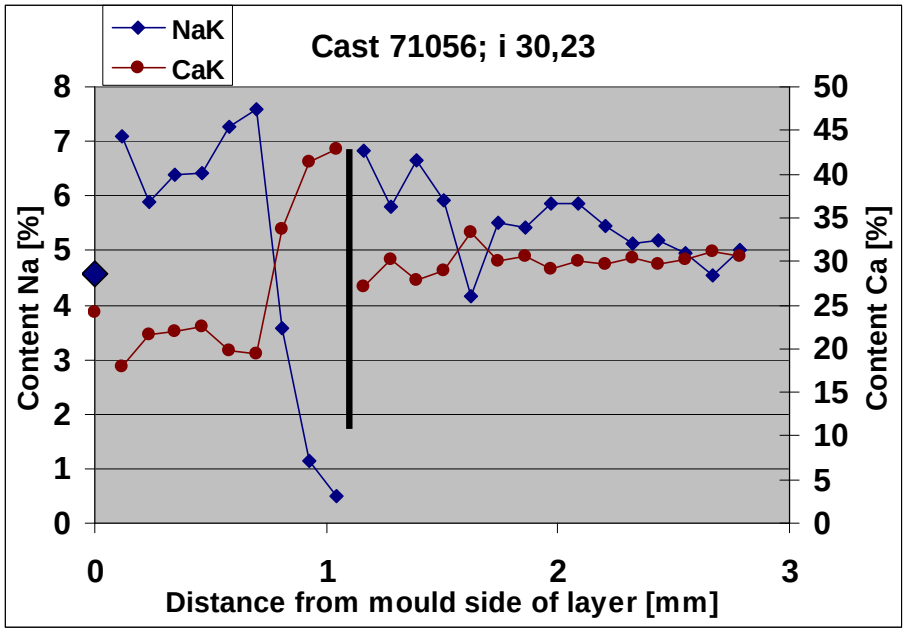

Figure 20. *The concentrations of Ca and Na in the layer shown in Figure 18.*

The powders used in the present work had a strong tendency to form cuspidine. When cuspidine formed, it expelled other compounds and with them many of the elements. As an

example of this, Figure 20 shows trends of Ca and Na concentration. When average Na concentration from the cuspidine layer to the mould side of the layer was calculated, it was only slightly lower than in the tail-out layer (from the vertical line to left; average value is shown at the distance of 0).

3.5 Microscopic features and phases in the layers of the film

In the previous chapter, the average concentrations of elements in the flux films were discussed. The layers consisted of several phases in the slag, and more specific analyses were conducted in order to determine the phases in different sub layers. Figure 21 shows an overall picture of the film; an increased magnification from the same film is presented in Figure 23, where it is possible to visually separate different areas by chromatic variation. This was used to select points for analyses by SEM. This film was chosen for more precise analysis, because it appeared to incorporate the whole film almost to the mould wall, and it also contained several interesting sub layers. In this cast, Zr-oxide doped powder was used during the last 20 minutes of casting, and Ba-oxide doped powder was added during tail-out.

When comparing concentrations of the elements shown in Figure 19, the most remarkable difference was in the concentration of Na in the mould side from the cuspidine layer. Na content here reached a value of approximately 50%.

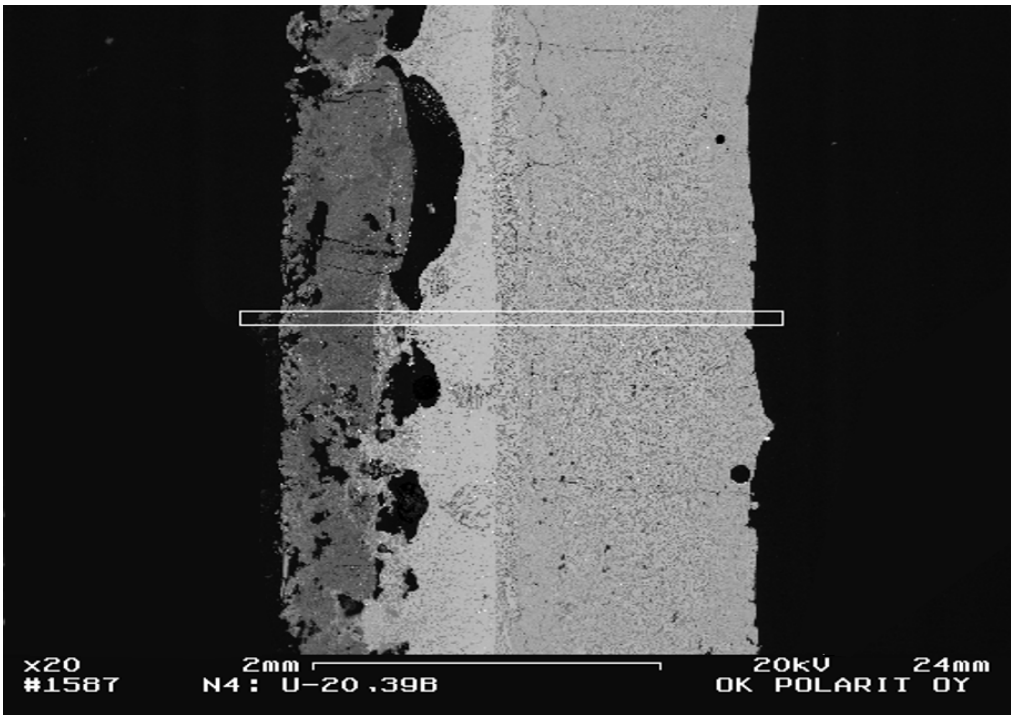

Figure 21. *One of the most complicated layers, found at 71056 U-20.39B i.e. the outer bow side 20 cm from SEN and 39 cm below the meniscus.*

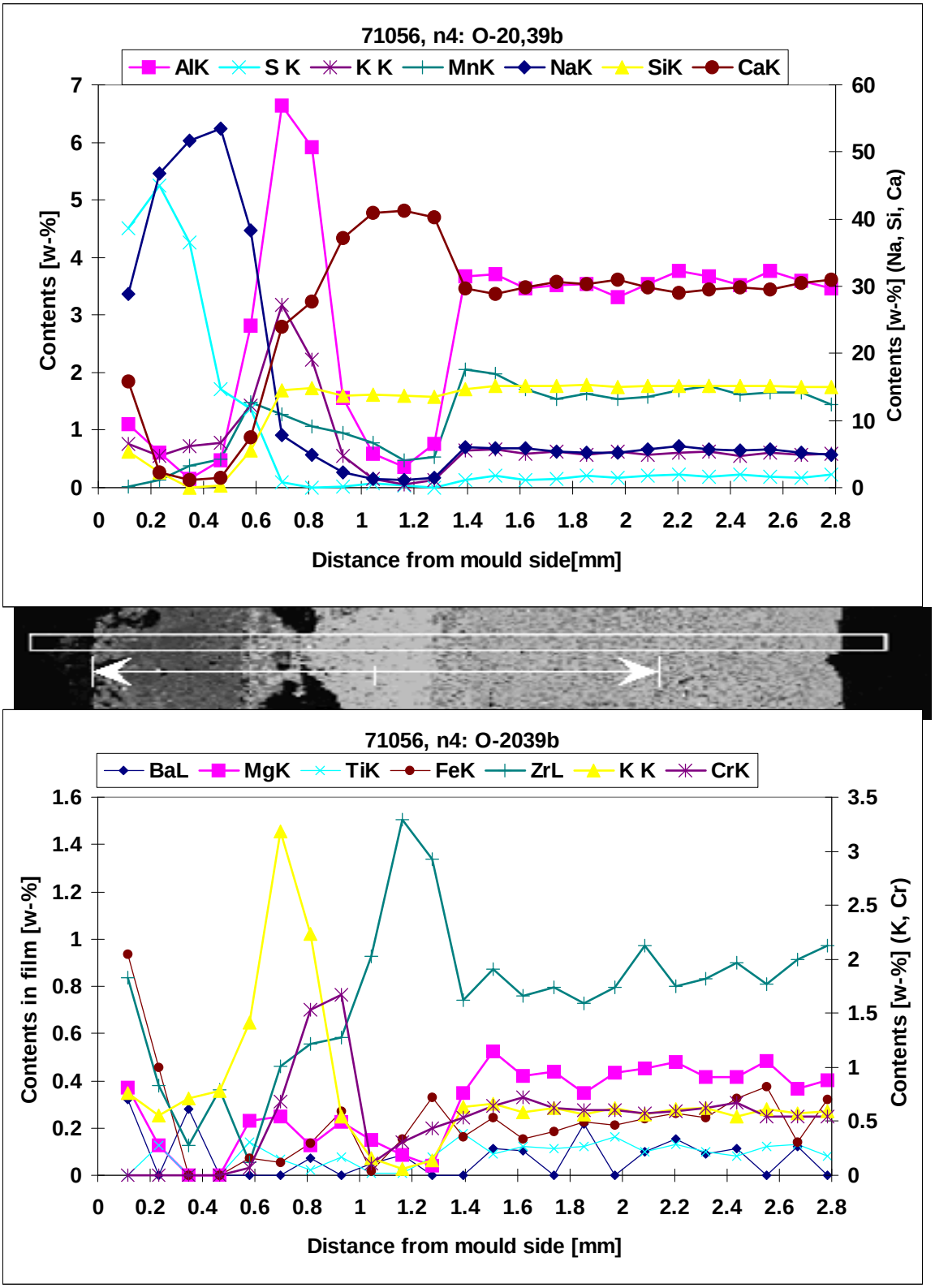

Figure 22. *The average concentrations of elements in different layers in the film shown in Figure 21 (Scheller et al. 1998, Hooli 2000(1), Spaccarotella et al. 2000).*

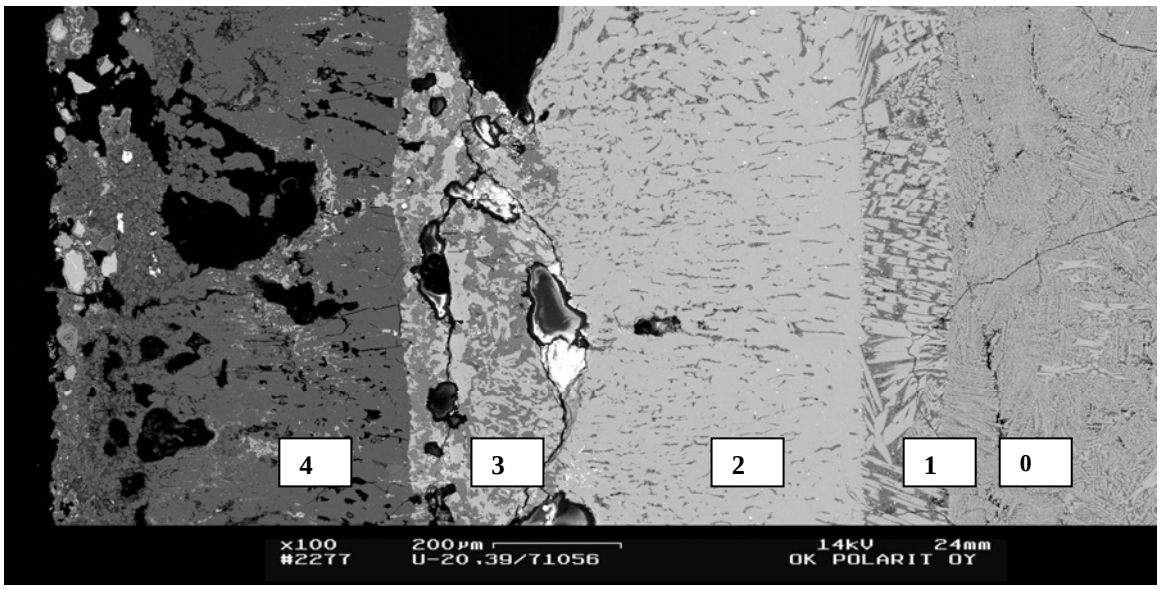

Figure 23. *The cross-section of a film 39 cm below the meniscus is shown (cast 71056). Areas are numbered from 0 to 4. Numbers refer to Tables 6-10 below.*

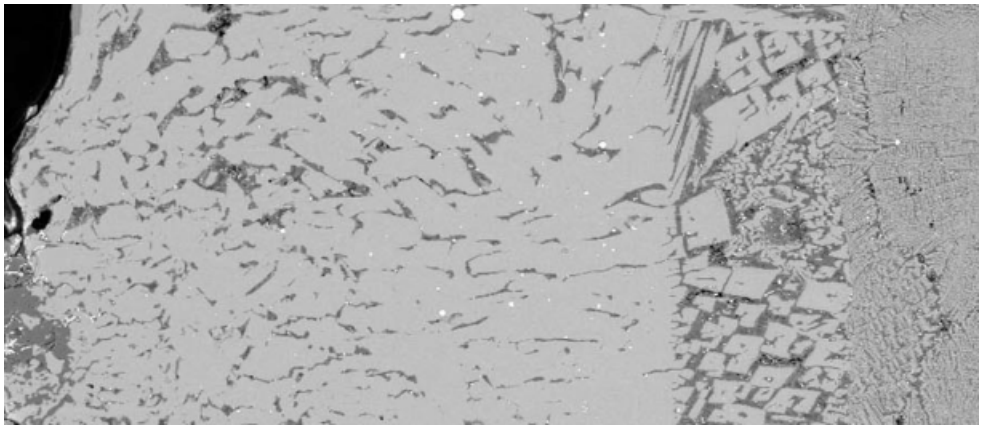

Figure 24. *Detail from Figure 23 (Areas 0, 1 and 2).*

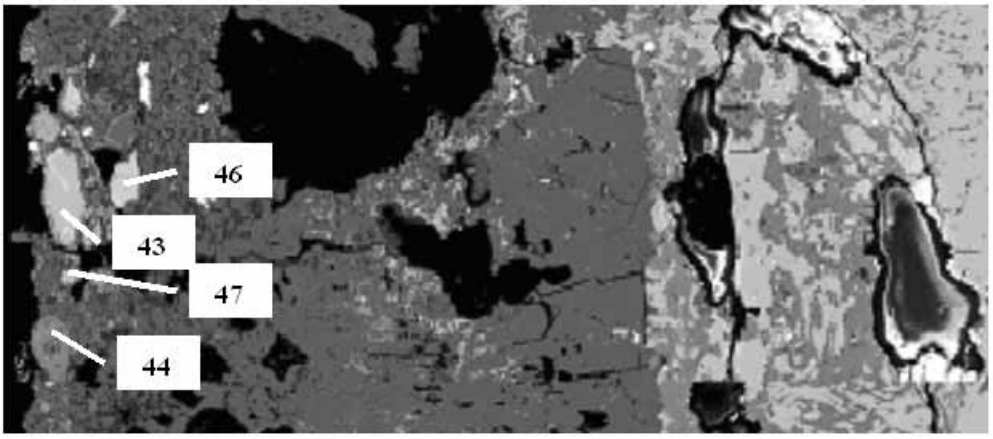

Figure 25. *Detail from figure 23 (areas 3 and 4).*

Concentrations of elements are shown in tables 6-10. Phases in different areas (see Figure 23) are numbered. The average concentrations of elements in different layers in the film are shown in Figure 22.

Different phases were analyzed with SEM/EDS analyzer, the results of which are presented in Tables 6-10 below.

Table 6. The concentrations of elements in area 0 (wt%).

Area 0	O	F	Na	Si	Ca	Mn	Fe	Zr	Ti	Mg	Al	K
Phase 01	30.1	10.0	1.6	15.1	41.6	0.6	0.1	1.0	0.1	0.2	0.9	0
Phase 02	40.6	2.7	7.5	16.7	21.3	2.1	0.0	0.7	0.1	0.8	7.2	0.4

In area 0, which formed during tail-out, several points were analyzed, but it was possible to find only two phases. The whitish phase resembled dendrite arms and was a cuspidine phase. The other phase was more complex and consisted of several compounds. Some notes: Na and F were usually in separate phases, whereas both phases contained Ca and Si. Phase 01 covered about 65% of the area. This layer was not present during casting, but formed during tail-out. The average content of Ca was approximately 30%.

Table 7. The concentrations of elements in area 1 (wt%).

Area 1	O	F	Na	Si	Ca	Mn	Fe	Zr	Ti	Mg	Al
Phase 11	29	9	0.3	15.2	44.4	0.4	0.4	1.5	0	0	0
Phase 12	29.6	9.3	0.3	15.3	44.4	0.2	0.1	1.2	0	0	0
Phase 13	34.2	1.7	11.2	17.6	3.2	6.6	0	0	0.1	1.4	9.2
Phase 14	31.6	3.7	8	17.5	3.5	7.6	0	0	0.3	1.8	6
Phase 15	27	6.5	20	12.7	0.6	3	0	0	0.3	0.9	9.7
Phase 16	11.4	26.5	28	8.3	1.5	3.1	0	0	0.2	0.4	4
Phase 17	6	44	45	3	0.5	1.7	0	0.1	0.5	0.1	0

In area 1, several phases were found. Phases 11 and 12 were composed of cuspidine, as was in area 0 phase 01. However, phase 02 was not at all found in area 1. The phase P17 was observed in a number of small areas, and its composition clearly corresponded to NaF. There were also phases that had low Ca concentration, but which contained several other oxides and fluorine.

In phase P13-16, the sum of the analyzed elements was only 80-86%, which means that some of the elements were missing. Nevertheless, these phases cover a very small proportion of the area. As is area 1, the average content of Ca was approximately 30%.

Table 8. The concentrations of elements in area 2 (wt%).

Area 2	O	F	Na	Si	Ca	Mn	Fe	Zr	Mg	Al	K	Cr
Phase 21	29.3	9.2	0.3	15.2	44.4	0.4	0.1	1.3	0.0	0.0	0.0	0.1
Phase 22	1.4	47.3	50.0	0.7	1.4	0.0	0.1	0.2	0.0	0.0	0.0	0.0
Phase 23	37-44	0-6	11-15	17-19	0.5-10	0-5	0.1	0	0-1	11-18	0-5	0-12
Phase 24	some small metallic droplets containing Fe, Cr											

Area/layer 2 is fully dominated by cuspidine, which had a share of over 90% of the total area. The remainder consisted of small areas of a nepheline phase with O, Si, Al, Na some K, and NaF. The average concentration of Ca, at approximately 40%, was clearly higher than in the areas 0 and 1.

The white spots in the areas 0, 1, and 2 (which are easier to detect in Figure 24), are Zr-oxides. There are clearly more these spots on the right side area of the cuspidine layer.

Table 9. The concentrations of elements in area 3 (wt%).

Area 3	O	F	Na	Si	Ca	Mn	Fe	Zr	Ti	Mg	Al	K
Phase 31	28	9.2	0.3	15	43.8	0.5	0	0.5	0	0	0	0.05
Phase 32	36	0	15	16.6	0.1	7.2	0	0	0	1.2	12.8	2
Phase 33	39	0	11	18.6	0.7	0	0	0	0	0	18.7	6.3
Phase 34	0.8	49.8	51.0	0.2	0.3	0	0	0	0	0	0	0
Phase 35	some CrMn oxides, and metallic droplets with Mn and Cr											

In area/layer 3, there were two main phases: a whitish cuspidine phase, and a darker, nepheline phase, which was especially evident in phase 33. Sodium and potassium are always present in naturally occurring nepheline in approximately the atomic ratio (3:1); (Na,K)AlSiO4 represents the true composition of nepheline (Wikipedia, Nepheline n.d.). There were also small areas of NaF. The average concentration of Ca decreased towards the mould side.

Table 10. The concentrations of elements in area 4 (wt%).

Area 4	O	F	Na	Si	Ca	Mn	Fe	Zr	Ti	Mg	Al	K
Phase 41	0	47.8	51.9	0.1	0.2	0	0	0	0	0	0	0
Phase 42	0	0	0	0.4	0.2	94.8	0.3	0	0	0	0	0
Phase 43	34.4	0	0	14	49.4	0.2	0.6	0.1	0.1	0.3	0.7	0.2
Phase 44	42.4	1.4	5.3	19.8	0.6	0	3.8	0.2	0.5	0.7	16.4	2.4
Phase 45	31.9	0	0	1.8	35.7	0.7	16.1	0.1	1.2	1.8	10.3	0
Phase 46	34.2	0	0.3	1.6	44.1	0	3.7	0	0.2	0.4	16.7	0.2
Phase 47	39.3	1.4	9.2	9.3	30.2	0	0.3	0.1	0.1	0	1.3	0.1

Area/layer 4 was dominated fully by the NaF phase, with only small islands of other phases. The locations of phases 43, 44, 46 and 47 are shown in Figure 25. Phase 45 resembled thin, white hair within phase 44. The largest islands were dicalcium silicates. Some islands, including phase 44, contained O,Na, Si,Al and K (nepheline type, similar to P33 in area 3), and others, including phase 46, contained calcium aluminate. One small island contained only Mn. This area contained a lot of voids.

3.6 Flux film with Ti stabilized steel

In flux films from Ti stabilised steel grades, it is possible to observe the same basic principles as with standard grades, both in appearance (see Figure 26) and in the concentration of elements (Figure 27). The main difference is the occurrence of a calcium titanate phase.

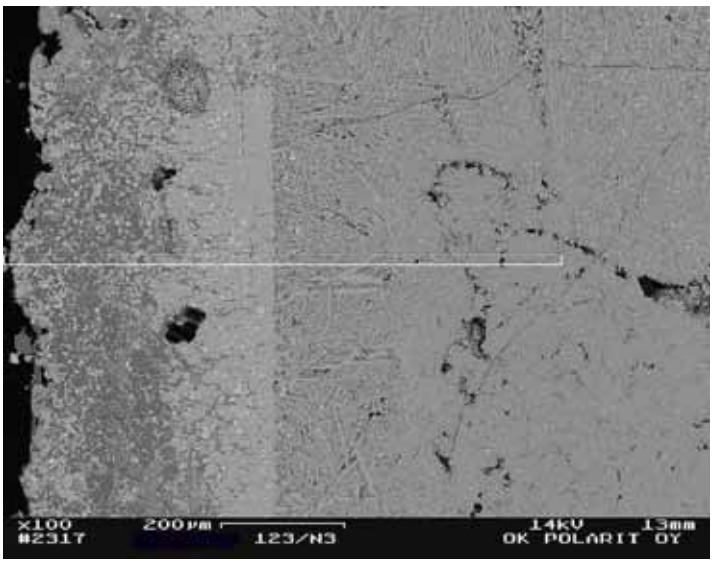

Figure 26. *Example of cross-section of slag film with Ti stabilized steel grade as an overview. The mould side is on the left. The layer with the dendritic structure formed during tail-out.*

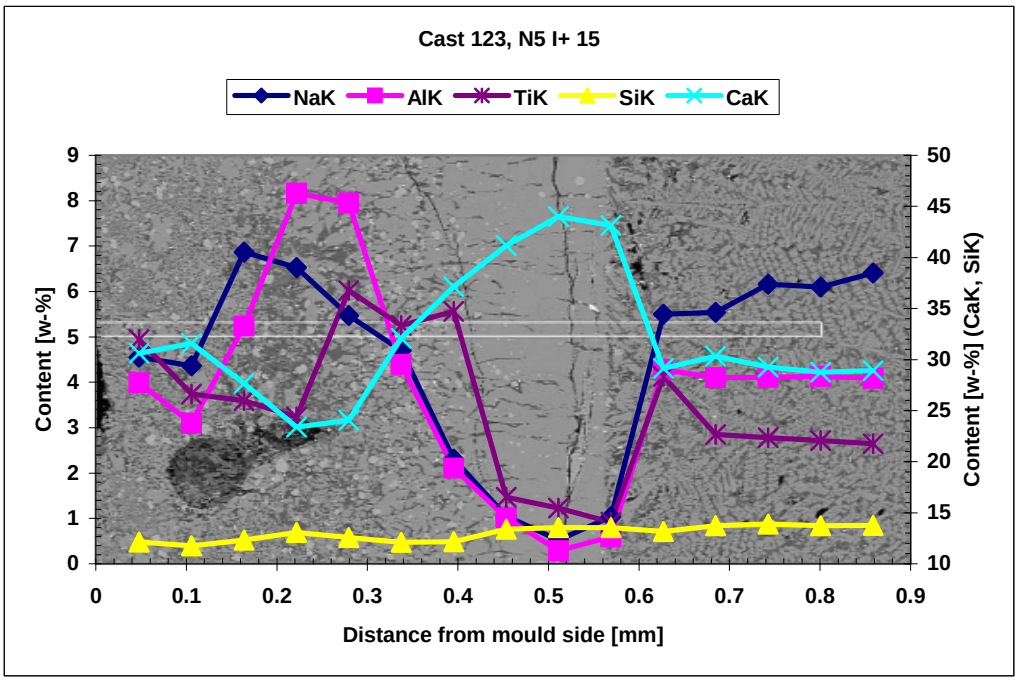

Figure 27*. A layer in the film from Ti alloyed steel grade. Concentrations of elements are drawn on the layer. The mould side is on the left. The layer with the dendritic structure formed during tail-out (only part of that layer is in this Figure). Powder A.*

The whitish coloured layer with a high Ca concentration indicated the presence of a cuspidine phase. The slag layer with a dendritic structure on the right hand side was formed during tail-out. The solidification rate has been the correct one for dendritic growth. On the mould side of the cuspidine layer, there was a layer with a high concentration of Al, which was also fairly typical. In those compositions of points, where Al concentration has the highest value, K also has its highest value (not shown in Figure) and the Na/K ratio is 4.3 and 3.4.

The most significant differences when compared with steel grades without Ti alloying were the presence of small whitish spots (Figures 26-29). The concentrations of elements in different phases shown in Figure 28 are presented in Table 11 and in Figure 29 in Table 12.

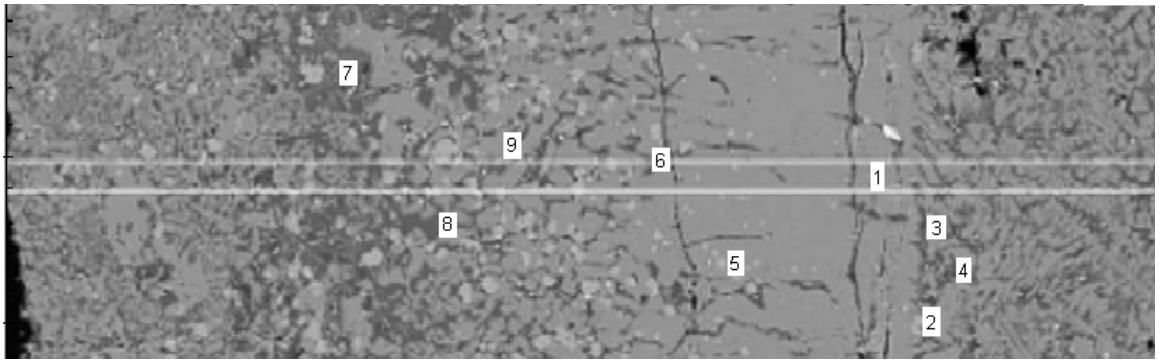

Figure 28. *The flux film from the cast of Ti stabilized steel. Concentrations of elements in the numbered spots are shown in Table 11. Distance from the meniscus was 15cm on the inner bow side on the wide face. Points 2, 3 and 4 are in the layer formed during tail-out. Numbers are to the right of analyzed spots (Powder A). Distance from the left hand side of the film to the point 2 is 0.6 mm.*

Table 11. Concentrations of the elements in the points in Figure 28 (wt%).

Point No	O	F	Na	Si	Ca	Ti	Al	Mg	K	Mn
1	28	10	0.1	15	45	0.3	-	-	-	-
9	28	9	0.2	15	45	-	-	-	-	0.1
5	32	0.6	0.7	2	30	31	1	-	-	-
2	32	0.5	0.6	1	29	32	0.8	-	-	0.2
4	2	40	42	2	1.5	0.2	0.8	-	0.1	0.1
3	26	3	11	13	1	1	13	0.6	0.6	0.7
6	34	-	13	14	0.5	1	18	0.5	0.7	0.5
7	32	4	8	14	17	0.8	13	0.2	0.7	1.6
8	39	-	11	17	2.5	0.1	19	-	4	-

The film shown in Figure 28 has been cast with the standard powder for Ti stabilized steel grades (Powder A).

The dominating phase was cuspidine (points 1 and 9). In point 4 there is clearly a NaF phase. A “dark” phase (point 8) containing O, Si, Al, Na and K was clearly nepheline (Na/K is approximately 3). The composition of points 3, 6 and 7 suggest a nepheline base phase. The presence of nepheline is also a common feature of standard grade films. The whitish spots are a calcium titanate phase ($CaTiO_3$); analyses revealed that all the Ti in these layers was in this form. Other phases did not, therefore, contain any Ti, as shown in Table 11.

Titanium was found only in points 2 and 5, where the content was around 32%. It seems likely that the Ti in the steel forms calcium titanate after reacting with the liquid flux either on the steel surface in the mould or in the gap between the shell and the mould. In contrast, the remaining slag components behave in a similar way to those of other steel grades.

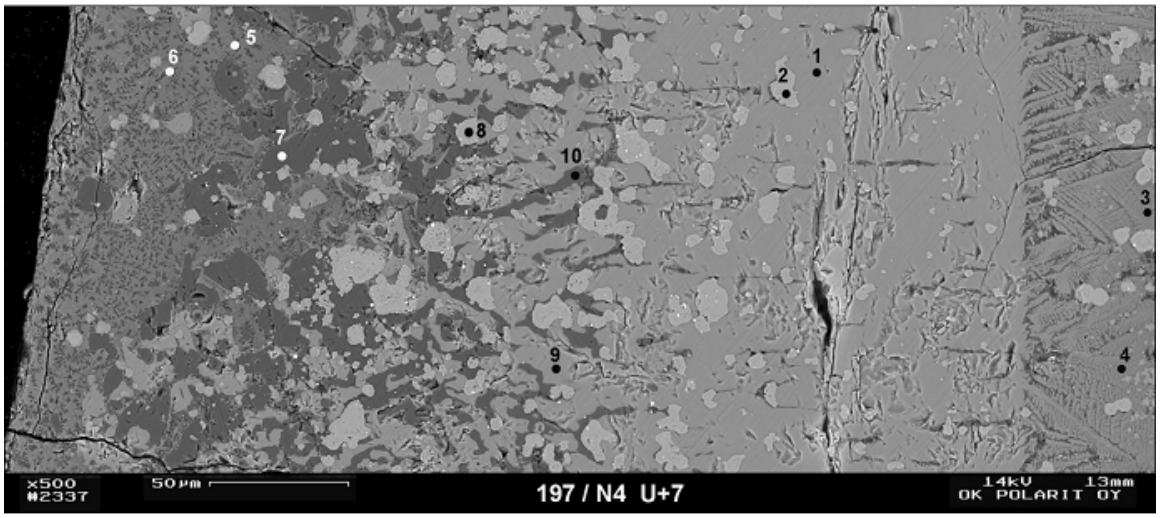

Figure 29. *The flux film from the cast of Ti stabilized steel. Concentrations of elements in the numbered spots are shown in Table 12. Distance from the meniscus was 7 cm on the outer bow side on the wide face. Points 3 and 4 are in the layer formed during tail-out. (Powder C).*

Table 12. Concentrations of the elements in the points in Figure 29 (wt%).

Point No	O	F	Na	Si	Ca	Ti	Al	Mg	K	Mn
1	29	10	0.2	15	45	0.3	0.1	0.1	-	0.1
9	28	10	0.3	15	44	0.3	0.2	-	-	-
8	32	0.3	1	2	30	32	0.5	-	-	0.2
2	31	0.4	1	2	29	32	0.5	-	-	0.2
4	29	9	3	14	35	2	3	0.2	0.7	0.4
3	30	8	4	15	31	1	4	0.4	1.3	0.5
5	33	7	5	16	23	2	5	1.4	1	1.9
6	8	27	27	7	9	1	2	0.7	0.7	1.2
7	40	0	12	19	0.4	0.1	18	0.2	4.2	0.1
10	40	0	12	19	0.5	0.2	19	-	4.1	-

The dominating phase here was also cuspidine (points 1 and 9). Concentrations of elements in points 3-5 were similar for cuspidine, except for the Ca content, which was lower than in cuspidine. In point 6, there was an indication of NaF (but maybe back scattering from the surroundings of a small spot has excited other elements too, same concerning also points 3, 4 and 5). A phase at points 7 and 10 containing O, Si, Al, Na and K, had a large share of the mould side of the cuspidine layer, but did not reach the mould wall. This phase was clearly nepheline. The whitish spots here were also a calcium titanate phase ($CaTiO_3$).

The phases from powders A and C were very similar.

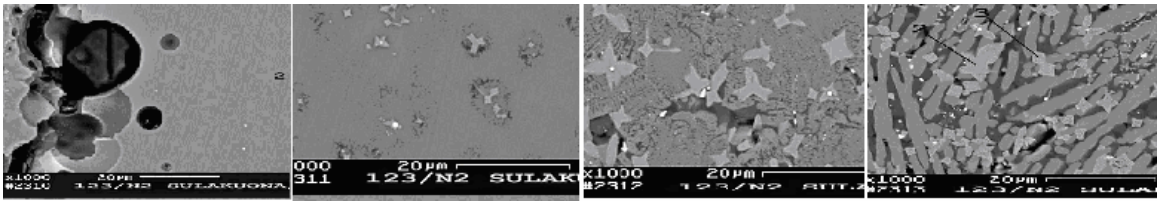

Figure 30 (a-d). *Structures formed when liquid slag was poured onto the surface of the steel plate (Cast 123).*

To compare structures on the films, liquid slag from the mould at the end of casting was poured onto the surface of the steel plate. The total thickness of the layer was about 5.5mm. The cooling rate therefore decreased from left to right. The area shown in Figure 30 a) covers the distance between 0 - 0.06mm from the surface of the steel plate. The distances of b), c) and d) from the surface of the steel plate are 0.7, 2.4 and 5 mm respectively. In the area shown in Figure 30 a), the structure was glassy and the composition of the two points is shown in Table 13. These represent the average composition of the slag at the end of casting. The concentration of Ti was about 5.5%. It is worth noting that concentrations of Mn, Cr, S and K were higher than in the original powder.

Table 13. Concentrations of elements in Figure 30 a) (wt%).

	O	F	Na	Mg	Al	Si	S	K	Ca	Ti	Cr	Mn	Fe
1	28.30	7.32	5.62	0.38	4.35	11.91	0.29	0.41	29.15	5.54	0.45	0.67	0.19
2	28.99	7.40	5.37	0.41	4.37	12.03	0.24	0.43	28.82	5.57	0.27	0.81	0.01

In Figure 30b), the star-shaped areas were probably calcium titanate, but the base matrix still contained approximately 6% Ti. In Figure 30c), there were several larger calcium titanate areas, but other phases were not clearly crystallized. In Figure 30d), there were long cuspidine crystals in addition to calcium titanate, and the darker areas between these contained a nepheline-type phase; segregation therefore took place. Solidification must only have taken minutes.

With the exception of NaF, the same phases as those in the films were also found in the layer of the slag poured onto the steel plate. However, the structure of these phases was different. Calcium titanate compound does not already exist in the liquid slag in the mould, as can be concluded from the fact that in Figure 30 a), there were no crystals of any phase. The calcium titanate was, nevertheless, the compound that crystallized first i.e. with the highest cooling rate.

In summary:

- cuspidine dominates in the layer on the shell side
- on the mould side of the cuspidine layer, there are phases of cuspidine and nepheline
- next to the mould side, NaF is the main phase
- calcium titanate is found in all layers as spots

The presence of titanium in the steel, at a concentration of approximately 0.4%, causes changes in the composition of the flux slag on the steel surface in the mould. Ti reacts with slag and reduces some oxides from the slag, including Si- and Mn-oxides, which results in Ti-containing oxides in the slag. This is also reflected in the slag film. Ti caused a decrease in Si content (with approximately 3% units) and in Mn content (with approximately 1.5% units), as shown in Figure 31. At the start of casting, changes in concentration were small (Figure 32), and this fact could be used when analyzing the film layers.

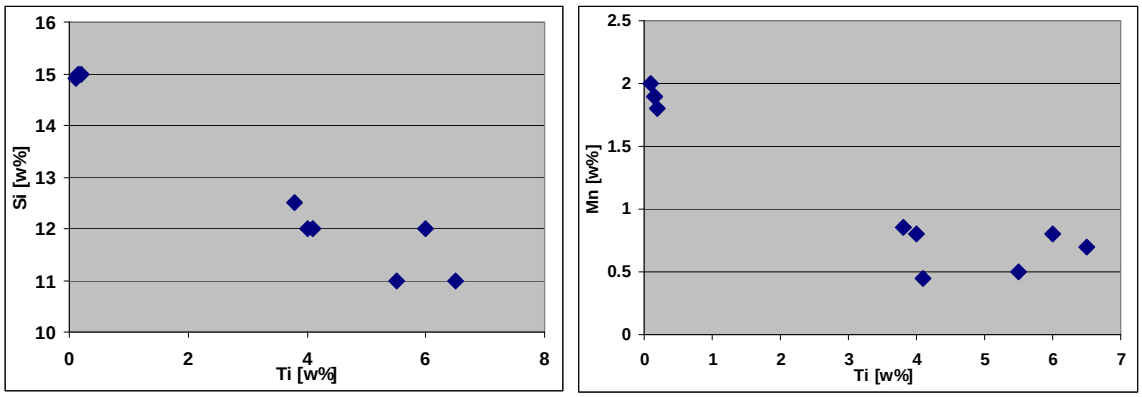

Figure 31 (a-b). *Ti content versus Si and Mn contents in the layer of films formed during the tail-out. Points where Ti content is nearly zero are from casts without Ti alloying.*

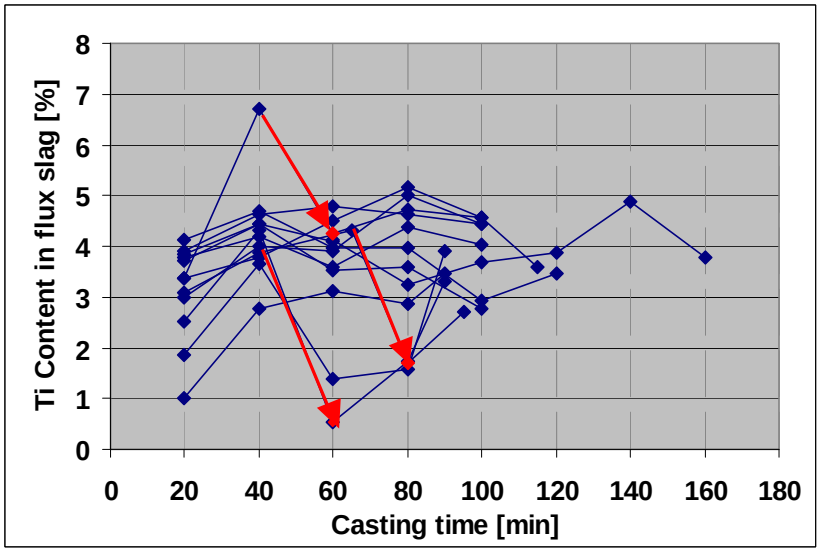

Figure 32. *Casting time and Ti concentrations in mould slags from Ti stabilized casts (Jokisaari 2000).*

The Ti concentration in the slag reached saturation level after 40 minutes of casting, but did not reach these concentrations after 20 minutes casting in any of the samples. As shown in Figure 32, in all samples, Ti content increased between 20 and 40 minutes. In the early stages of casting, Ti concentration is probably lower, but as the amount of liquid slag in the mould is small, concentrations can increase quite rapidly. Consequently, in the film layers formed at the beginning of casting, Ti concentrations may be smaller. Partition between different phases and apparent fractures in film layers must both be taken into account. Especially with Ti alloyed steel grades frequently occurred sticking cases indicated fractures in film layers.

After approximately 20 minutes of casting time, the consumption of casting powder decreased to very low levels. This means either a thin lubricating layer, or that the lubricating liquid layer is moving slowly, because of its high viscosity. Calcium titanate has a high melting point, which means that it can also behave like solid particles in the liquid slag.

Figure 32 shows four cases where Ti content has dropped approximately 3% units between samples, and, simultaneously, Si concentration (SiO_2) has clearly increased towards virtually the original concentration of the powder. In three of these cases (indicated with arrows), a sticking defect was found on the slab cast between sampling periods. Sticking-related phenomena triggered a brief increase in powder consumption in the cap between the shell and the mould; fresh powder melted onto the steel surface in the mould, and the Si content increased. The liquid flux may have been thin and viscous and thus badly lubricating, which led to a breakdown in the solid film, which in turn increased powder consumption momentarily. Other effects typical for Ti alloyed steel grades include rapid decreases in heat flux, especially after the beginning of casting, and rapid increases.

3.7 Flux film with sodium free powder

Due to the discovery of the special role played by sodium in the layer next to the mould, it was decided to test a sodium-free powder. Sodium, together with its compounds, has a significant influence on the properties of casting powder. Although the sodium-free powder was chosen so that its "indices" were in the right ranges, the powder's functioning was very different from that of a normal powder, and therefore its use had to be limited to the finishing periods of casting.

Table 14. Composition and some properties of the Na-free powder (D), with powder B as a reference (wt%).

	Powder B	**Powder D**
Basicity	1.14	1.17
Al_2O_3	6.4 %	2.5 %
SiO_2	31.0 %	41.0 %
CaO	34.5 %	44.1 %
Na_2O	8.0 %	**< 0.1 %**
MnO	< 0.1 %	< 0.1 %
MgO	0.7 %	4.8 %
F	7 %	8.4 %
C_{free}	2.4 %	0.4 %
Viscosity, dPa∗s, 1300 °C	1.3	2.2
Melting point (°C)	1100	1270

Viscosity and melting points of Na-free powder were higher (Table 14) than those of the standard powder. SiO_2, CaO and MgO concentrations were higher, but Al_2O_3 concentration was lower.

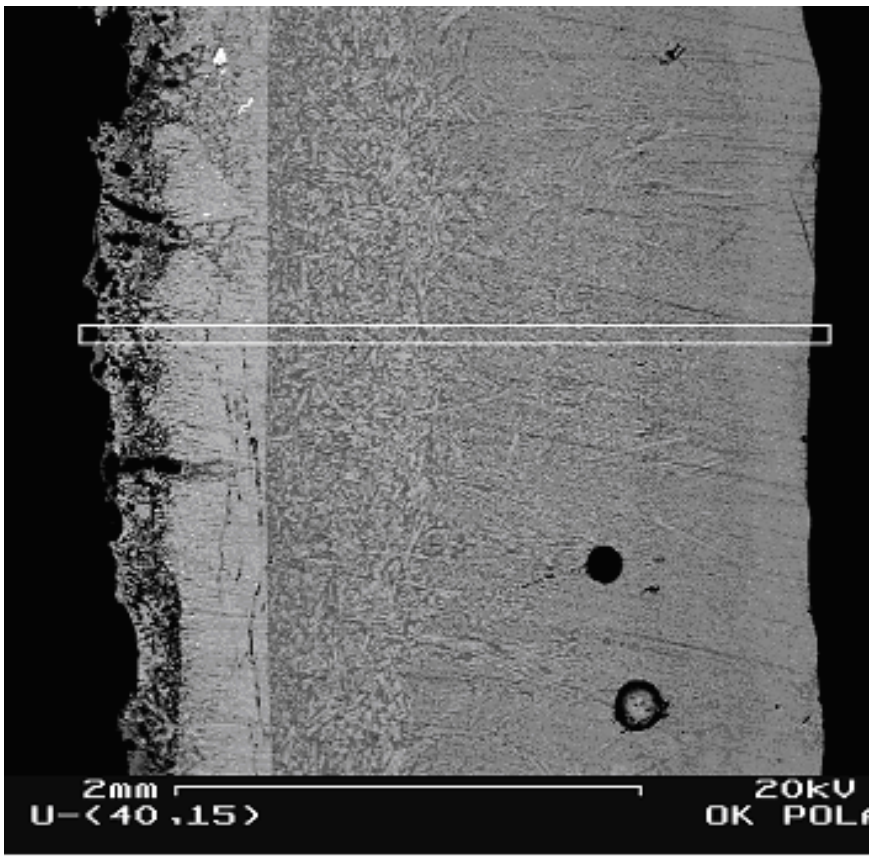

Figure 33. *Film from cast 90586, 15cm below the meniscus. Na-free powder was used for half of the casting time (50 minutes). The mould side is on the left.*

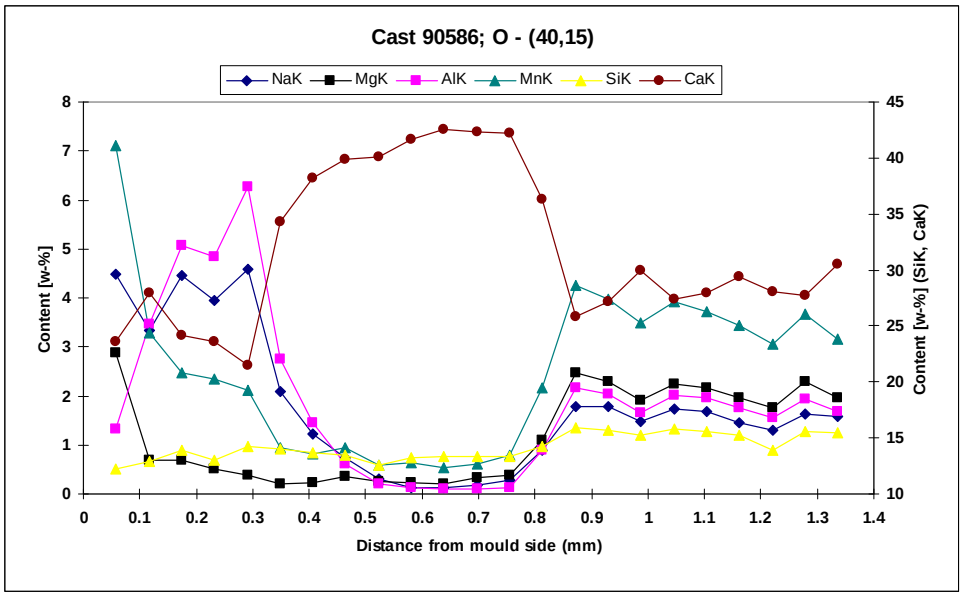

Figure 34. *Concentrations of elements in the film shown in Fig. 33. Analyses were made along the line indicated, up to the distance of 1.33 mm from the mould side.*

Sodium-free powder was used during the last 50 minutes in cast 90586. A picture of the film layer 15cm below the meniscus is shown in Figure 33, and the elemental composition is

shown in Figure 34. The vertically oriented whitish area has a high Ca content (cuspidine). On the mould side of this, there is a fairly typical layer containing a higher Al content.

The following can be stated concerning the behaviour of certain elements:

- flux slag at the end of casting (tail-out slag) was a mixture of powders B and D, indicating that powder B has a long residence time in the mould
- On the mould side of the high Ca layer, Na content was 4%
- Mg content in tail-out slag was 2%, except for the mould side, where, except for one point, it was below 1%
- Al content in tail-out slag was 2 %, but on the mould side it was up to 5%

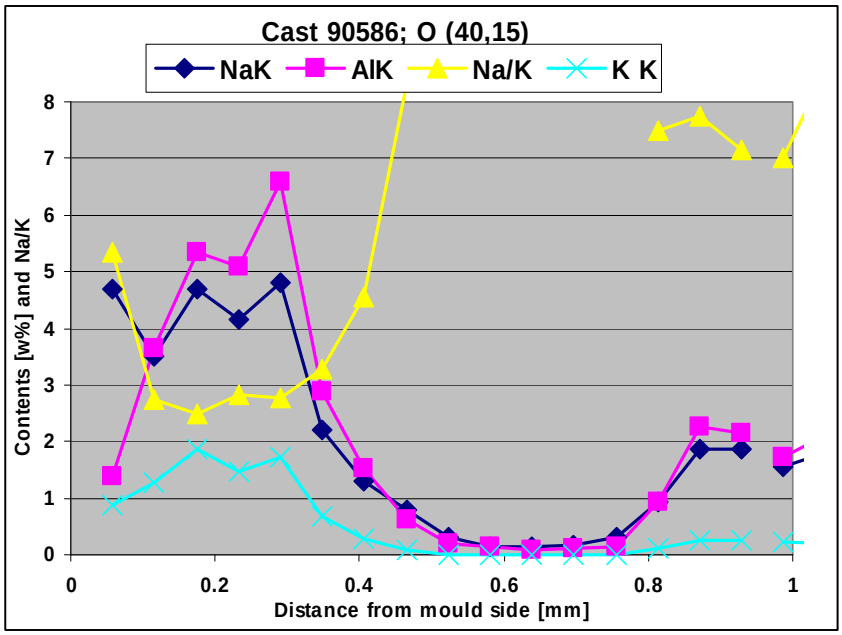

Figure 35. *Concentrations of Na, Al and K and Na/K ratio (the film is shown in Figure 33).*

In nepheline-type phases the typical Na/K relation is approximately 3. This could be used to predict the presence of nepheline. Figure 35 shows the Na/K relation together with Na, K and Al concentrations. As shown the Na/K relation was very near 3 in the area between 0.15 and 0.3mm, and at the same time, the Al and K concentrations were high. This indicates the presence of nepheline. Near the mould side, Al and K concentrations were decreasing and Na/K increasing, but Na concentrations remained the same. This indicates that a larger proportion of Na was in the form of NaF.

High Na and Al concentration and low Mg concentration in the layer on the mould side left from the high Ca layer indicates that this layer formed during the casting of the first heat in this sequence casting. The effect of powder D was a decrease in heat transfer after the powder change. The difference was approximately 10%. Another effect was that oscillation marks were shallower. The proportion of deep oscillation marks (over 0.22mm) was approximately 1-2% of all marks compared with the standard powder, for which the figure was approximately 3-4%. The surfaces also appeared to be very smooth.

3.8 Film remaining adhered to the mould walls

After the end of casting and sampling of the "main" slag film, a "white" layer of film remained on the mould, as shown in Figure 34. This flamed when water was sprayed onto it, but if excess water was used in tail-out to cool the tail of the last slab, it vanished. On the broad faces, this layer almost reached the exit of the mould and on the narrow faces it reached to 20-30cm below the meniscus. This layer therefore extended further below the meniscus than the sampled "main" layers. Samples from this layer were loosened for analysis. The layer varied in thickness from 0.16 to 0.33mm, with an average of 0.25mm.

After oxidizing this layer with flame, it no longer reacted with water, which might indicate that oxidation of Na and K occurred. The example of Figure 22 show that the K content had a strong tendency to rise on the mould side of the cuspidine layer, from level 0.5% up to 2-3%. Melting points of metallic Na and K are low, at 98°C and 64°C, respectively. If formed in the high temperature zone by reduction/vaporization, the vapour must have found its way outwards, then condensed to liquid, which could then flow or trickle onto the mould wall.

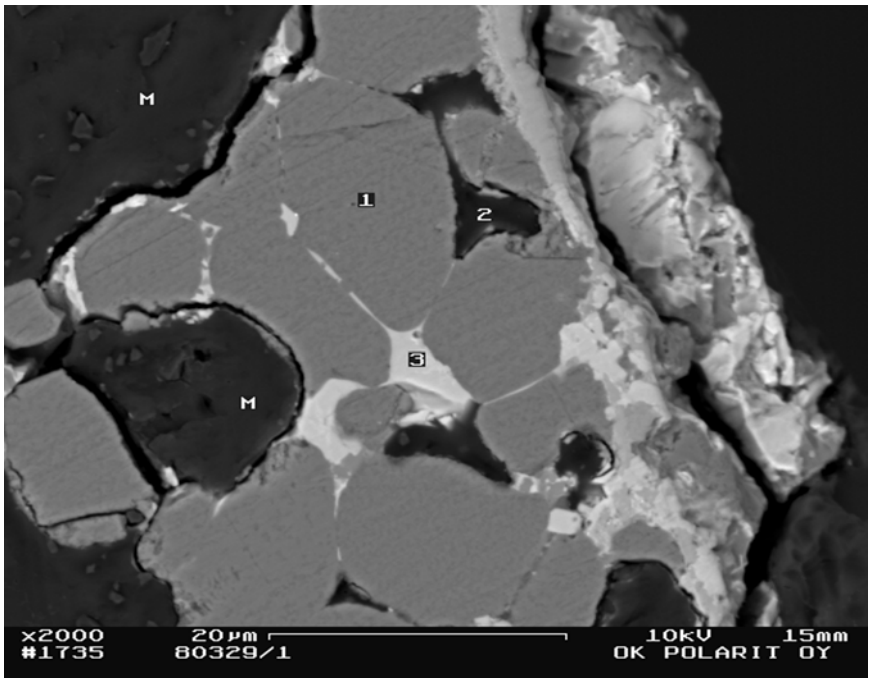

Figure 36. *A piece of the "white" layer film against the mould. (sample No. 80329/1)*

In the "white" film, two phases were found, as shown in Figure 36. The concentrations of elements are shown in Table 15 ("phases" M and 2 are plastic).

Table 15. Concentrations of elements in different areas in Figure 36 (wt%).

Area No	O	F	Na	Si	Ca	Mn	Fe	Ba	C	Cr	Al	K
1		48	52	0.2								
3	33	13	4	13	30	0.9	0.7	2	3	0.6	0.6	0.9

The film contained two phases: NaF and a complex phase containing several elements, including carbon (somewhat similar to cuspidine). In samples of this film from certain casts, carbon was analyzed separately, and C content was found to vary from 2.6% to 3.9%. Carbon could react with Na and K compounds and as a result produce Na and K. This "white" layer appeared to be a part of the NaF rich layer found in some of the films, but remained adhered to the mould wall.

3.9 Thermodynamic calculations

There are special problems concerning thermodynamic calculations. In certain steps in the formation of the layers in the film, macro segregation and separation of the phases takes place. This should be included in thermodynamic calculations; otherwise such calculations will be impossible. A thermodynamic study of mould flux used as slag in the continuous casting of stainless steel was carried out using the software program HSC (Karlemo 1997). A special emphasis was placed on investigating the behaviour of sodium in the slag.

The conclusions of the work were as follows:

- At temperatures under 500°C, sodium carbonate is the dominating phase of sodium. At temperatures between 500 and 1300°C, sodium fluoride and different sodium silicates are stable. When the temperature rises above 1300°C, the sodium silicates start to decompose and sodium gas and sodium fluoride gas begins to form.
- At high temperatures (over 1300°C), the thermodynamic conditions favour the formation of sodium gas, and sodium fluoride gas begins to form. The steep temperature gradient in the solidifying slag makes it possible for these components to nucleate in the slag. In lower temperatures, the formation of sodium from sodium oxide needs reducing conditions, which can be developed locally by segregation of coke in the mould flux.
- Water vapour from the secondary cooling, without the presence of coke, does not favour the formation of sodium from sodium oxides.
- The temperature of the slag can rise to over 1300°C only in the mould or in the gap very near the meniscus, where the formation of sodium or sodium fluoride gas formation can take place without carbon.

A thermodynamic study was carried out also using the program FactSage (by Nurmi, 2006). Calculations gave the following results:

- CaF_2 was solidified at 1418°C
- $Ca_3Si_2O_7$, rankinite, started to freeze at 1158°C
- $CaSiO_3$, wollastonite, started to freeze at 1100°C
- $Ca_2Al_2SiO_7$, gehlenite, started to freeze at 870°C
- $Na_2CaSi_3O_9$ started to freeze at 970°C and the amount increased sharply at 870°C
- there was no further liquid phase below 850°C

The first two compounds together contained the same elements as cuspidine. Unfortunately, the software did not contain the phase cuspidine, but based on the formation of the first two phases, formation of a cuspidine type phase is most reasonable at the highest temperature. From the first solid compound to the last, the temperature difference was about 590°C, so the mushy zone was very wide.

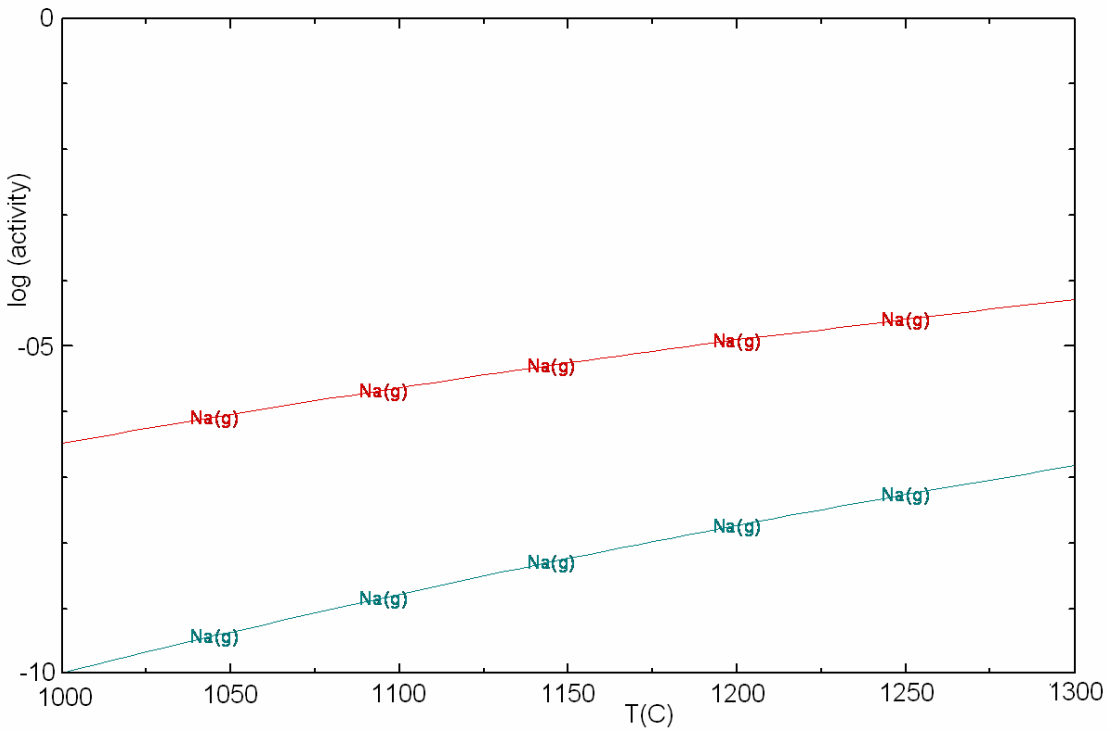

Figure 37. *Activity of Na gas in vapour as a function of temperature. Slag composition used in calculation was as follows: SiO_2 37%, CaO 28%, Al_2O_3 7.5%, Na_2O 9.5%, CaF_2 18%. Lower curve is for carbon-free slag and upper curve for slag with 2.8 % carbon. Calculation was made with FactSage programme (Nurmi 2006).*

Considering formation of sodium vapour a calculation was performed for a slag shown in the caption of Figure 37 above. The results show relatively high Na vapour pressures, especially at high temperatures (over 1200ºC), and in the presence of carbon. This confirms the mechanism of the formation of Na rich layers on the mould wall discussed previously and later.

3.10 Some observations and discussion on phases in slag layers

This discussion principally concerns the results shown in Figures 23-35 and tables 6-12.

Layer 0 was formed during tail-out and contained the average content of the casting powder flux, which had been in the mould at the end of the casting. Two phases were found: cuspidine, and another phase containing several elements. Because of its finer structure, this layer had solidified and cooled faster than layer 1. A phase 02 was found in area 0, but not in any other areas.

Cuspidine was dominant in area 1, with a proportion of approximately 60% of the area. The layer where area 1 was located was eventually part of the lubricating layer during casting. Based on the trials of Kashiwaya et al. (1998), the block faceted crystals indicate that the cooling rate was low in this area. This confirms the assumption that area/layer 1 has its own history of formation, compared with the areas 0 or 2, and that it was probably the lubricating layer during casting. In fact, inside this layer, the cooling rate was 0.

In area 2 (Figure 23), cuspidine was the dominating phase, as in area 1, although it now covered approximately 90% of the whole area. Between cuspidine crystals, there were phases with low Ca content and some small NaF islands. So the proportion of phases other than

cuspidine had decreased dramatically. The other phases appeared to have moved towards the mould, possibly with the aid of some kind of pumping effect caused by mould oscillation. In all layers of the film, there were small amounts of tiny metal droplets and Cr and Mn oxides among the slag phases. The cuspidine layer had a reasonably sharp boundary against area 1, with cuspidine "fingers" reaching in. There were thus certain common features in these areas.

Between the Ca and Na rich layers, area 3 contained a lot of voids or pores, indicating gas formation or eventual shrinking cavities. Cuspidine was also found in this layer, but it was no longer a dominating phase. Another major phase contained Al, Na, Si and K (F=0, Ca=0), making it a nepheline-type phase. There were some rests of nepheline type phase in the area 2, which confirms that phases in area 3 originated from area 2. NaF was also found.

Layer 4 nearest to the mould side contained a lot of voids. The dominating phase was NaF. On the mould side of this layer, there were islands of different phases, including phases containing Ca, Si, Al and O. The largest islands were dicalcium silicates. The dicalcium silicate phase was probably the first solid phase nucleating from the liquid slag, but this disappeared after the formation of cuspidine. It is interesting to note that there were no cuspidine islands.

Areas 0, 1 and 2 contained Zr-oxide spots. In this case, most of the Zr came from the doped powder, but some came from the ZrO_2 sleeve mounted in the SEN, which had been dissolved by the liquid powder flux in the mould. In Ti stabilized grades, the features in the film were similar to that of standard grades, except for the presence of calcium titanate.

When sodium-free powder was used, the slag in the mould still contained nearly 2% Na at the end of the casting, which means that there was in fact no casting with truly sodium-free flux. In these trials, the typical features of the films were also similar to those of films from casts made with the standard powder.

3.11 Trials with tracers

The first results concerning the composition of elements in the flux film were highly unexpected, and therefore interesting. It was soon found, however, that the entire sampled film was not formed during the steady state casting, but during tail-out. Tracers were used to study which layers in the film were formed during tail-out, and to study the residence times of the layers in the film formed during casting.

Figure 38 shows an example of the results of tests with tracers. Near the meniscus (0-80mm), Zr was found through all the films, which indicates that there was no such layer in those films that had been there during the last 30 minutes of casting. If there was such a layer, it had remained adhered to the mould wall. Further away from the meniscus, Zr was not found in the layer on the mould side. This "permanent" layer (solid during casting) increased in thickness as it went downwards. With the present sampling technique, the maximum distance where a layer could be found on the mould wall was 40cm. Below, it is possible that the layer might have fractured into pieces. However, the "white layer" still covered the surface of the mould almost down to the mould exit.

The width of the thin layer next to the Ca rich layer on the shell side (see Figure 24, area 1) varied between 0.05 – 0.15mm. In the film shown in Figure 17 (case 38cm), the thin layer was located at a distance of 1.7 - 1.8mm from the mould side. In Figure 39, the location of this thin layer was between the points where Ba concentration changed from 0 to 0.9 %, when

BaO doped powder was used during the last 15min. This might indicate that this layer had been partially liquid (mushy) during casting, with more solid on the mould side and more liquid on the shell side. The solidified structure in this layer was different to that of the next layers.

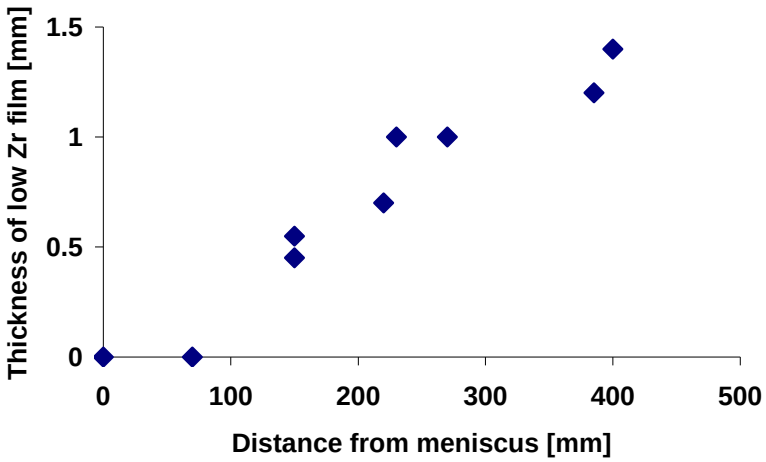

Figure 38. *Thickness of film with low Zr content in a trial where ZrO_2-containing tracer powder was used during the last 30 min (Hooli 2002(3)).*

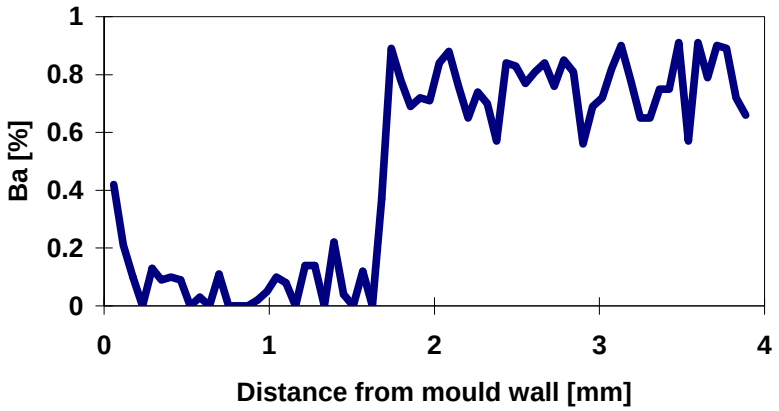

Figure 39. *Ba content in the cross-section of the slag layer at 38cm level below the meniscus (Hooli 2002(2), Hooli 2002(3)).*

These results are in good agreement with those of Ogibayashi et al. (1987).

3.12 Minor elements in the main phases

There was a tendency for those compounds of minor elements (impurities in powder, from steel or refractories, or added as tracer) to be distributed unevenly in the main phases. The main phases were for example cuspidine or nepheline, and minor elements were in this case Mg, Mn, Zr, S, K and Ti. Data used here were from the layer film shown in Figure 23.

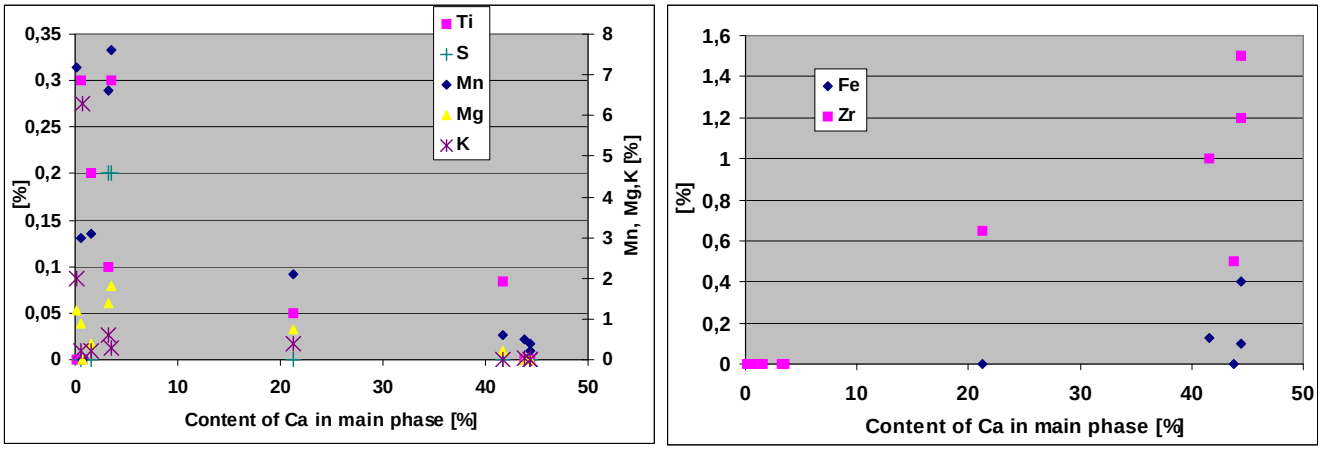

Figure 40. *Concentrations of minor elements vs. Ca content in the main phases. Main phases (such as cuspidine) are "indicated" as based on Ca content of the phase.*

Figure 40 shows concentrations of minor elements against Ca concentration in the main phases (NaF phase was excluded). Ca was used to represent the type of main phase studied. If Ca-concentration in the main phase was over 40%, only Zr and Fe favoured that phase. Other minor elements were higher in phases containing no Ca. The phase with approximately 21% Ca contained minor elements with moderate concentrations (this main phase was present only in area 0). As Zr was used as a tracer, the phenomenon above makes it more difficult to read information from Zr concentrations. Phases containing no Ca contained no Zr either. Unfortunately, barium, which was also used as a tracer in this case, was not included in these field analyses. Concentrations of minor elements can give a hint as to the phase or compound concerned. For example, potassium (K) concentrations of over 2% probably indicate the presence of nepheline.

3.13 Fracturing off

In several layers, it was possible to observe features, which indicated fractures in layers during casting. When cases of sticking are considered, fractures in the film might represent a starting event. Appendix 2 presents a series of flux films showing apparent fracturing. In some of the films, whitish pieces of cuspidine are separated from each other, i.e., the cuspidine layer is not continuous.

The temperatures of thermocouples with Ti-stabilized steel grade had different behaviour from those of un-Ti stabilized grades. Temperatures had a strong tendency to decrease during casting, but they specialised in "jumps" following a certain period of decreasing. This behaviour is shown in Figure 41. One such "jump" is observed at 20000mm due to increased casting speed. The temperatures of the thermocouples "x,50 " are on a lower level than the temperatures of "x,35". This is because they were located at a distance of only 30mm from the mould corner.

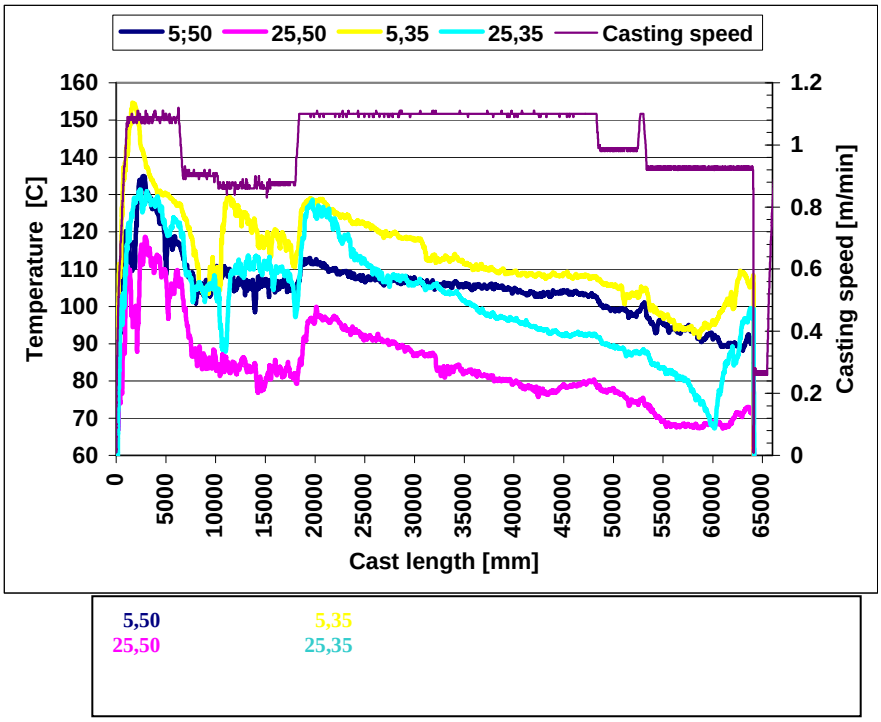

Figure 41. *Cast length and temperatures of thermocouples and casting speed (cast 189, AISI 316Ti, mould width 1050mm). The thermocouple locations are indicated as follows: 5,50 = 5 cm below meniscus, and 50cm from the middle of the wide face. In the lower part of the figure, the thermocouple locations are depicted schematically.*

The temperatures of the thermocouples ”5,35” and “25,35” had a ”jump” about 5m before the end of casting. This indicates sudden increase in the heat flux (see Figure 41). An example of slag film taken from the area of the thermocouples “5,35” and “25,35” is shown in Figure 42 together with the contents of some elements.

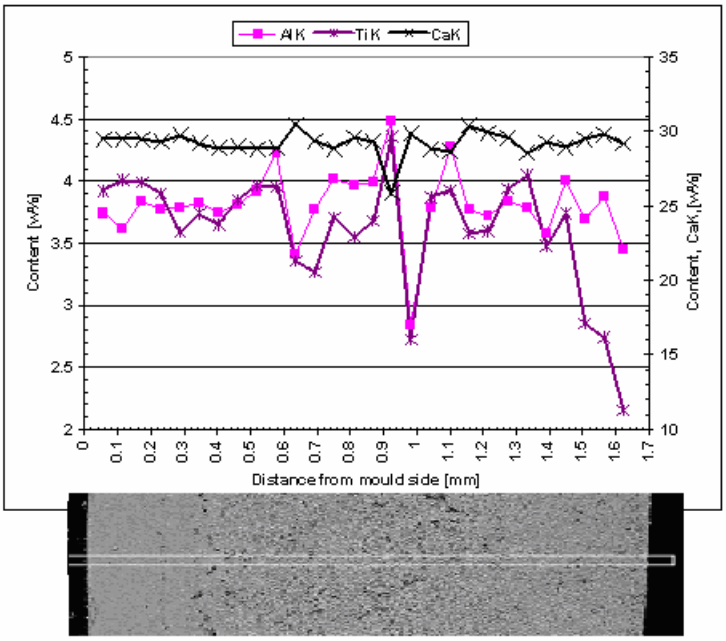

Figure 42. *Flux film and concentration of some elements. (10cm below the meniscus, Cast 189) (mould side on the left).*

There were no visually detectable layers with different colour shades in the flux film, and the structure in the area next to the mould side was of glassy appearance. Either there was no variation in the concentrations of elements, as there was in the typical film structures described earlier. Therefore, it seems obvious that the slag film had fractured about 5m (~5 minutes) before the end of casting, which was indicated by the "jump" in the thermocouple temperatures, and the tail-out samples were formed only during the last 5 minutes of casting. The slag films taken from the Ti stabilized steel grades were extremely brittle, making sampling difficult (Jokisaari 2000). From the thermocouple temperature data, and from the many cases of sticking, it seems reasonable to assume that the slag film was also brittle during casting.

During the cast of Ti stabilized steel grades, the flux slag in the mould was contaminated with Ti; Ti reacted with less stable oxides, resulting in the formation of calcium titanate in the gap. This led to low powder consumption and, therefore, poor lubrication, fast growth of the solid flux film, possibly as a consequence of the nucleating effect of calcium titanate particles, and finally, a weak, brittle solid flux film. This combination led to regular fracturing of the solid flux film and finally to numerous cases of sticking.

3.14 Glassy vs. crystalline phases in layers

Layers or areas in the films composed of a glassy phase were found only occasionally. When a layer is formed directly on the mould surface either at the beginning of casting or later on, it will form in a glassy state. If there is enough driving potential, in other words, if there is enough time and the temperature is sufficiently high, devitrification of the layer will take place, resulting in a crystalline phase. Glassy phases were also found locally, when the liquid slag entered the mould surface through fractures in the solid layer and there was not enough time for crystallization. This took place near the end of casting and examples are provided in Figures 14 b and c.

Mould oscillation, or mechanical forming, probably favours crystallization of glassy phases on the mould surface. There was no orientation in the phases, which were originally glassy and crystallized later (O'Malley & Neal, 1999). This information can be used when evaluating the history of the phases. In Figure 23, a clear orientation in the structure in areas 0, 1 and 2 can be seen.

There are two possible ways in which the layers might have formed:

(i) layers on the mould surface formed in glassy state, and crystallization took place during casting.
(ii) layers solidified with a lower solidification and cooling rate on the existing solid layers, then crystallized readily during or after solidification.

This might be taken into account when studying the differences in the layer structures near the surface of the mould or near the steel shell.

3.15 Heat flux and temperatures of thermocouples

Thermocouple temperatures were used to determine whether or not the different film structures might be connected to local heat fluxes. Heat flux behaviour and thermocouple temperatures have been discussed many times. How is it possible that the heat flux, and especially the temperatures of thermocouples in the middle part of the wide faces of the mould, decrease as much as is observed? Three explanations were considered: (i) the glassy layer formed at the beginning of casting was crystallizing, (ii) the increase in thickness of the flux film between the shell and the mould (iii) the complexity of layers with pores or voids was increasing.

The behaviour of both heat fluxes and thermocouple temperature were similar in all casts with similar steel grades. The degree of changes could vary to some extent, therefore it was interesting to find out if the flux films offered any explanation for the above mentioned heat flux behaviour.

Locations of thermocouples have already been shown in Figure 7. Examples of the temperatures of the thermocouples are shown in Figures 43, 44 and 45, and Figure 46 shows examples of the heat flux. Figure 43 shows the temperatures of different thermocouples in a short cast (with one heat) to observe the behaviour of temperatures at the beginning stage of the cast. The biggest changes in temperature took place during a period of approximately 40 minutes. Figure 44 presents the behaviour of the temperatures of two thermocouples in the middle part of the wide faces during a longer cast lasting several hours, when heat fluxes in all parts of the mould had stabilized. These two thermocouples took the longest time to stabilize, and at those locations was also produced the thickest and most complex films.

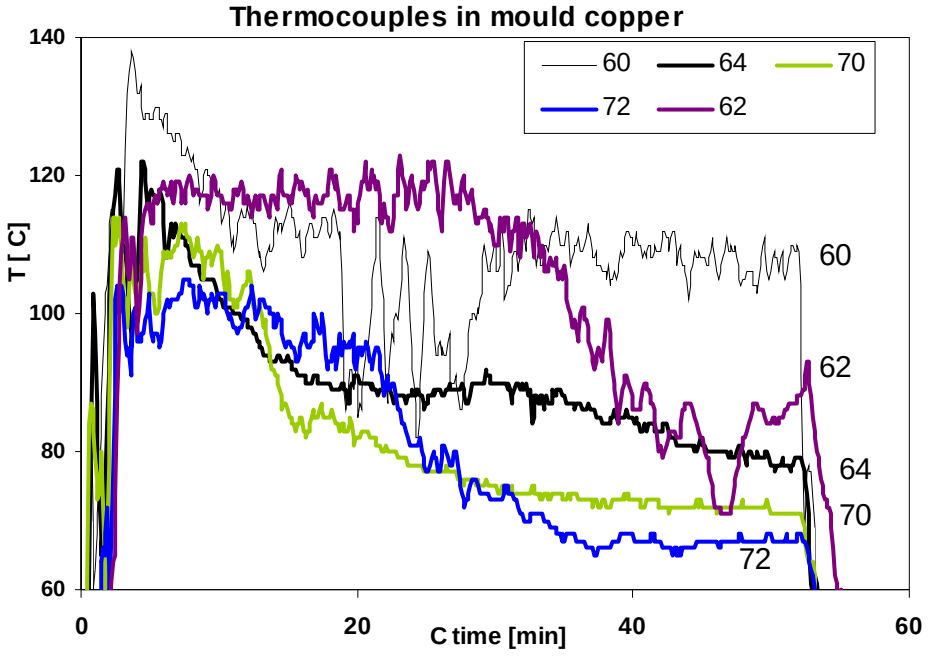

Figure 43. *Behaviour of the temperatures of the thermocouples in the mould copper. All thermocouples were in the middle area of the wide face: 60 was very near the meniscus, 64 - 25cm, 70 - 34cm, 72 - 38cm and 62 - 64cm below the meniscus.*

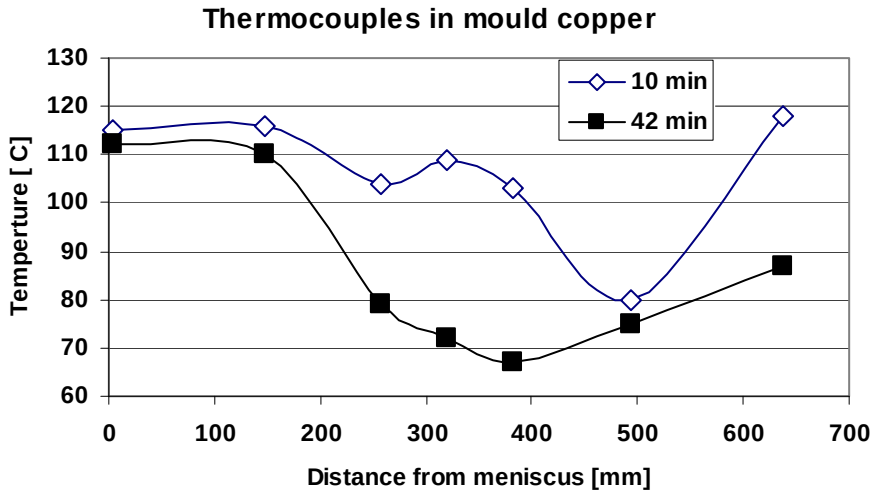

Figure 44. *Temperatures of thermocouples as a function of distance from the meniscus and with two casting times (Hooli 2003).*

Thermocouple temperatures were lowest at a distance of approximately 35-40cm below the meniscus, as can be seen in Figures 43 and 44. This means that the heat transfer in this zone was low. Although the thermocouples in Figure 43 were not exactly on the same vertical line, it is possible to see the principal trends. Temperatures near the meniscus and the heat flux only decreased slightly during casting, but in the middle area, the decrease was clear.

"The first" reason for the decrease in heat flux was that the glassy layer formed at the beginning of casting and it was crystallizing, thus heat conductivity of the layer was decreasing. During longer casts, temperatures could decrease to very low levels in the middle area of the mould wide face, as shown in Figure 45.

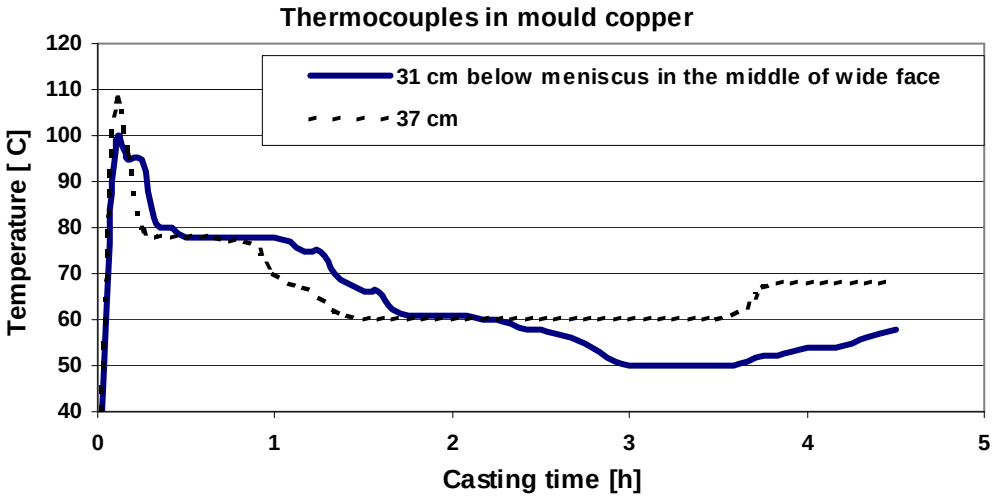

Figure 45. *Casting time and temperatures of thermocouples in the middle of wide faces (Hooli 2002(3)).*

The longest flux films reached approximately 40cm below the meniscus. These cases presented the largest and thickest layers; their structure was often the most complex, with high porosity and/or voids. These observations on the heat flux and the layers in the film sit well together. Near the mould exit, heat flux was higher than in the middle area (see element 62 in Figure 43; all the corresponding 4 elements displayed similar behaviour). This could be explained by the fact that the film was fracturing into pieces below 40cm from the meniscus,

and contact between the shell and the mould improved, although the variation was possibly large because pieces of the film were carried out. Below 40cm, the film had fractured into pieces, possibly because of the increasing friction between the shell and the film layer due to lack of liquid flux film below this distance.

Figure 46 shows the behaviour of temperature differences of mould cooling water. Temperature difference decreases down to the level of 80% of the initial level. Some thermocouple temperatures could decrease from 100ºC to 50ºC during casting. This means that a large proportion of the decrease in total heat flux was caused by the decrease in the heat flux on the middle area of the wide face of the mould. The function of the casting powder near the meniscus is anyhow more essential considering results of casting.

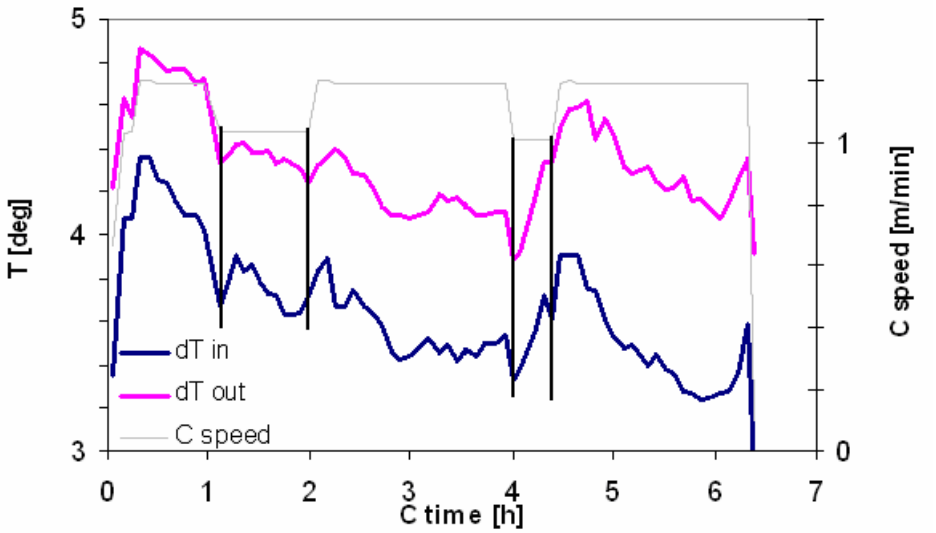

*Figure **46.** Temperature differences [ºC] of the cooling water on the wide faces during casting of over 6 hours. dT_{in} = inner bow side, dT_{out} =outer bow side, C_{speed} = casting speed*

Changes in casting speed sometimes cause surprising changes in heat flux, as shown in Figure 46. When casting had been underway for 1h, casting speed was decreased and, as expected, heat flux decreased, with a small increase at the beginning of the period with lower casting speed. But when casting speed was decreased at 4h, heat flux first decreased, and then already during the lower speed period, it clearly increased. This increase continued when the casting speed was increased. After 4h of casting time, layers in the film between the shell and the mould were thick and complex and a decrease in the casting speed could cause fracturing of the film or peeling off some layers, leading to improved contact between the mould and the shell and the increased heat flux. After the increase, the heat flux started to decrease again (from a time of approximately 4.5 hours) due to the formation of new film. Near the end of casting, there was again an increase in temperature, indicating changes in the film.

Powder consumption is one of the parameters which can give additional information concerning phenomena related to lubrication and formation of the solid film. When ‘granulated powder’ was used, a powder feeder was employed. Only one example is shown in Figure 47, because the measurement of the consumption was not very accurate due to the use of a small gas flow to aid the flow of the powder in the feeding tube. Thus the powder flow was not fully free, but a little forced. The gas (Ar) was used because the angle of the tubes was not large enough for gravimetric feeding alone.

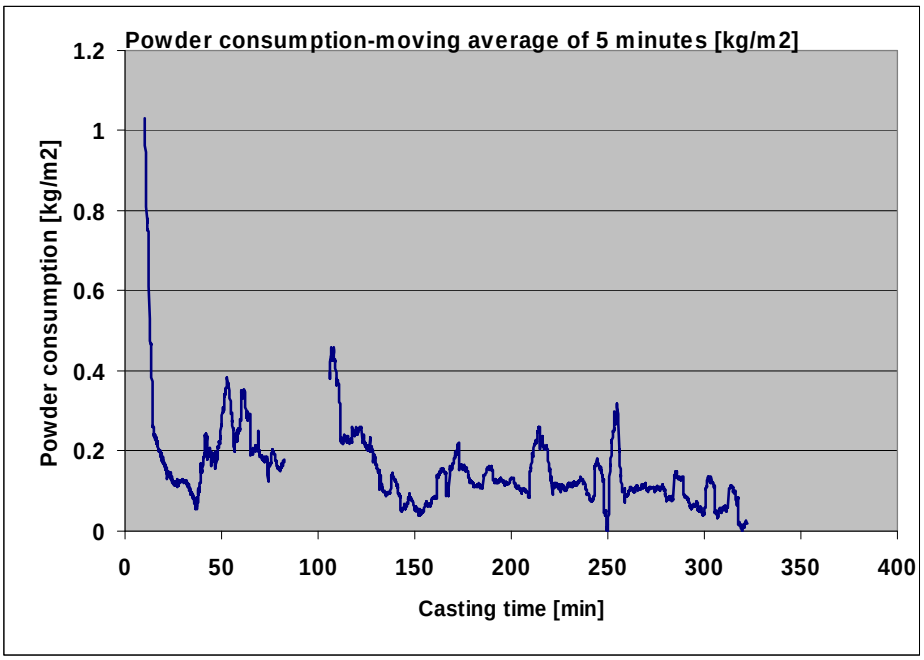

Figure 47. *Casting powder consumption in a cast of AISI 304.*

Powder consumption was high during the first ten minutes of the cast. There were fairly big variations during casting, many of which being caused by the function of the feeder. The level of consumption was approximately 0.1-0.2 kg/m^2. Calculation of the thickness of the liquid flux layer could be possible, but would, nevertheless, require assumptions as to how the liquid flux was divided around the perimeter of the mould. If it was assumed that powder consumption was 0.2 kg/m^2, and that this was evenly distributed over the surface (3 kg/dm^3 was used as the density of liquid flux), the thickness of the liquid flux film would be about 70µm. The thickness of the liquid flux film was not, in fact, uniform layer in the gap around the perimeter of the mould or in the different distances from the meniscus.

Near the meniscus it had a higher temperature and higher fluidity. The film was thin and flow speed was high. Lower down in the mould, the average viscosity increased, flow speed decreased and the film thickness probably increased. Consequently, liquid flux film thickness could reach the thickness shown in Figure 23 (area 1) i.e. 120µm, which was suggested as the liquid, lubricating layer during casting.

3.16 Layer structures and heat flux calculations through flux layers between solidified steel shell and mould

The flux film between the steel shell and the mould has an important role concerning the heat flux from the steel shell to the mould. The flux films found in the present study ought to have responded to the heat flux in accordance with their structures, specifically their thickness and porosity. The aim of these calculations was thus to determine whether or not the layer films could explain the local heat fluxes observed i.e. the measured temperatures with the thermocouples. Using a spreadsheet, temperature gradients and temperatures in different points in the flux film structure were calculated for some of the observed layers. Commonly used formulas were used to calculate heat fluxes.

Heat flux can be calculated with the following equations:

$$q = \frac{k(T_i - T_{i-1})}{s} \quad [4]$$

$$q_i = q_{i-1} \quad [5]$$

$$T_i = \frac{qs}{k} + T_{i-1} \quad [6]$$

If the layer contains porosity, the conductivity is calculated based on the fractional areas of solid material and pores

$$k_{layerwithpores} = (1 - f_{pores})k_{solid} + f_{pores}k_{gas} \quad [7]$$

If contact resistance is used on the interface (which has no thickness), the temperature change was calculated by the formula:

$$\Delta T = rq \quad [8]$$

where:

q is local heat flux	[kW/m^2]
k is heat conductivity	[W/mK]
T is temperature	[º C]
s is layer thickness	[µm]
f is fraction	[-]
ΔT is temperature difference	[º C]
r is contact resistance	[m^{2}K/W]

T_i and T_{i-1} are the temperatures from one interface to the other interface of the layer or on different sides of the interface in the case of the contact resistance.

Certain measured values were used in the calculations. The heat flux was set so that the temperature in the mould in the location of the thermocouple was the same as the measured temperature. It was then assumed that this same heat flux continued through all the sub layers. The thickness of different sub layers was measured on the photographs of films prepared with the microscope. Fractions of pores were also estimated. Heat conductivity of air was used for pores. The gas in the pores was probably not air, but because the gas composition was not known, heat conductivity of air was chosen. Mould cooling water temperature was set based on the measured values. The principles presented by Meng and Thomas (2006) and Thomas (2004) were adopted for these calculations. The majority of the basic data were also from Meng and Thomas.

The layers and contact resistances included in this calculation were:

- heat resistance (as contact resistance) from average cooling water to cooling water near the surface of the mould
- heat resistance (as contact resistance) between cooling water and the mould surface
- from mould cold surface to the thermocouple location
- from thermocouple location to the hot surface of the mould
- contact resistance between the hot surface of the mould and the solid flux film based on an equivalent air cap
- from the cold surface to the hot surface of solid layer # 1 (“white layer)

- the second solid layer (if porous, this was taken into account)
- a possible third solid layer
- from the colder surface to the hot surface of the liquid slag layer
- from the cold surface to the hot surface of the steel shell (hot surface temperature was assumed to be the calculated solidus temperature i.e. 1380°C

Shell thicknesses were calculated with the simple formula:

$$s = k\sqrt{t} \qquad [9]$$

where:
s is the shell thickness [mm]
k is sc. solidification constant; for austenitic steel grades its value is 25 [mm/min$^{1/2}$]
t is the residence time of the shell from the meniscus [min]

Shell thicknesses were modified slightly, depending on the heat flux level. For example, for a high heat flux (higher temperature of the thermocouples) the shell thickness was assumed to be somewhat bigger than that calculated with the formula 9. Two film cases shown on the lowest row in Figure 17 were used in the calculations, and also for corresponding temperatures of thermocouples. The third case represents conditions at the beginning of casting. The thermocouple reading presents the only measured value, and the aim is to get an estimate for flux film thicknesses to compare with observed films at the end of casting. Three cases were calculated. Results are largely estimates for temperatures in different positions, thus trends for temperature gradients are given for different films.

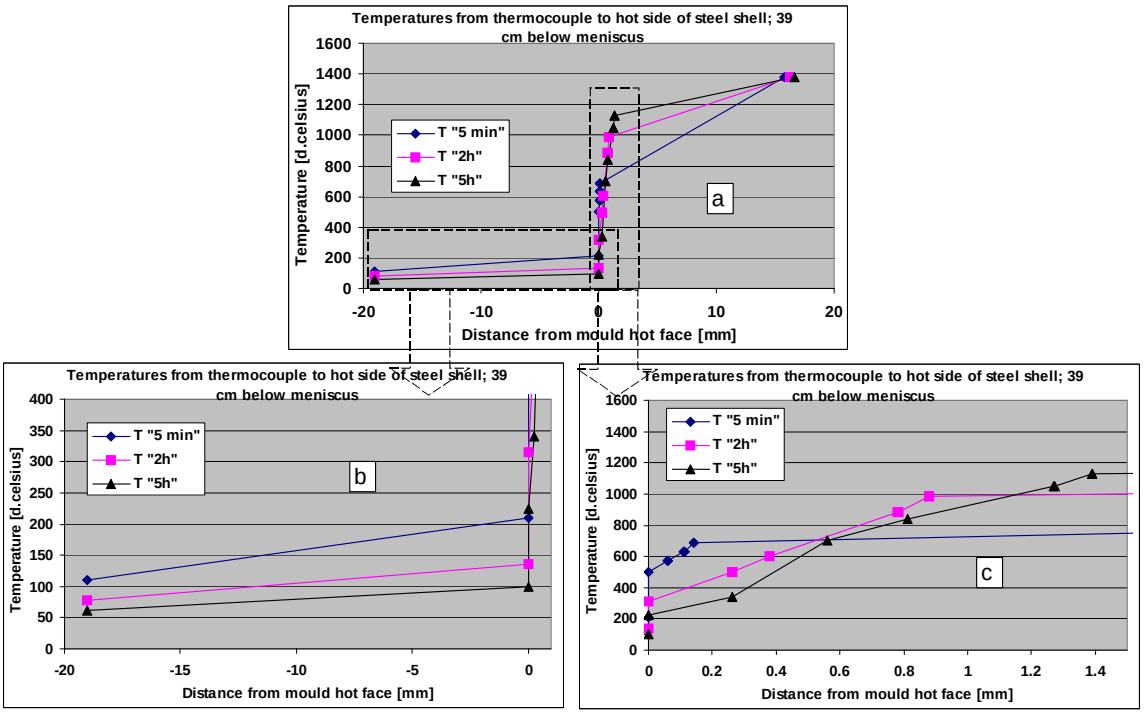

Figure 48 (a-c). *Calculated temperatures through the layers in films.*

Cases “2h” and “5h” in Figure 48 are based on the films shown in Figure 17, cases 38 and 39cm below the meniscus with different casting times. Case “5 min” is based on the assumed layers in the film after 5 minutes casting time. The hot face of the mould was set to be 0 on the x-axis. Figure 48a) shows temperatures from the thermocouple to the hot surface of the

steel shell. Figure 48b) and c) are "magnifications" from Figure 48a). Thus b) is from the thermocouple to the mould hot face, and c) from the mould hot face to the cold surface of the steel shell.

The porosities were estimated respectively. The calculation began from cooling water and ended at the hot surface of the shell, i.e., to the solidus temperature of the stainless steel (calculated to be 1380ºC). Heat flux was set so that the temperature in the mould wall at the point of the thermocouple was the same as that measured via thermocouple in the same case. Because all the layers seemed to have a crystalline structure, radiation was not taken into account. In the case of "5 min" a glassy layer was also possible, but despite this, the film ought to have been very thin. This case was included in order to estimate trends in temperature gradients with different film thicknesses. The data used in these calculations are given in Tables 16 and 17.

Table 16. Measured, estimated or given thickness [µm] and portions of pores of layers used in calculations and contact resistances on the boundary mould/solid slag [m^2K/W] ([estimation] or (given) values are in parentheses).

Case	1.layer sc."white"	2.layer	3.layer	4.layer	liquid layer	$r_{mould\,/\,solidslag}$
"5 min"	(60, 0)	(50, 0)	-	-	(30, 0)	(0.00024)
"2 h"	[260, 0]	120, 0.2	400, 0	-	(73, 0)	(0.00026)
"5 h"	[260, 0]	560, 0.3	250, 0.2	460, 0	90, 0	(0.00028)

Thicknesses for "white" layers are based on measurements, but are not necessarily exactly true for these cases. In the last stage of calculation, the contact resistances were adjusted, so that the solidus temperature of the steel on the inner side of the shell was reached. For the contact resistance from the graph of Meng and Thomas (2006) for the distance of 390mm, the value is around 0.0002 m^2K/W. So the values used in the calculations (Table 16) are in the acceptable range. The values of the adjusted resistances are also principally in the correct order: the thin layer ("5min") has the lowest value and the thickest layer ("5h") has the highest value.

Table 17. Input data for calculations

Solid slag conductivity	k_{solid}	1.0	W/mK
Liquid slag conductivity	k_{liquid}	0.66	W/mK
Copper conductivity	k_{Cu}	315	W/mK
Steel conductivity	k_{steel}	27.5	W/mK
Air conductivity	k_{air}	0.06	W/mK

As expected, in the case of the thick layer with pores (case "5h"), the temperature gradient over the whole film was the shallowest, but the total temperature difference was the largest. The calculation gave a temperature range from 1049 to 1131ºC for the liquid flux layer, which meant that it could, in fact, be fully liquid. For the next layer, the temperature range was from 842 to 1049ºC. Within these temperatures, the slag ought to be fully solid if the main phase was cuspidine; this has the high solidification temperature of 1407ºC (Watanabe et al. 2000), which is high enough even when containing additional fluxing compounds. Formation of cuspidine with high solidification temperature is certainly an important factor when considering the possibility of the slag films growing in thickness. After cuspidine solidification, the residual liquid consists of several different compounds and is probably liquid at lower temperatures. It can thus be squeezed out by forces caused by mould oscillation.

In the case “2h”, the calculation gave for the liquid layer a temperature range from 882ºC to 987ºC. At the lower end of the temperature range, the flux was probably viscous, and might also contain crystalline phases. For the case “5 min”, the calculation gave a temperature range for the liquid layer from 632ºC to 688ºC. It is possible that only a small fraction of the slag could be liquid at such low temperatures. From these calculations, it is possible to state that the layers observed can serve as an explanation of these very low heat fluxes (i.e. the observed low thermocouple temperatures). The calculations also gave further information concerning the role of cuspidine in the formation of flux films, especially the formation of thick films.

3.17 Relations to surface defects

When liquid casting flux infiltrates into the gap between the mould and the shell, part of it solidifies on the mould surface. This slag layer can grow in thickness and can change its structure during hours of casting, leading to a reduction in heat flux and an increase in the frequency of surface defects.

At the Tornio Works, there are certain quality aspects known to be related to the casting process. One of these is called “slag defect”. This defect is detectible only on hot rolled strip and cannot be found on slabs, probably because it resembles a thin film on the surface. The reason that these defects can be connected to the casting process originates from the fact that traces of casting powder (Na!) were detected in the defect zone of hot rolled strip.

As shown in Figure 49, the frequency of the defect is very low but increases with casting time. In addition, the severity of the defect is minor, which means that an enormous volume of data is required to find a trend. In earlier times, when this type of defect was a bigger problem, it was found to be related to the type of powder used. Changing the casting powder brought about a significant decrease in the frequency of this defect. This defect also has a correlation with casting time, and in addition, the increasing thickness and complexity of the solid film during hours of casting probably changed the behaviour of the lubricating layer.

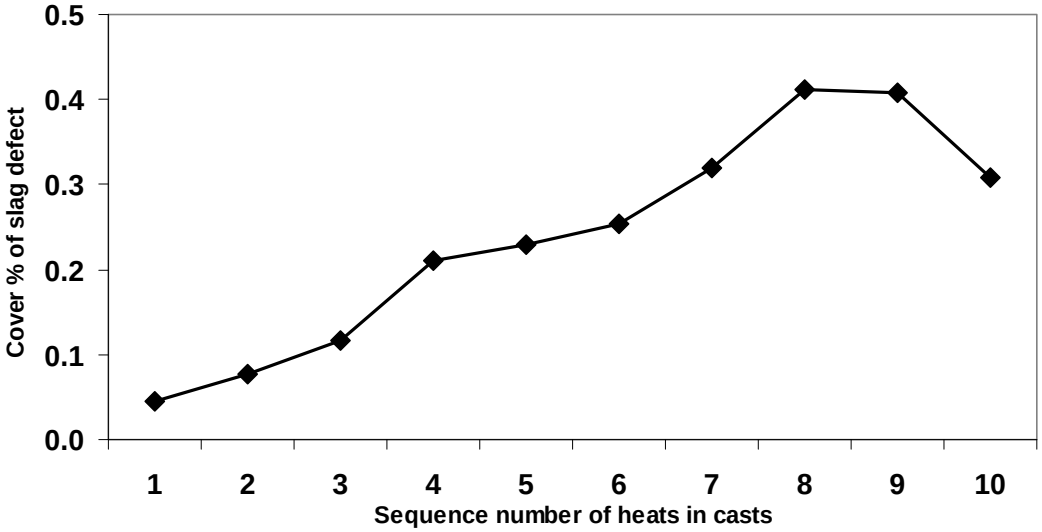

Figure 49. *So-called cover % (i.e. % of the total length of the strip covered with the slag defect) vs. duration of casting. (In this case, one heat corresponds to approximately one hour of time, AISI 304) (Hooli 2002(1)).*

3.18 Evidence regarding reactions between steel and mould flux

With Ti stabilized steel grades, there is clear evidence of reactions between the steel and slag in the mould. However, with standard grades, there are also a number of changes in the flux slag composition, which indicates reactions between the steel and slag in the mould. In the flux in the mould at the end of casting, elements can be found which had very low original concentrations in the casting powder. MnO content could rise up to 3% in the mould slag, although its concentration in the powder was below 0.1%. There are two possible ways for Mn concentration to increase in the mould flux: i) Mn in the steel reduces some oxides in the flux oxidising itself; ii) inclusions from steel are dissolved into the mould slag. In addition to oxides, inclusions also contain manganese sulphides, which could also explain the presence of higher sulphur concentrations in the slag than in the powder.

4 DISCUSSION

In the literature, few observations of flux films were presented. The results found in the present study do, therefore, present new prospects for this field of research.

4.1 Discussion concerning conditions in the gap between mould and steel shell

The conditions in the mould gap are schematized in Figure 50. The steel shell near the meniscus is very thin, has a high temperature and is very weak. Lower in the mould, the shell increases in thickness, the temperature is lower and the steel strength is little higher. The hot surface of the mould wall has clearly lower temperature than the steel shell. There is therefore a steep temperature gradient across the flux film resulting in special thermodynamic and kinetic conditions.

The steel shell moves downwards and the mould is oscillating, therefore there are certain mechanical forces concentrated on the flux film. Ferro-static pressure increases downwards from the meniscus, therefore a certain amount of pressure is focused on the flux film. Duration of casts can be several hours, which means that there is enough time for the occurrence of phenomena which need hours of time to occur in the flux film.

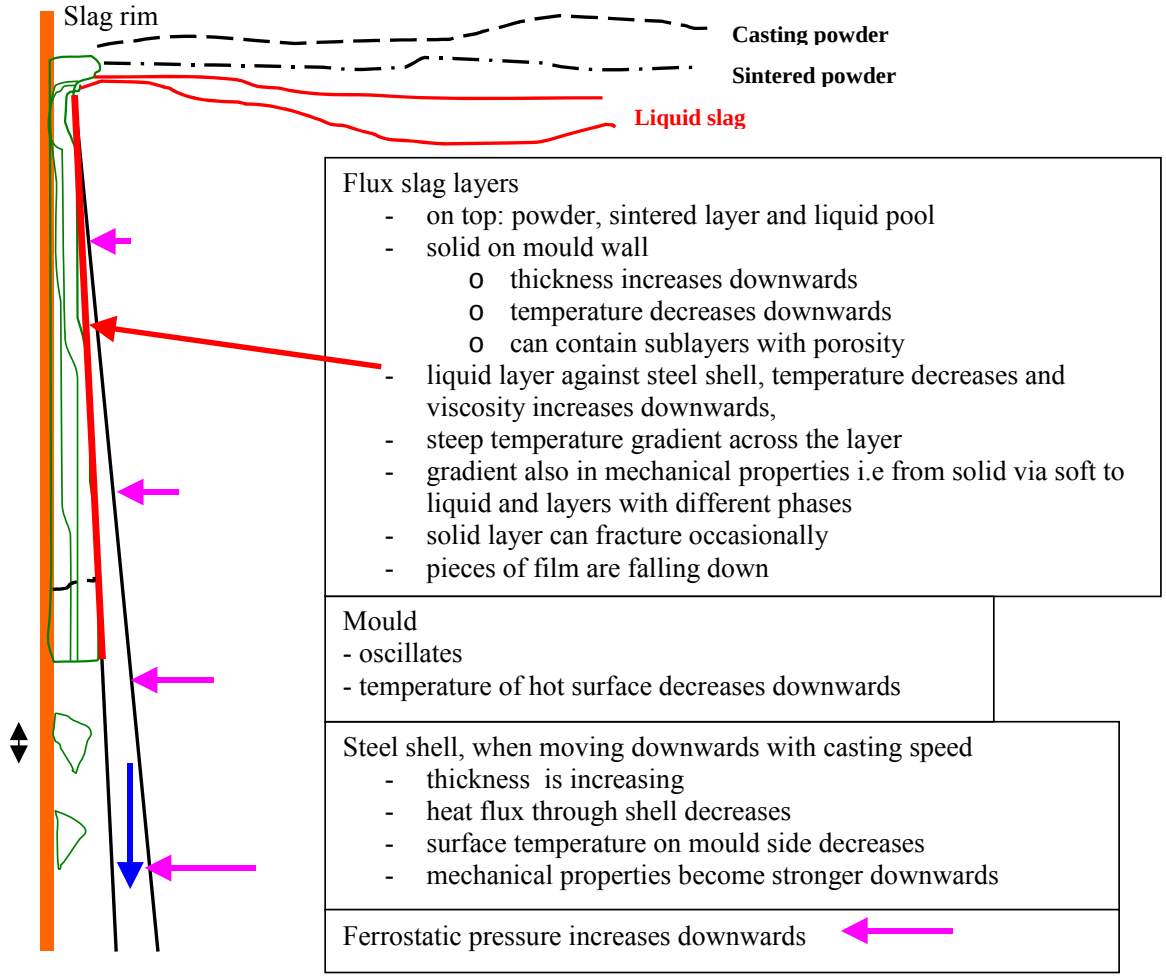

Figure 50. *Schematic presentation of the conditions in the gap between mould and steel shell.*

The flux, infiltrated into the gap in the meniscus between the steel shell and the mould, is experiencing extraordinary conditions and is going through a unique "process". It is easy to understand that these conditions are difficult to simulate both physically and mathematically.

4.2 Discussion on formation mechanisms for the flux film structures found in the present study, and some associated phenomena

The following layers and phenomena found or observed in the experiments are summarized below:

- residence times of the films could be several hours
- formation of cuspidine, which is a common phenomenon for fluorine containing powders
- the cuspidine layer had an increasing distance from the mould wall with increasing distance from the meniscus (i.e. lower in the mould)
- formation of NaF was distinctly verified
- formation of nepheline
- formation of other phases with complex compositions, such as those found in the areas 0 and 1 (see Figure 23)
- relatively high concentrations of minor elements, such as Mn, K, S
- the layers in the film had a mostly crystalline structure; glassy phases were observed in few cases
- voids and porosity were commonly observed
- In Ti stabilized grades calcium titanate was observed to form in the film but not yet in the casting slag in the mould
- heat transfer could decrease significantly, especially in the middle area of the wide faces, which contained the thickest slag layers

There were some cases among the flux films with quite surprising structures. This chapter will attempt to describe how these structures might have formed. Some features are to be expected, but some are very difficult to explain. Sampling was made in the tail-out of casts, therefore so sampled flux films had structures corresponding to at least 1 hour of casting time, and often to several hours. An exception includes those cases where fracturing of the film had removed the old film, and a new film had formed later, sometimes near the end of casting.

During tail-out, liquid flux was left on the steel surface in the mould. Tail-out was carried out with a low casting speed, and a layer from this liquid flux adhered to the film formed during casting. This extra layer was easiest of all to distinguish, either visually in the photographs from the optical microscope (dendritic structure and colour shade) or by analyzing the composition of elements as these are the same as in the flux slag in the mould at the end of casting, and especially if a tracer was used. This layer was also useful because it served as a reference showing the composition of the liquid flux at the end of casting. In this way, if the layers in the films had a different composition and/or structure, one could assume that these layers were not formed during tail-out.

Formation of the film at the beginning of the cast

The discussion concerning the film structures at the beginning of casting are based on local heat flux behaviour and on the indirect observations of the behaviour of some elements in the film layers next to the mould wall, as well as on conclusions gleaned from the literature.

After the start of casting, a thin, glassy film formed on the surface of the mould wall. The heat flux was high. In the glassy form there were no separate phases; these formed later via devitrification. Because of poor wetting of liquid flux on the nickel surface, the first layer formed unevenly and its shape could be related to the mould oscillation. Such shapes were found on some of the film surfaces against the mould. From this, it could be construed that some of the films had been in the gap during the entire casting period.

Formation of the cuspidine layer in the film

When the solid film thickness increased and there were no more glassy layers, the solidification and cooling rates of new flux layers decreased. Solidification could then take place directly via nucleation of crystallines, which formed a dendritic structure. Several phases could possibly precipitate during solidification. Phase relations detected in the areas 1, 2 and 3 (see Figure 23 or 51) as the share of cuspidine/the share of nepheline was 0.6/0.35, 0.9/0.05 and 0.35/0.4 respectively, could thus become possible.

Kashiwaya et al. (1998) found that the precipitation of dicalcium silicate takes place at temperatures over 1050ºC and of cuspidine at temperatures below 1050ºC and that the onset of crystallization is a function of cooling rate. The aforesaid is fully valid only in the closed system. However, if the liquid remaining among the crystals is even partially removed (for example the liquid among dicalcium silicate), the final result will be somewhat different from that in a closed system. The present study indicates that liquid between crystals became detached due to pressure or mechanical “pumping”. When a solid, glassy structure is formed, all elements are evenly distributed in the phase and changes are much slower while diffusion is controlling.

Crystallization of the cuspidine phase can act as a driving force for the first separation of compounds (see Figure 20).

Formation mechanism of nepheline

Nepheline was often found on the mould side of the cuspidine layer. The nepheline-type phase had probably squeezed off from the cuspidine grains. Nepheline was found via spot analyses, and its presence is also possible to predict from the average compositions of sub layers. Nepheline formation is favoured by high Al and K concentrations and a value of Na/K ratio of approximately 3. So if the relation is exactly 3, it can be assumed that all Na is in the nepheline phase.

In Figure 27 on the mould side of the cuspidine layer, there was a layer with a high Al content and an Na/K ratio close to 3 indicates the presence of nepheline. Next to the mould side, where Al and K concentrations are lower, Na is probably chiefly in the form of NaF.

Formation mechanism of NaF

The interface between NaF and adjacent layer could be distinguished both visually in BE images and with the spot analyses made by SEM/EDS over the cross cuts of the films (see Figure a16).

When the cuspidine layer moves step by step inwards from the mould wall towards the solidifying shell, a liquid phase containing Na and F in the upper part of the gap flows downwards. When the liquid enters the lower zone in the gap with lower temperature, NaF formed and crystallized. In the literature, NaF was very seldom found in the powder fluxes. Li et al. (2004) mentioned that during heating of a casting powder, NaF was found to be stable only up to 800ºC in high vacuum conditions. Chilov (2005) also found that NaF starts to vaporize between 800 and 900ºC depending on the composition of the powder. The vapour

pressure of NaF has been given as $1.33 \cdot 10^{-3}$ bar (1 mmHg) at 1077ºC (data for sodium fluoride, n.d.). This means that NaF is readily vaporized in mould gap conditions. The melting point of NaF is 980ºC respectively (data for sodium fluoride, n.d.).

The temperatures at which NaF can vaporize are very close to those of the mould wall near the meniscus, but have increasing distance lower in the mould. So lower in the mould, a NaF rich layer could grow thicker. When the mould is decelerating near the lowest position or accelerating upwards, liquid slag among the solid phases can move downwards somewhat. Gases can become squeezed downwards when the mould is moving upwards. When the mould is moving upwards, the pressure in the gap between the mould and the shell is increasing, and gases could be pushed downwards. On the other hand, gases can be compressed, but liquids cannot, and this makes a significant difference in the behaviour of these states.

Formation of Na

There were indirect observations which indicated the existence of elemental sodium on the mould wall. Based on the observation of flaming when sprayed with water on the layer adhering to the mould wall, there was a considerable amount of Na (and K) in the layer.

Other associated phenomena

Fracturing or shearing in the film

Chapter 3.14 presents evidence of fracturing with Ti stabilized grades and Appendix 3 shows slag films with indications of fracturing of the film. Fracturing causes changes in the heat flux, and can lead to sticking and finally break-out in the steel shell. Therefore, measures to decrease fracturing also decrease sticking frequency. In the Tornio Works, one mould is now equipped with thermocouples also lower in the mould, in order to study fracturing of the films lower in the mould.

Residence times of the films

In the case of powders doped with a tracer, it was shown that the film could remain on the mould wall for at least 45 minutes. Trials with the sodium-free powder indicated even longer residence times. The long periods (hours) during which the temperatures of the thermocouples were lowered (see Figure 45), indicates that the film could remain in the gap and its thickness and structure could change during hours of casting.

Discussion concerning the film structure from cast 71056

Figure 51 shows the film from cast 71056 once more, which was taken from 39cm below the meniscus. It is especially interesting because it contains the widest variety of different sub layers. Concentrations of the elements of the different phases and compounds were shown in Tables 6-10. When considering zones 0 and 1, it is difficult to understand whether or not area 1 was formed directly from area 0. Except for cuspidine, there were no clear relations between the other phases in areas 0 and 1. In fact, area 0 did not exist during casting; the steel shell was present instead, which means that the connection of areas 0 and 1 did not exist during casting. Layer 1 did not, therefore, form directly from layer 0. The area/layer 0 (formed during tail-out) represents a result from relatively slow (some minutes) solidification and cooling of liquid flux slag from the top surface of liquid steel in the mould during tail-out.

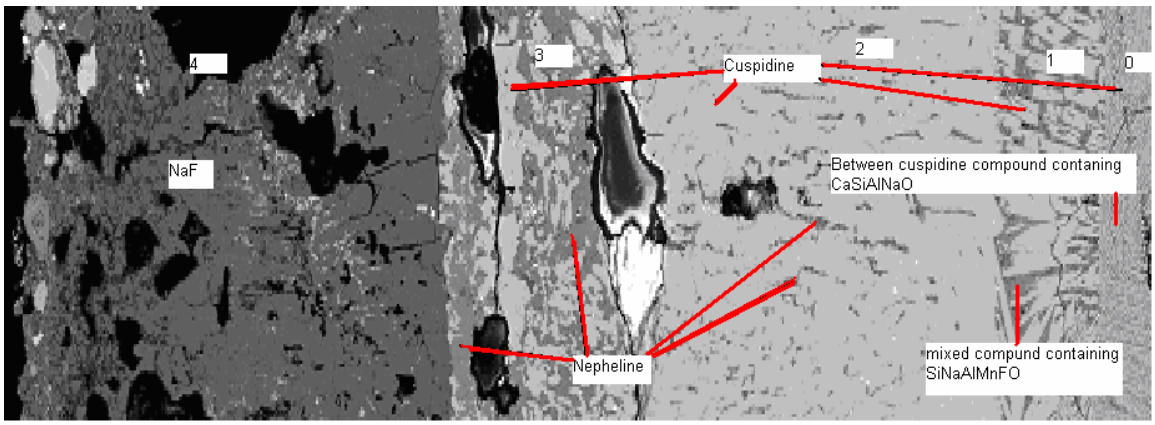

Figure 51. *The cross-section of a film (shown previously in Figure 23). Different phases or compounds are shown with lines in the different layers. Numbers of areas/layers are also shown.*

One explanation for this could be that phase 02 (see Figure 23 and Table 6) went with the steel shell. When comparing average concentrations of elements between areas 0 and 1, there is slightly more O, Si, Ca and Al in area 0. When looking at the differences, a gehlenite-type phase may have separated from area 0. Did this phase disappear with the steel shell? The steel shell did, in any case, removed certain parts of the flux on its surface. Nevertheless, area 1 must have originated from the flux slag on the top of the mould, having the same composition as area 0. One hypothesis could be that the lubricating liquid flux, when solidifying slowly, separated into two parts: a gehlenite-type phase (C2AS with some Na) removed by the steel shell, and remained phases are left in the area 1. Gehlenite was found to form in the highest test temperature, 1100 ºC, in the devitrification test (Meng et al. 2006(2)).

Another explanation was found in a paper by Scheller (2005), who reported a thin layer next on the steel, where the Mn, Mg, Ti and Na concentrations could be clearly higher, and Al and F concentrations lower than in the bulk of the casting flux on the liquid steel. Area 1 contained phases with high concentrations of the above mentioned elements, but also higher concentrations of Al and F. This mechanism does not, therefore, provide an explanation covering all elements.

It was also suggested that layer 1 had acted as the lubricating layer during casting. If so, it was finally solidified during or after tail-out. Perhaps some of the phases, evidently cuspidine, were already solid during casting. Solidification was very slow because the temperature was high, probably near the melting point of the powder flux. Solidification seems to take place with two main phases: cuspidine (no Na!) and another phase containing several elements but not Ca. Additionally, there were small islands of almost pure NaF.

In area 2, the cuspidine-type phase was fully dominant. The proportion of cuspidine increased with decreasing cooling rate, as shown by Kashiwaya et al. (1998(2)) (Figure 6). The cooling rate decreased with increasing distance from the mould wall, and the proportion of cuspidine could thus increase. At any rate, there is a maximum proportion of cuspidine that can be formed, because cuspidine does not contain Na or Al. Based on the mass balance calculations, the maximum proportion of cuspidine is finally limited by Ca and could be in the range of order 0.7 (with powder B). But the proportion of cuspidine in area/layer 2 was estimated to be over 0.9 (based on the distribution of the area and the average composition of layer 2), which indicates that at least a certain proportion of other phases were removed, probably including nepheline in the liquid form. Based on mass balance calculations, the proportion of nepheline could have been at a level of 0.15-0.2. NaF was probably present among the other phases. On the other hand, the large proportion of cuspidine indicates slow cooling rates.

Ca content in the area 2 was clearly higher than in area 0 or 1. This area could not, therefore, have formed as a direct result of areas 0 or 1. Some phases must have been removed. The darker phase (mainly nepheline) between cuspidine has a horizontal orientation. This might indicate that phases which had existed in this area were removed horizontally towards the mould.

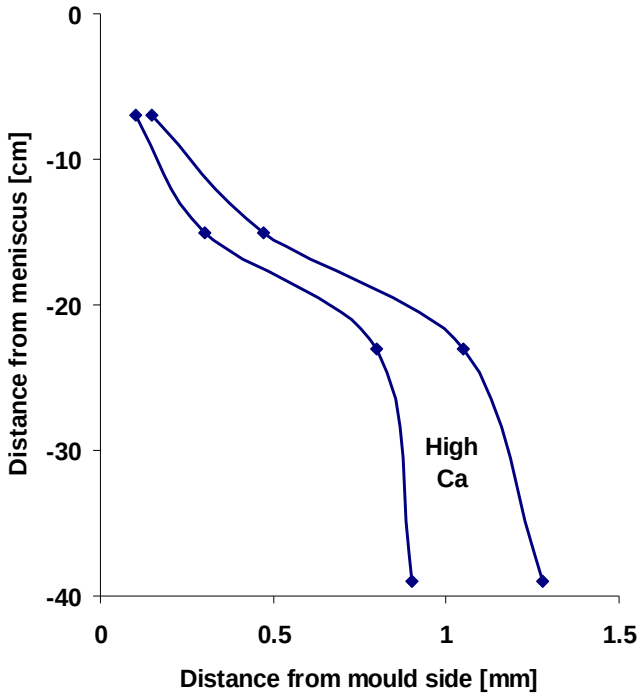

Figure 52. *Location and width of cuspidine (high Ca) layer in cast 71056. Values used in this Figure are based on the layers shown in pictures in Appendix 1.*

Figure 52 shows the location and width of the layer with high Ca, which denotes the presence of cuspidine. It can be seen that the distance from the mould wall and the width increase downwards from the meniscus. The distance from the mould wall might possibly follow a temperature isotherm, where conditions are suitable for solidification so that the solidification rate is low and a crystalline phase is formed directly. On the mould side, the solidification rate was higher, and layers have solidified as a glassy phase and crystallized later. The temperature in the layers next to the mould can rise up to over 400°C when contact resistance increases with the thickness of the solid layer. In these temperatures, the time needed for crystallization can be under half an hour (see Figure 2). Similar behaviour of "high Ca" layer was found also with other cast.

The film shown in Figures 23, 24 and 25 has an exceptional structure in relation to a layer containing only a NaF phase. In the same cast and from the same distance from the meniscus, but from the inner bow side (see Figure 53), the NaF layer is different. NaF phase is present only in the spot-like areas, and does not have a wide coverage.

Appendix 1 shows a series of layers, and a NaF layer could be observed only in one of the transverse cuts (o20,39b, a). This NaF layer was virtually missing from the other film sample near the same location, as can be seen when comparing films o20,39b and o20,39 shown in Appendix 1. In the case of o20,39, the NaF layer remained adhered to the mould wall forming a "white" layer.

Perhaps Na gas formed by vaporization or sublimation and ended up on the mould wall, where it condensed and froze. It may have made tight contact with the mould wall and finally

acted as a glue between the mould wall and the main part of the solid film, especially at the end of casting when mould wall temperatures are lowering during the low tail-out speed.

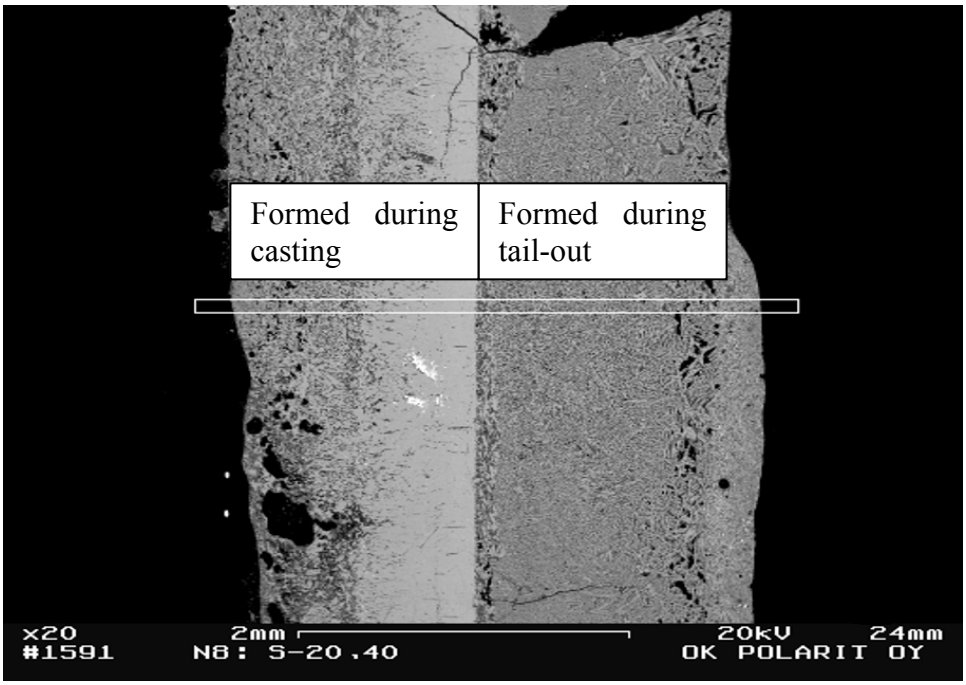

Figure 53. *Cross-section of a film (cast 71056, 40 cm below meniscus on the inner bow side, Mould side is on the left).*

Pores and voids either indicate the formation of gases, or they are shrinking cavities. For example, in Figures 21 and 53, there are roundish pores, which indicate that they are created by Na or NaF vapour. These gases moved outwards towards the mould and then condensed, which might explain that the other phases were virtually missing in this layer.

In area 3, the pores were more rounded than in area 4 (see Figure 51 or 23). Thus in area 3, pores were possibly caused by gas formation, and in area 4, voids were caused by the volume change in condensation of NaF vapour. If the formation of the NaF phase is a consequence of condensing of NaF gas, no liquid was formed, which could have filled the empty space. This resulted in the formation of voids, and during further cooling, more voids were formed due to shrinkage. Pores could also be caused by other gases, including hydrogen, as suggested by Cho et al. (2005).

Some extra trials were made to verify the location of the boundary between the layer formed during casting and that formed during tail-out. (More details were given by Scheller et al, 1999.) These trials did not lead in this sense to a clear solution, but provided some other interesting points. The boundaries between the layers were very sharp in the films from the lower zone in the mould. Usually, the structure, colour shade and changes in concentrations of elements at the boundaries supported each other well.

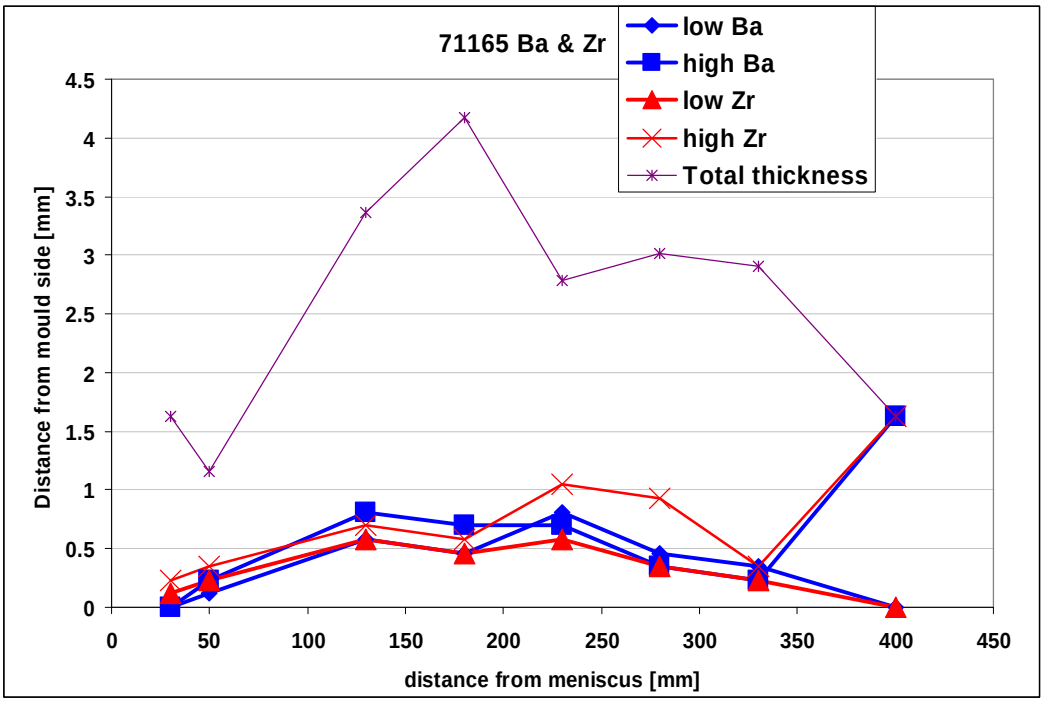

Figure 54. *Distances from meniscus versus distances from mould side showing the regions where Ba or Zr concentrations were especially low or high, respectively.*

Data used in Figure 54 needs some clarification. ”Low Ba” means the layer thickness, where Ba content was clearly lower than in the tail-out layer. Ba containing powder was added between 45 to 10 minutes before the end of casting and Zr containing powder during the last 10 minutes. So if in a layer both are low, this layer had formed at least 45 minutes before tail-out. If only Zr was low in a layer, it must have formed between 45 to 10 minutes before the end of casting (Photographs of the films from cast 71165 are shown in Appendix 3).

The layer containing “low” concentrations was an older layer, the layer thickness between “low” and “high” was a transition between low and high. The layer between “high” and total thickness was formed during tail-out. The film “400mm” concentrations were only “high” i.e. the whole sampled film was formed in the tail-out. To a distance of 330mm, there was a layer older than 45 minutes. At a distances of 230 and 280mm, the high Zr layer was thicker than the high Ba layer. This might indicate that certain layers formed during the last 10 minutes.

Series of events leading to sticking

Sticking of the solidifying shell onto the mould wall is the most important metallurgical problem when aiming for increasing casting speed in the slab casting. The following hypotheses can be presented for the events leading to sticking based on the results in the present study:

- solid film layer fractures off lower down in the gap (20-40cm below the meniscus)
- liquid slag in the gap between the fracture point and the meniscus will flow rapidly downwards to fill the area below the fracture
- lubrication in the gap deteriorates temporarily as a consequence
- weak steel shell near the meniscus comes into contact with the solid film layer and ruptures

A similar mechanism was also suggested by O’Malley and Neal (1999).

4.3 Proposed mechanisms for the growth of the thickness of flux film during casting

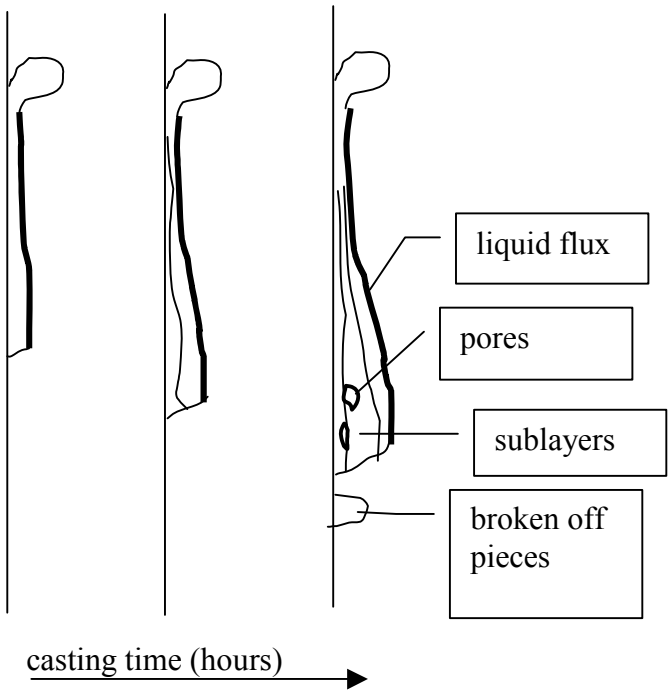

Figure 55. *Presentation of changes in flux film during casting schematically.*

Figure 55 schematically shows the concept of the increase in film thickness. The crystallinity of the film also increases along the casting time. Next to the liquid flux layer, a layer with liquid and solid phases formed, with the solid phase being cuspidine. When the proportion of cuspidine became big enough, the liquid phases were partially squeezed towards the mould wall, and the layer behaved like a solid. When the mould moved upwards, the cap between the flux film and the steel shell opened slightly, leaving space for cuspidine to move a little way towards the shell. Liquid phases gradually moved towards the mould at the same time, and in this way, the almost solid cuspidine rich zone grew away from the mould. In this proposed mechanism, the explanation of how phases other than cuspidine could travel through the cuspidine rich layer onto the inner side of this layer remains a problem.

The formation of cuspidine and Al rich layers are consequences of the same process, but the formation of the NaF layer has a separate mechanism. The NaF rich layer has a very sharp boundary against area 3 (see Figure 23) with a high average Al content, which is possible to see visually and also from analyses. For example, in Figure a16 in Appendix 4, Na and Al concentrations have an abrupt change. Areas/layers 3 and 4 have fully different phases. How could such a sharp boundary have formed? The conclusion is that area 4 formed with an independent mechanism rather than as a consequence of any modification of area 3.

Shrinking of the solid layer can cause voids and also reduce pressure, which could contribute to the formation of gas phases, including Na gas.

5 CONCLUSIONS

The slag film samples were taken from the mould at the end of casting sequences of stainless steel heats. A special tail-out practice was developed in order to get massive samples so that the original location of each sample was properly known. The structures of the films and their compositions were then investigated.

No study was found in the literature with an equal number of massive samples, or with known locations and concentrations of elements analyzed through cross cuts of the samples. Therefore the present study contains several new findings concerning the behaviour of the flux slag in the gap between the mould and the steel shell.

Studies were also made concerning the connection of several associated phenomena to the structures of the films. The final aim was to construct a kind of temporal, thermal, chemical and spatial history of the slag layer between the mould wall and the solidifying steel shell.

Central results

- The most typical feature in the sampled films was the layer in which the cuspidine phase was dominant.
- The films had a crystalline structure which either formed during solidification or via devitrification.
- When the cooling rate had been high enough and the residence time before sampling was short, glassy structures were also found.

These findings are in very good accordance with information found in the literature, especially the formation of cuspidine. In addition, the formation of crystalline structures was as expected, via direct formation or via devitrification. The accordance with information from the literature, along with other evidence, confirms that the layers in the films were not formed during tail-out, but during longer periods of the casting process.

- The most unexpected feature was the formation of a separate NaF layer, and the formation of elemental Na (and/or K) against the mould wall.
- It was shown that films can have long residence times (even hours) on the mould wall, and complex structures can develop, containing several sub layers, voids and pores.
- With the aid of thermocouple temperature recording, evidence of fracturing was found in the sampled films.
- Surfaces on the mould side varied in appearance, not only between samples from different heats, but also locally in centimetre scale.

Results can be concluded as follows:

1. The slag films taken with the sampling method used in the present study contained both a layer formed during casting and a layer formed during tail-out.
2. Most of the phases found in the films were as expected, and were compatible with those in the literature.
3. In the film formed during casting, the layer of cuspidine was, as expected, the dominating phase both with powders for austenitic standard grades and Ti stabilized grades.
4. Nepheline and NaF also had an important role in the structure of the films.

5. The layer responsible for lubrication during casting was recognisable in several of the films.
6. The powders used formed both glassy and crystalline layers depending on solidification and cooling rates.
7. During casting, glassy layers displayed devitrification and all layers in the film in the end of the cast were crystalline.
8. The film structure had an influence on the heat flux in the mould.
9. This method can be used when evaluating the functioning of different casting powders.

The formation of NaF vapour and elemental Na and their traversing outward and condensing when approaching the mould wall were qualitatively experienced and stated by thermodynamic calculations. These phenomena also have a role in the heat flux and other important functions of the mould powder.

Further studies can be proposed based on this work and its results:

- casting with tracer (e.g. radioactive isotope) doped powder at some period at the beginning of the cast.
- more comprehensive parameter data collection together with sampling of the films.
- formation of NaF and Na were proximately studied, but further investigations are required.
- the influence of mechanical “pumping” on the film.
- sampling after an observed sticking case during casting could give interesting information concerning the role of fracturing of the solid film.

REFERENCES

Bagha, S., Machingawuta, N.C., Grieveson, P. 1998: 'Heat transfer simulation for continuous casting', *3rd Intertional Conference on Molten Slags and Fluxes*, The Institute of Metals, London, pp. 235-240.

Brandalese, E., Benavidez, E., Castella, L., Madias, J. 2004, 'Behaviour of continuous casting fluxes during heating and coolig', *VII International conference on MOLTEN SLAGS FLUXES AND SALTS*, January, pp. 807-811.

Carli, R., Righi, C. 2004, 'Mould flux crystallisation: A kinetic study', *VII International conference on MOLTEN SLAGS FLUXES AND SALTS*, January, pp. 821-826.

Chilov, A. 2005 'Mass spectrometric study of volatile components in mould powders', Doctoral Thesis, Helsinki University of Technology, Department of Materials and Engineering, Laboratory of Metallurgy, p.61.

Cho, J.W., Emi, T., Shibata, H., Suzuki, M. 1998: 'Heat Transfer across Mould Flux Film in Mould during Initial Solidification in Continuous Casting of Steel', ISIJ Intl., 38: pp. 834-842.

Cho, J.W, Ryu, H.G. 2005: Effect of hydrogen of molten steel on the mould heat transfer during continuous casting of steel; *5th ECCC*, Nice, France, p.19.

Cho, J.W., Shibata, H., Emi, T., Suzuki, M. 1998: 'Thermal Resistance at the Interface between Mould Flux and Mould for Continuous Casting of Steels', ISIJ int., 38, No. 5, pp. 440 - 446.

Courtney, L., Nuortie-Perkkiö, S., Valadares, C.A.G., Richardson, M.J., Mills, K.C. 2001: 'Crystallisation of slag films formed in continuous casting', *Ironmaking & Steelmaking*, Volume 28, Number 5, October, pp. 412-417.

Cramb, A.W. 2007: 'From Liquid to Solid: Key Issues in the Future of Steel Casting', *AISTech*, Indianapolis, USA, pp. 59-75.

Grieveson, P., Bagha, S., Machingawuta, N., Liddell, K. and Mills, K.C. 1988: 'Physical properties of casting powders: Part 2 Mineralogical constitution of slags formed by powders', *Ironmaking and Steelmaking* Vol.15 No.4, pp. 181-186.

Hautamäki, T., Hooli, P. 1992: 'Valupulverien ominaisuudet ja sulattoperäiset pintavirheet' ('Properties of casting powders and melting shop origin surface defects', in Finnish), Outokumpu Tornio Works internal report 5397-133/, p.5.

Hayashi, M., Watanabe, T., Nakada, H. and Nagata, K. 2006: 'Effect of Na_2O on Crystallisation of Mould Fluxes for Continuous Casting of Steel'. *ISIJ International*, Vol. 46, No. 12, pp. 1805-1809.

Hooli, P. 2000: 'Study of the Mould Flux Film between Mould and Steel Shell', *Sixth International Conference Molten Slags, Fluxes and Salts*, Stockholm-Helsinki.

Hooli, P. 2002. 'Study of the Mould Flux Film between Mould and Steel Shell', Influence of Solidification Phenomena on Quality Aspects of CC Semi-Products. *ECSC STEEL WORKSHOP*, Luxembourg.

Hooli, P. 2002: 'Mould Flux Film between Mould and Steel Shell', *Ironmaking & Steelmaking*, August, Volume 29, Number 4, pp. 293-296.

Hooli.P. 2002: 'Study of the Mould Flux Film between Mould and Steel Shell'. *4th European Continuous Casting Conference*, Birmingham, UK.

Hooli, P. 2003: 'Mould Flux Film between Mould and Steel Shell - Effect on Heat Flux and Defect Formation', *Steel Research International*, Issue 8.

Jokisaari, J. 2000: 'Ti-seostettujen erityisongelmat sekvenssivalussa' ('Special problems with Ti-alloyed steel grades in sequence casting', in Finnish), Master's Thesis, University of Oulu, p.114.

Kallio, K., Petäjäjärvi, M., Vatanen, J., Mattila, R., Kokkonen, T., Härkki, J., 2004: 'Mikroskooppitarkastelua kiinteille valupulverikerrosnäytteille, Tutkimusraportti' ('Microscopic study of solid casting powder films', in Finnish), Department of Process and Enviromental Engineering, Laboratory of Process Metallurgy, University of Oulu, Finland, 33 p.

Karlemo, B. 1997: 'Teräksen jatkuvavalussa käytetyn valupulverin termodynaaminen tarkastelu' ('A thermodynamic study of mould flux used in continuous casting of stainless steel', in Finnish). P. 20.

Kashiwaya, Y., Cicutti, C.E., Cramb, A.W., Ishii, K. 1998: 'Development of Douple and Single Hot Thermocouple Technique for in Situ Observations and Measurement of Mould Slag Crystallization', *ISIJ International*, Vol. 38, No. 4, pp. 348-356.

Kashiwaya, Y., Cicutti, C.E., Cramb, A.W. 1998: 'An investigation of the Crystallization of a Continuous casting Mould Slag Using the Single Hot Thermocouple Technique', *ISIJ International*, Vol. 38, No. 4, pp. 357-365.

Kawamoto, M., Tsukaguchi, Y., Nishida, N., Kanazawa, T., Hiraki, S. 1997: 'Improvement of the Initial Stage of Solidification by Using Mild Cooling Mould Powder', *ISIJ international*, 37, No. 2, pp. 134-139.

Li, Z., Thackray, R., Mills, K.C. 2004: 'A test to determine crystallinity of mould fluxes', *VII International conference on MOLTEN SLAGS FLUXES AND SALTS*, January, pp. 813- 819.

Ludlow, V., Harris, B., Riaz, S., and Normanton, A. 2004: 'Continuous casting mould powder and casting process interaction: why powders do not always work as expected', *VII International conference on MOLTEN SLAGS FLUXES AND SALTS*, Cape Town, RSA, January, pp. 723-729.

Meng, Y., Thomas, B.G. 2006: 'Simulation of microstructure and Behavior of Interfacial Mold Slag Layers in Continuous Casting of Steel', *ISIJ International*, Vol. 46, No. 5, pp. 660-669.

Meng, Y., Thomas, B.G., Polycarpou, A.A., Prasad, A., Henein, H. 2006(2): 'Mould Slag Property Measurements to characterize CC Mould – Shell Gap Phenomena', *Canadian Metallurgical Quarterly*, Vol.45, No1, pp. 79-94.

Mills, K.C. 2003: "Mould powders for Continuous Casting" in *The Making, Shaping and Treating of Steel*, 11th Edition, The AISE Steel Foundation, Chapter 8, pp. 1-41.

Mills, K.C., Fox, A.B., Normanton, A. 2003: 'Powder Consumption and Heat Transfer for Mould Fluxes', *ISSTech Conference Proceedings*, Indianapolis, USA, pp.693-701.

Nakada, H., Fukuyama, H., Nagata, K. 2006: 'Effect of NaF Addition to Mould Flux on Cuspidine Primary Field', *ISIJ International*, Vol. 46, No. 11, pp. 1660-1667.

http://en.wikipedia.org/wiki/Nepheline

Nurmi, S. 2006: Personal communication. Helsinki University of Technology, Department of Materials and Engineering, Laboratory of Metallurgy.

Ogibayashi, S., Yamaguchi, K., Mukai, T., Takahashi, T., Mimura, Y., Koyama, K., Nagano, Y., Nakano, T. 1987: 'Mould Powder Technology for Continuous Casting of Low-Carbon Aluminium-Killed Steel', Nippon Steel Technical Report No.34 July, pp. 1-10.

O'Malley, R.J., Neal, J. 1999: 'An Examination of Mould Flux Film Structures and Mould Gap Behavior Using Mould Thermal Monitoring and Petrographic Analysis at Armcos's Mansfield operations', *International Conference on New Developments in Metallurgical Process Technology*. Düsseldorf: METEC Congress 99, pp. 188-195.

Pesonen, K. 1998: 'Voitelukerros ruostumattoman teräksen jatkuvavalussa' ('Lubricating layer in the continuous casting of stainless steel', in Finnish), Master's Thesis, University of Oulu, p.119.

Petäjäjärvi, M., *in press.* Laboratory trials in Laboratory of Metallurgy of University of Oulu, Part of a research project.

Scheller, P, Spaccarotella, A, Hooli, P. 1999: 'Development of high speed casting in conventional cc stainless steel slab production', ECSC steel RTD programme report.

Scheller, P.R. 2005: 'Interfacial Phenomena between Fluxes for Continuous Casting and Liquid Steel', *ICS Proceedings*, pp. 763-772.

Shilov, A., Holappa, L. 2006: 'Mass spectrometric measurements of the gas phase composition over mould powder samples in vacuum conditions at 50-1550ºC'. *Steel Research. International*. 77, pp. 803-808

Spaccarotella, A, Scheller, P, Hooli, P. 2000: 'Development of high speed casting in conventional cc stainless steel slab production', *58th EAF and 17th PT Conference Proceedings*, Orlando, Florida, USA, November, pp. 833-850.

http://ptcl.chem.ox.ac.uk/MSDS/SO/sodium_fluoride.html. Safety data for sodium fluoride, 2 p.

Susa, M., Mills, K.C., Richardson, M.J., Taylor, R., Stewart, D. 1994: 'Thermal properties of slag films taken from continuous casting mould', *Ironmaking and Steelmaking*, Vol.21, No.4, pp. 279-286.

Susa, M., Nagata, K., Mills, K.C. 1993: 'Absorption coefficients and refractive indices of synthetic glassy slags containing transition metal oxides', *Ironmaking and Steelmaking*, 20, No. 5, pp. 372-378.

Taylor, R., Mills, K.C. 1998: 'Physical properties of casting powders: Part 3 Thermal conductivities of casting powders', *Ironmaking and Steelmaking*, 15, No. 4, pp. 187-194.

Terauchi, M., Nakata, H. 2002: 'Influence of mould powder on characteristics of heat transfer in continuous casting', Research and Development Laboratories, Kakogawa Works, Kobe Steel Ltd., Japan, p.8.

Thomas, B.G. 2004: CON1D Users manual, Version 8.0, May 26, p50.

Tsutsumi, K., Nagasaka, T., Hino, M. 1999: 'Surface roughness of solidified mould flux in continuous casting process', *ISIJ international*, 39, No. 11, pp. 1150-1159.

Wang, Q., Wang, Y., Chi, J., Xie, B., He, Y., Zhu, B., Chen, W. 2004: 'Effects Of Continuous Casting Mould Fluxes On Decreasing Of Longitudinal And Star Cracks On Slab Surface', *Journal of Chongqing University* (english edition abstract) Vol.3 No.1, pp. 65-68.

Watanabe, T., Fukuyama, H. Susa, M., Nagata, K. 2000: 'Phase Diagram Cuspidine (3CaO*2SiO2*CaF2)-CaF2', *Metallurgical and Materials Transactions B*, Volume 31B, December, pp. 1273-1281.

Yamauchi, A., Sorimachi, K., Yamauchi, T. 2002: 'Effects of solidus temperature and crystalline phase of mould flux on heat transfer in continuous casting mould', *Ironmaking Steelmaking*, 29, No. 3, pp. 203-207.

Yamauchi, A., Sorimachi, K., Sakuraya, T., Fujii, T. 1993: 'Heat Transfer between Mould and Strand through Mould Flux Film in Continuous Casting of Steel', *ISIJ international*, 33, No. 1, pp. 140-147.

Yamauchi, A. 2001: 'Heat Transfer Phenomena and Mould Flux Lubrication in Continuous Casting of Steel', Doctoral Thesis, Royal Institute of Technology, Stockholm, Sweden, p. 33.

APPENDICES

APPENDIX 1

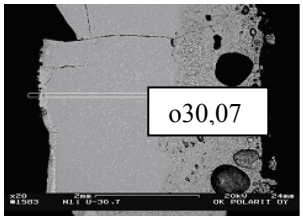

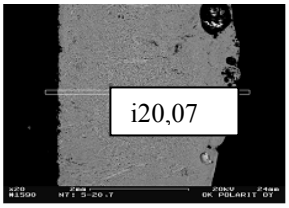

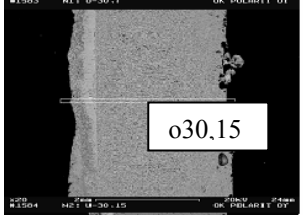

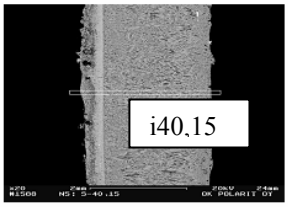

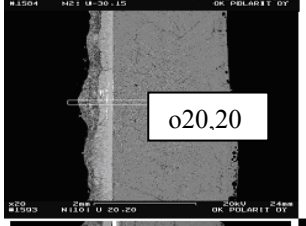

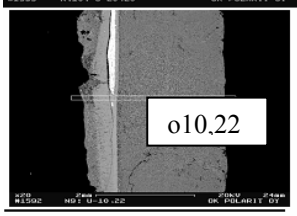

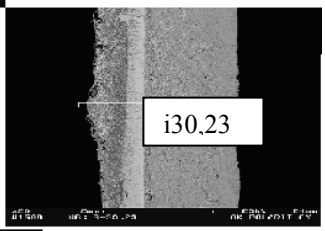

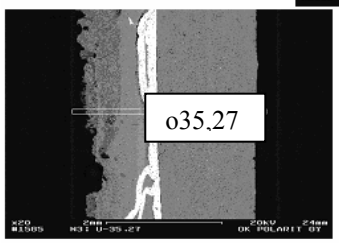

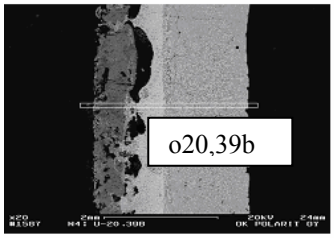

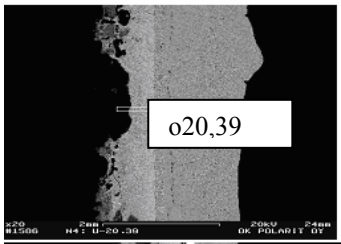

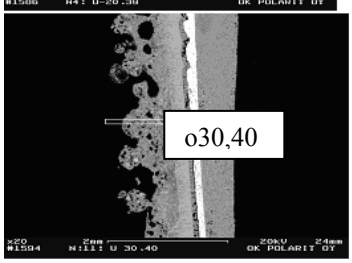

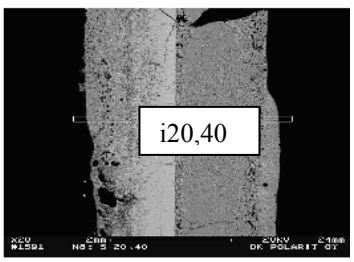

Figure a1. BE (Backscattered Electron) images of all analysed layer cuts from cast 71056.

Left column = **o**uter bow side
right column = **i**nner bow side

Pictures are in order down from meniscus.
First number=distance from SEN [cm].
Second number=distance from meniscus [cm]

ZrO_2 doped powder added during last 30 min, in tail-out BaO doped powder added in box.

Typical findings:

- whitish high Ca rich (cuspidine) layer
- a layer against mould is missing (remained on the mould wall), in most cases thin, but in some cases thicker (for example picture no 7 and 8 in left column)

Occasional findings:

- there is a steel layer in the borderline between layer formed in tail-out and the layer existed during casting
- some of the cross-sections are not representative (e.g. no 1 in left column)

APPENDIX 2

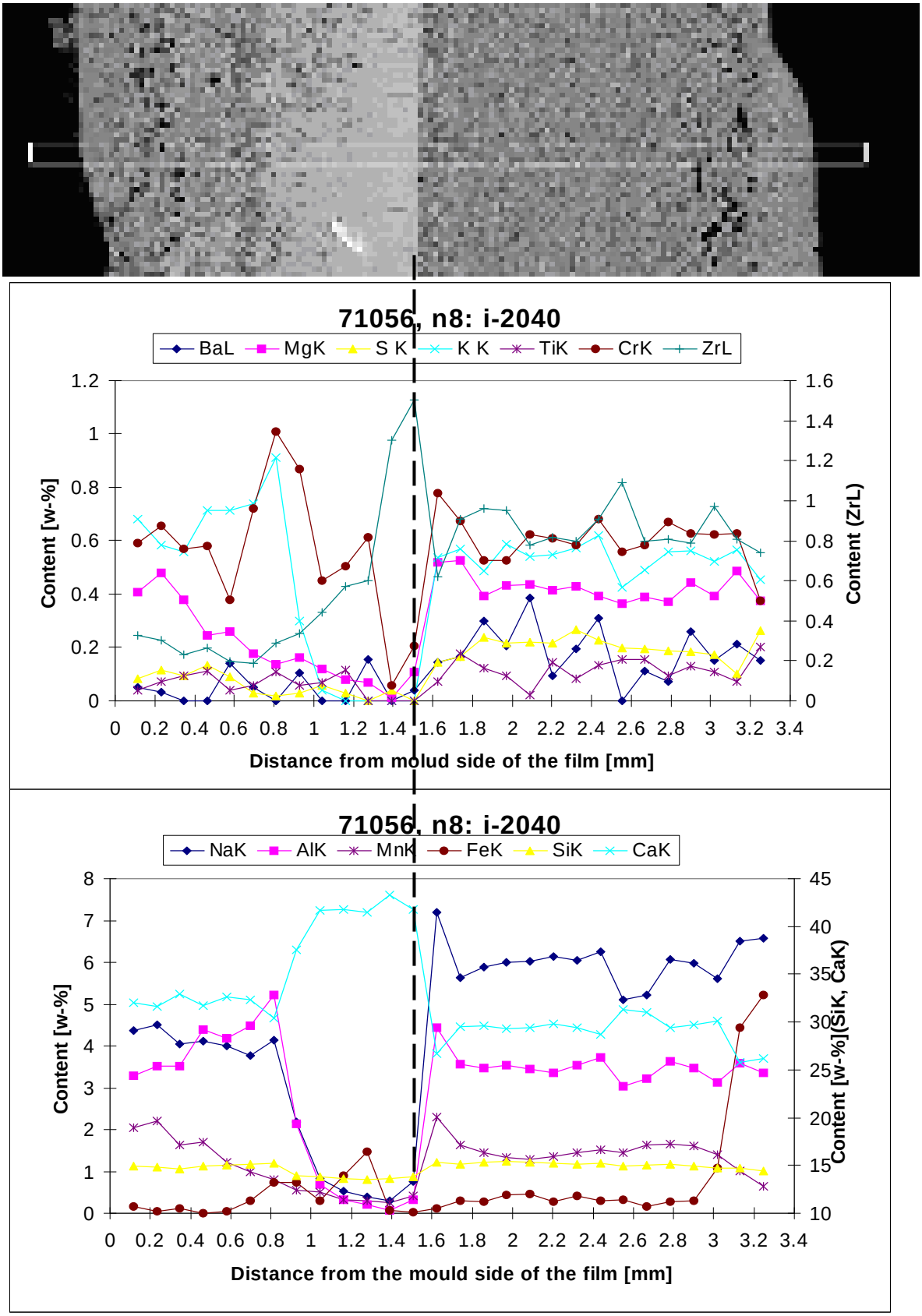

Figure a2. *Film from cast 71056, i 20,40, with concentrations of elements.*

APPENDIX 3

Photographs of the films with comments from cast 71165; the sequence consisted of 3 heats. BaO doped powder was used 45-15 min before the end, and ZrO_2 doped powder the last 10 min. In all pictures mould side is on the left. All layers were also analyzed along the marked line. Note: F was not usually analyzed.

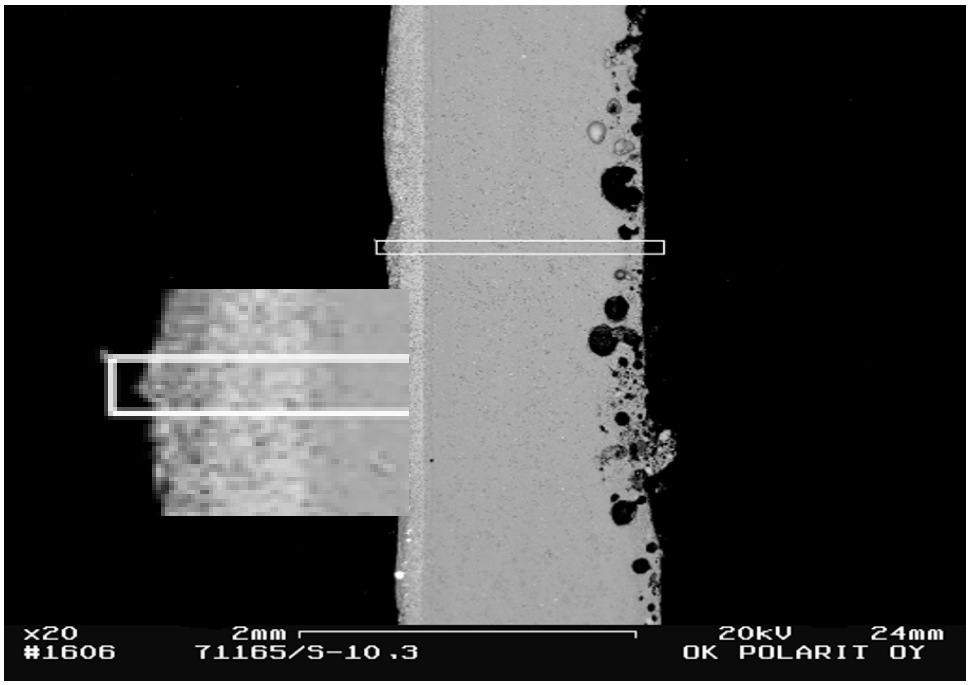

Figure a3. *Layer is 3 cm from the meniscus and 10 cm from SEN on the inner bow side (S).*

The layer formed during casting (thin whitish layer) is not complete because part of it remained adhered to the mould wall. Most of the film had formed during tail-out.

Layer thickness in the sample is 0.3-0.4 mm. Whitish Ca rich layer is clearly visible (0.2 mm). In the layer on the mould side Mg, Ti and Zr were lower than in the layer formed during tail-out, but Ba content was a little higher. It is possible to state that this layer did not form during the last 10 minutes. In enlargement, it is possible to see traces of the lubricating layer during casting.

APPENDIX 3

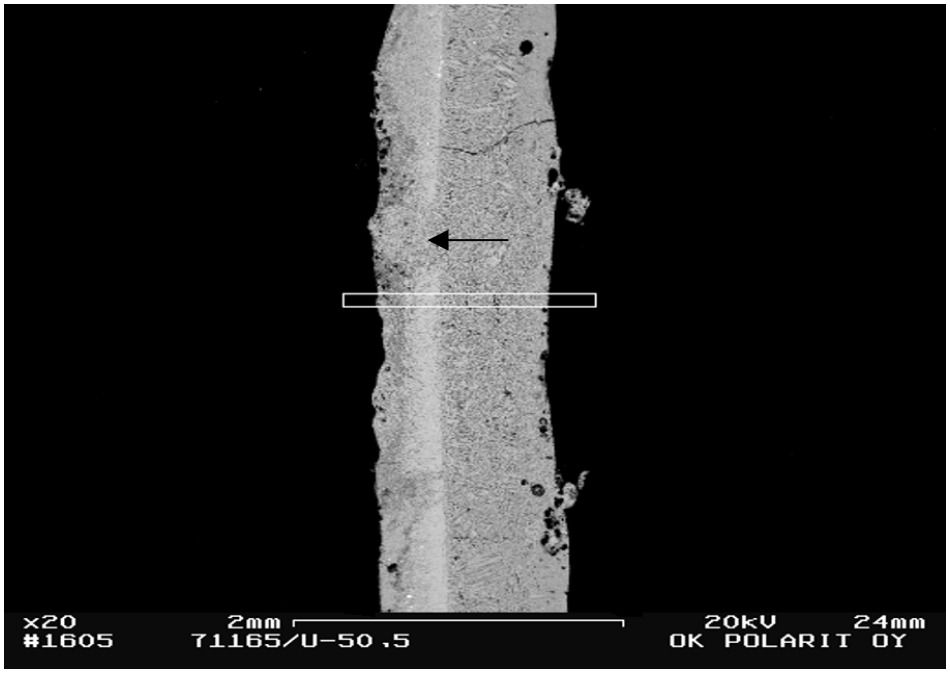

Figure a4. *Layer 5 cm from meniscus and 50 cm from SEN.*

It is a layer with high Ca where Zr is also high, but other elements are low. On the mould side Ba content is high, but Zr is low. Above analysis line there has been a fracture (indicated with arrow), and liquid slag has entered through that fracture, but obviously not during the last 10 minutes.

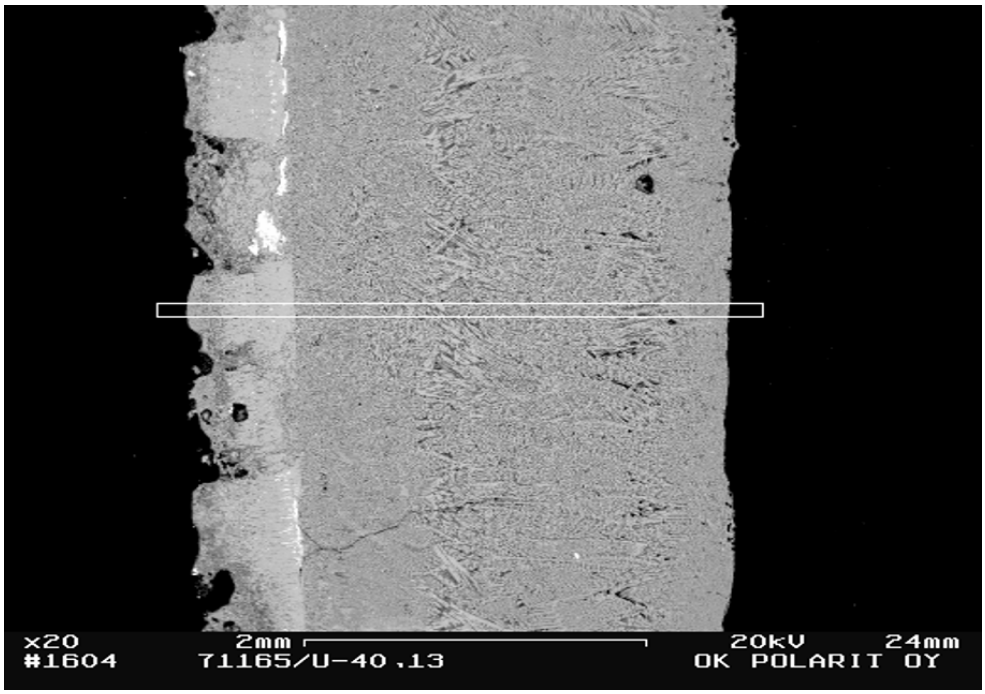

Figure a5. *Layer 13 cm from the meniscus.*

It looks like fracturing has taken place in this layer. Ca, Ba and Zr concentrations are shown in the graph below. Ba concentration is low through the whole layer, as is Zr except in the first point (0.7mm), which is in the high Ca layer. The analysed part was possibly older than 45 min. Between the cuspidine pieces, the layer looks dissimilar to the layer formed during tail-out, so it probably formed earlier. Thus fracturing has most probably happened earlier than in tail-out.

APPENDIX 3

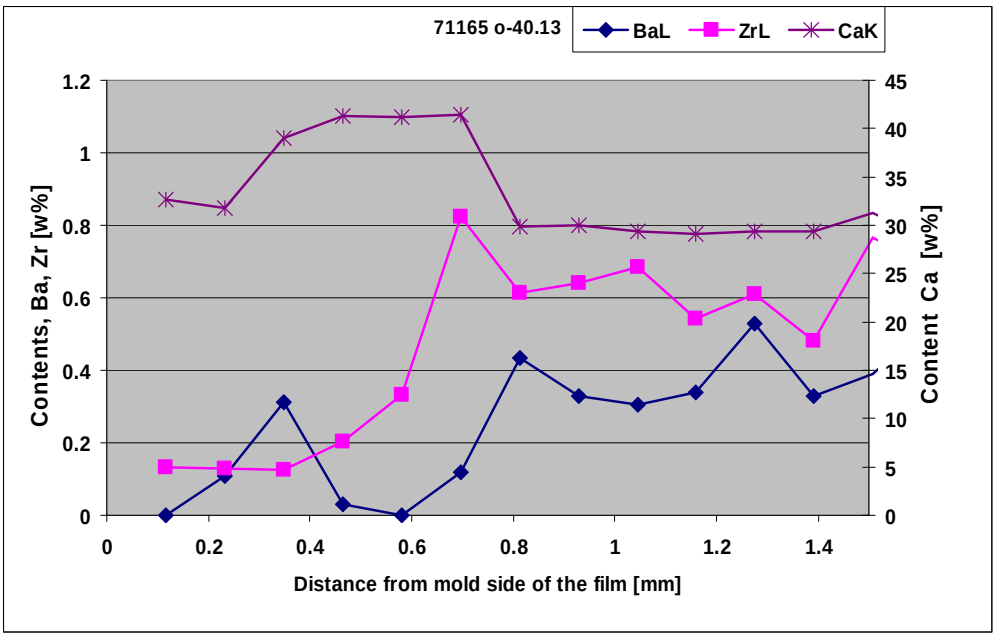

Figure a6. *Contents of Ba, Zr and Ca.*

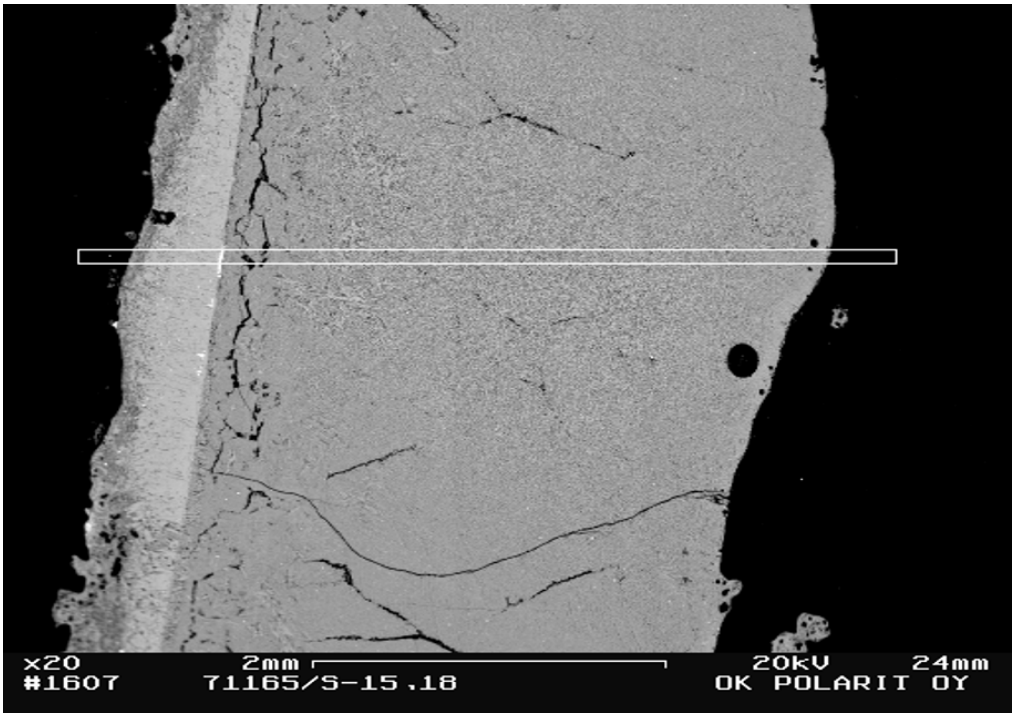

Figure a7. *Layer 18 cm below the meniscus.*

APPENDIX 3

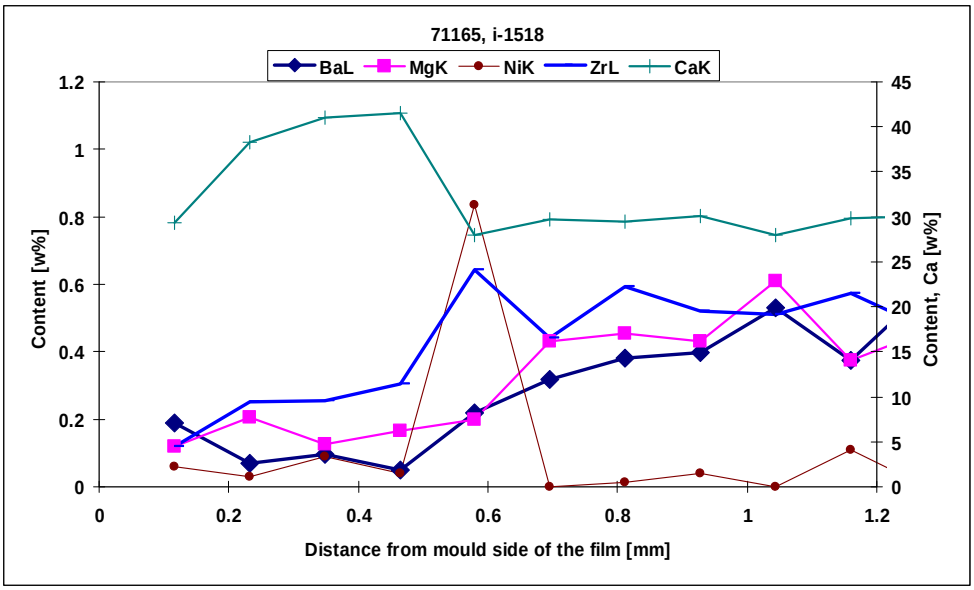

Figure a8. *High Ca layer is between 0.3-0.5 mm from left side.*

There is also a tiny steel layer on the border of tail-out slag and high Ca layer (indicated by Ni content). In the high Ca layer Ba, Zr and Mg concentrations are clearly lower than in tail-out slag (see graph below). The low Mg content is interesting, because it could indicate that the layer was from a very early period of casting - if not from the beginning. The cuspidine layer is rather undamaged.

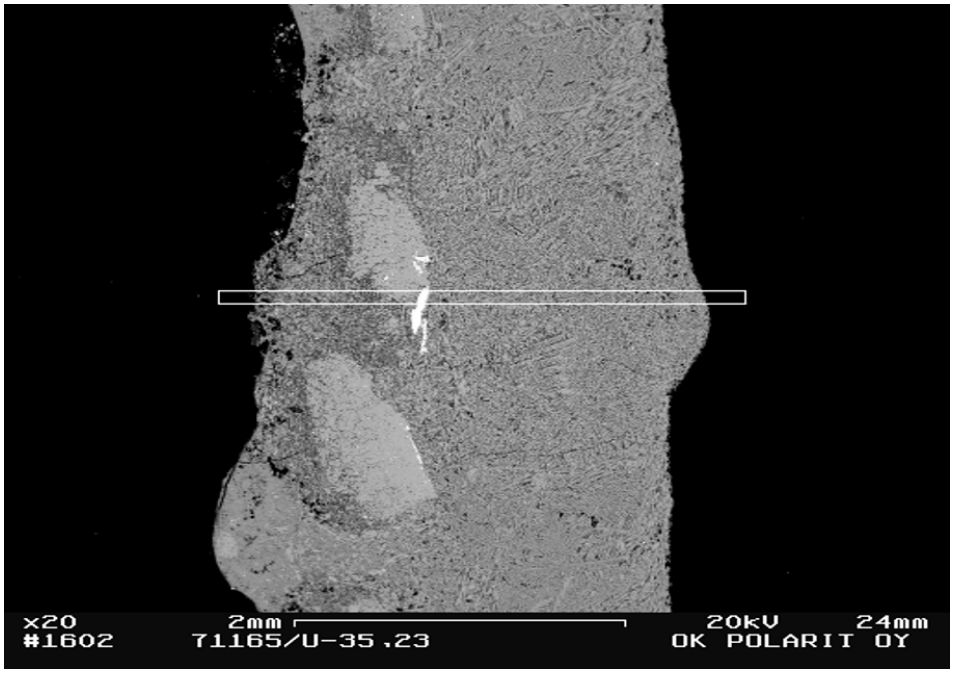

Figure a9. *Layer on outer bow side 23 cm from meniscus.*

There are clearly fractures in the layer. Light regions (cuspidine) are in pieces i.e. not as a continuous layer. In the line, there is a small white spot of steel. Steel layers, if they existed, were typically of this location between the layer formed during casting and the layer formed during tail-out. The steel layer also indicates that the layer on the left side did not form during tail-out, because steel layers were formed during tail-out. Concentrations of elements analysed along the line are presented in the graph below.

APPENDIX 3

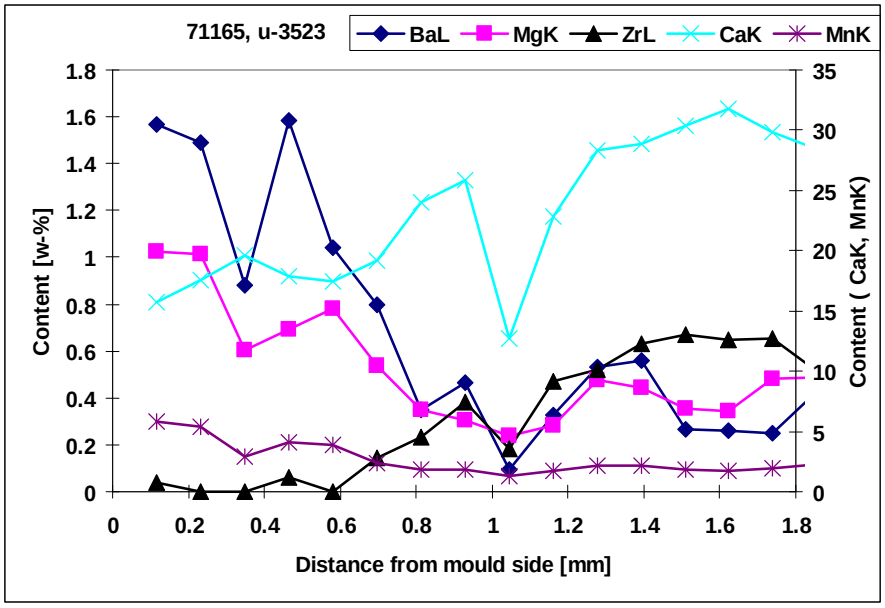

Figure a10. *Contents in the layer on outer bow side 23 cm from meniscus.*

Between 0-0.6 mm Zr concentration is zero, but in the tail-out slag it is about 0.6 %. This indicates that layer has not formed during last minutes of casting. Ba content is higher than in tail-out slag. This could indicate that the layer (or area) is formed during the use of BaO doped powder. Also Mg and Mn concentrations are higher than in tail-out slag, as are almost all other elements except Ca and Zr.

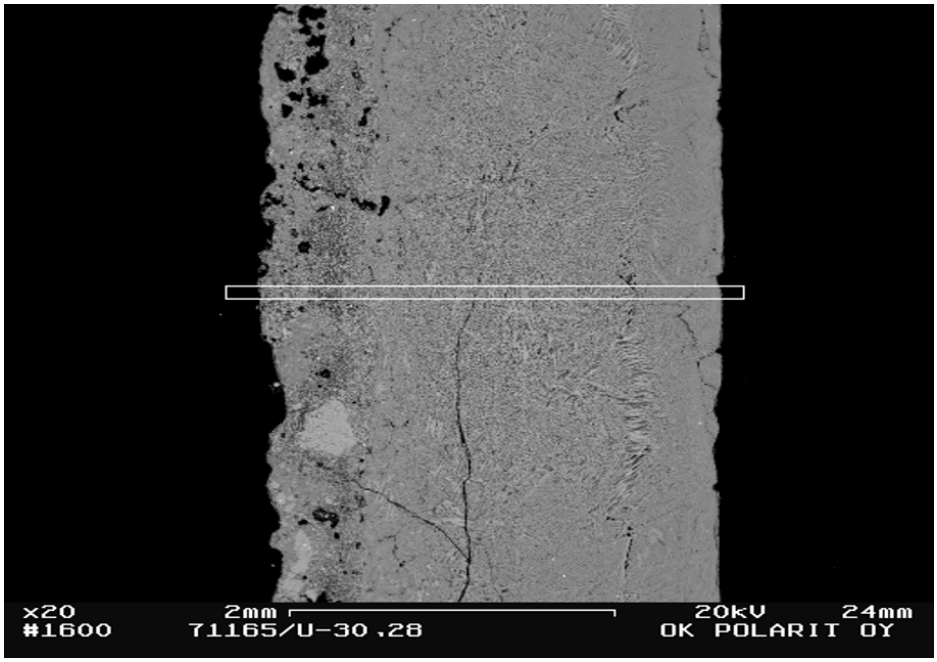

Figure a11. *Layer 28 cm below the meniscus.*

In this layer there are few pieces of cuspidine. Possibly, the main part of the "real" layer formed after the layer has broke off. In the analyzed line from distance of 0.8 mm Ca and Zr concentrations are gradually falling down to 0, but Ba concentration is increasing from 0.5 to 2.5 %. Behaviours of Ba and Zr could indicate, that the layer in the analyzed line was born between 45-15 min before the end of casting i.e. breaking has taken place between these time periods. Concentrations of elements are rather equal with previous layer (23 cm). Behaviour of Ca could indicate that cuspidine layer has broken later off from other layers.

APPENDIX 3

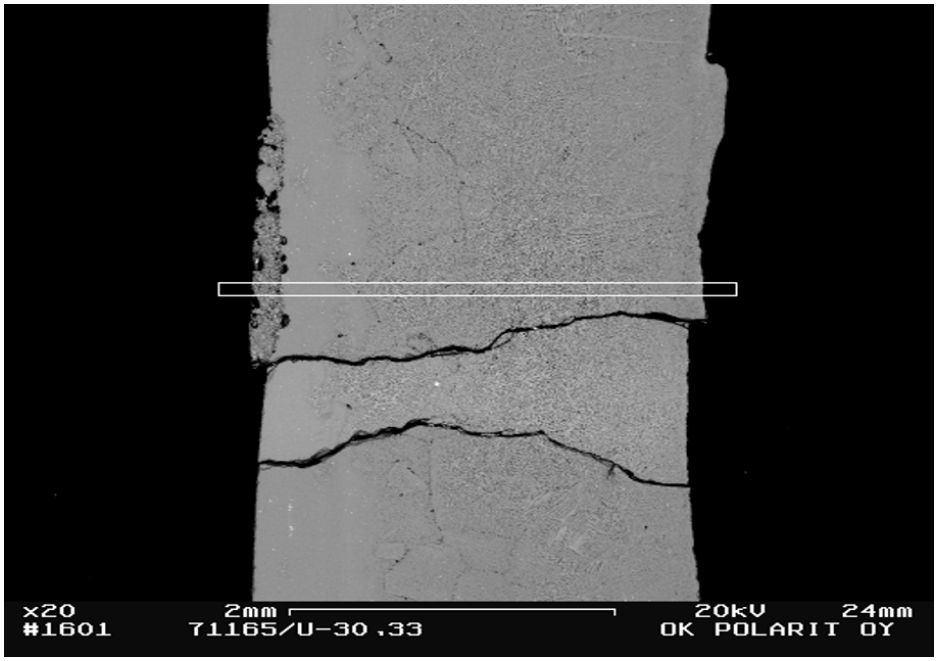

Figure a12. *Layer 33 cm from meniscus.*

Only the thin layer in the analyzed line has formed before tail-out. In that layer Zr and Ca are nearly zero and Ba concentration is high.

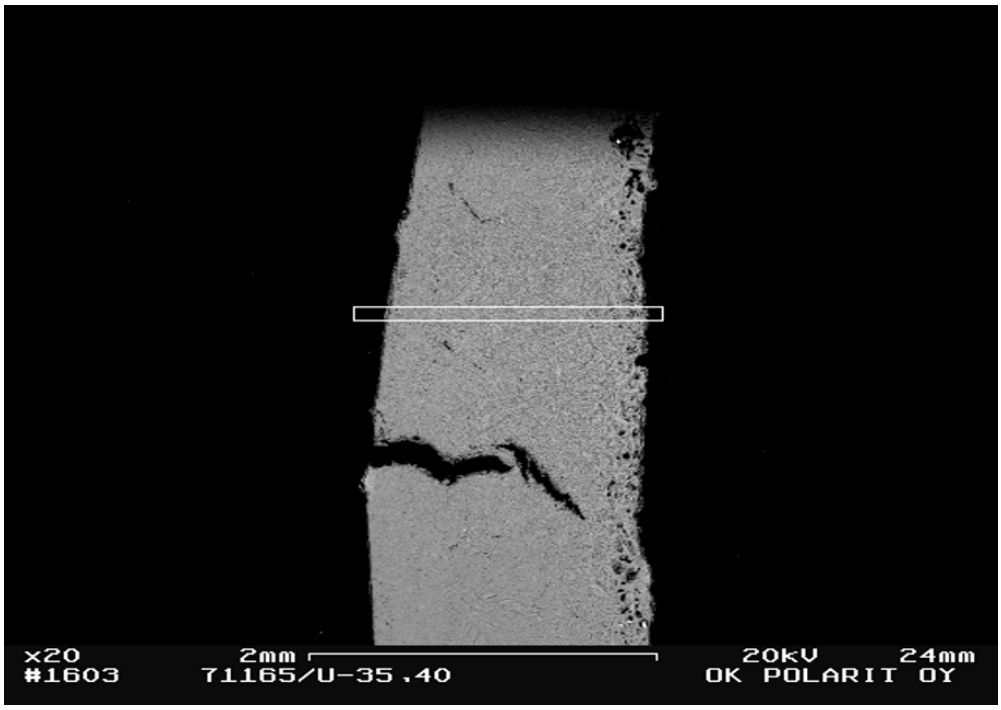

Figure a13. *Layer 40 cm from meniscus.*

In the layer in this picture there are no visible or compositional changes. Thus the whole layer formed during tail-out. This means that the layer existing during casting have not reached this distance (only after tail-out).

APPENDIX 4; BE images of the film shown in Figure 23.

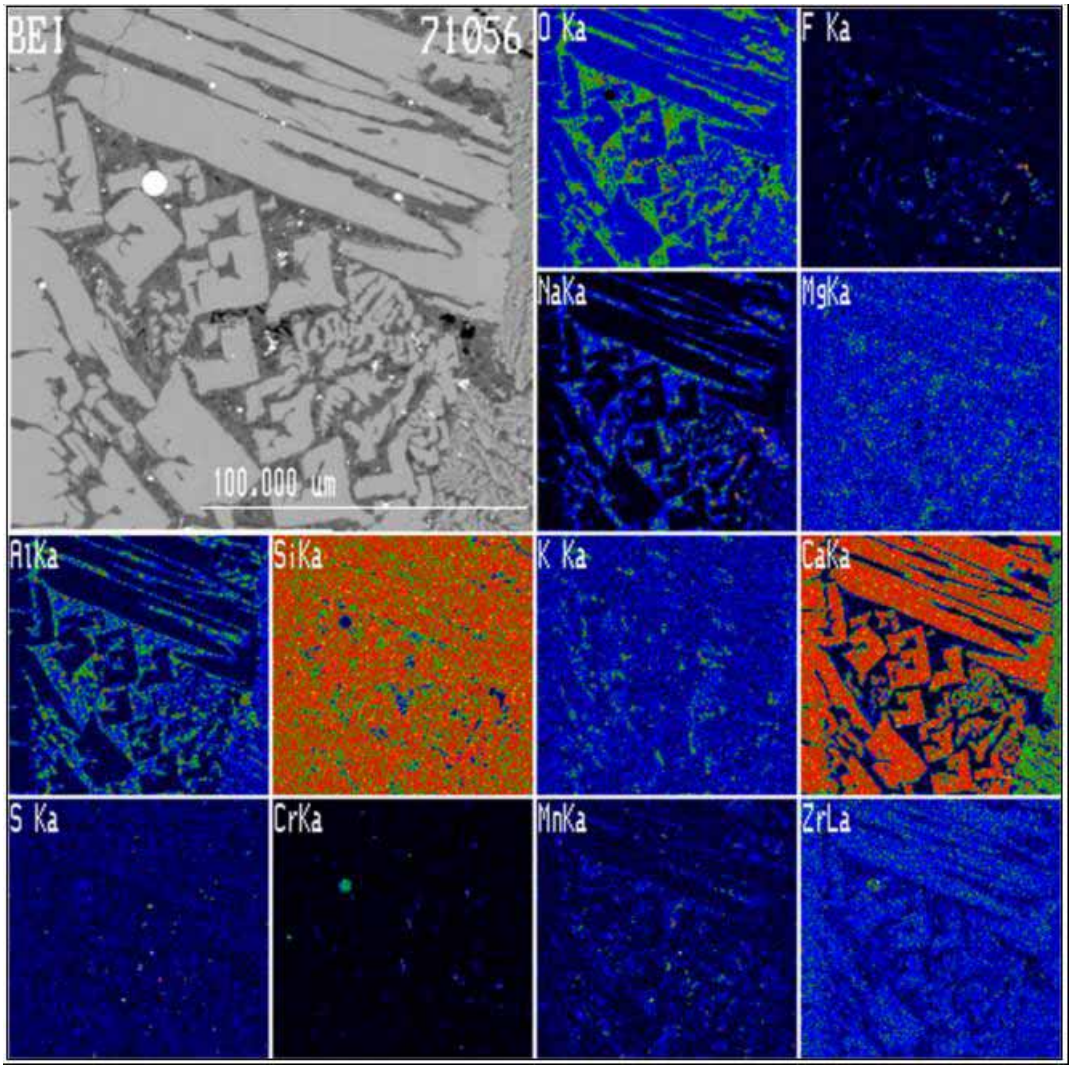

Figure a14. *BE Images of the sub layers in the film 71056 shown in Figure 23. Layer 1 in the middle and small strips of 0 (formed during tail-out), and 2 (cuspidine).*

APPENDIX 4

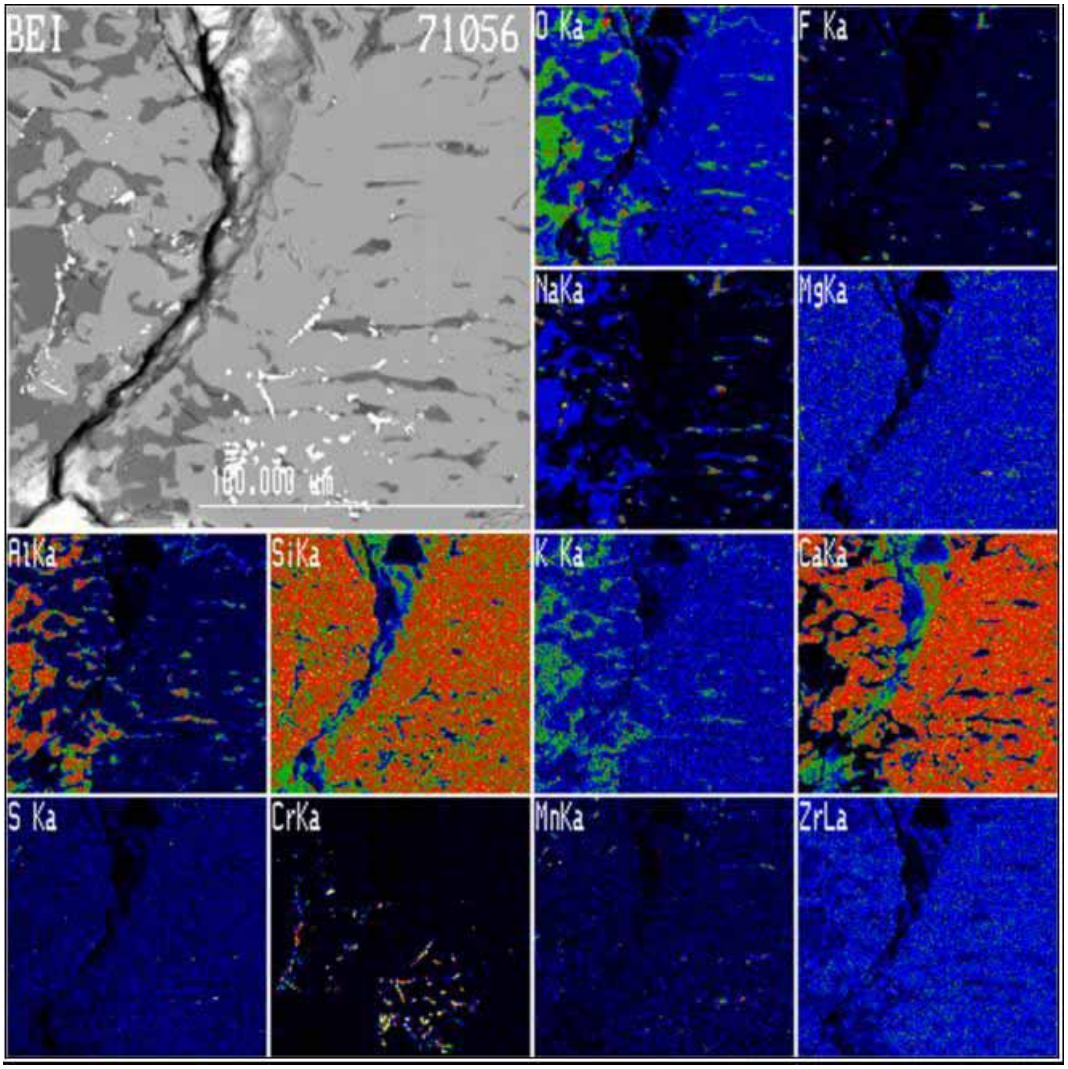

Figure a15. *Layer 2 on the right side and layer 3 on the left side.*

APPENDIX 4

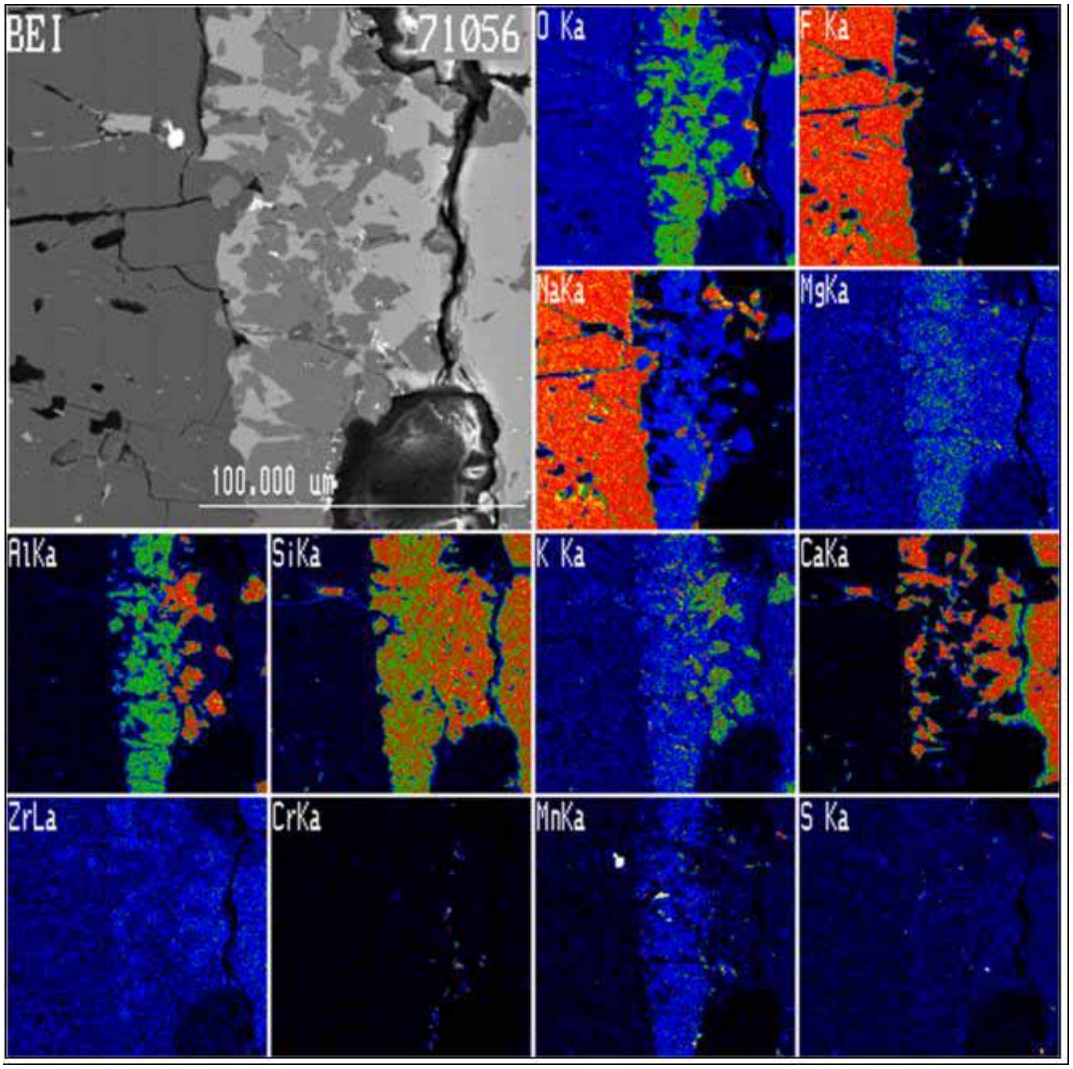

Figure a16. *Layer 3 on the right side and layer 4 on the left side.*

APPENDIX 4

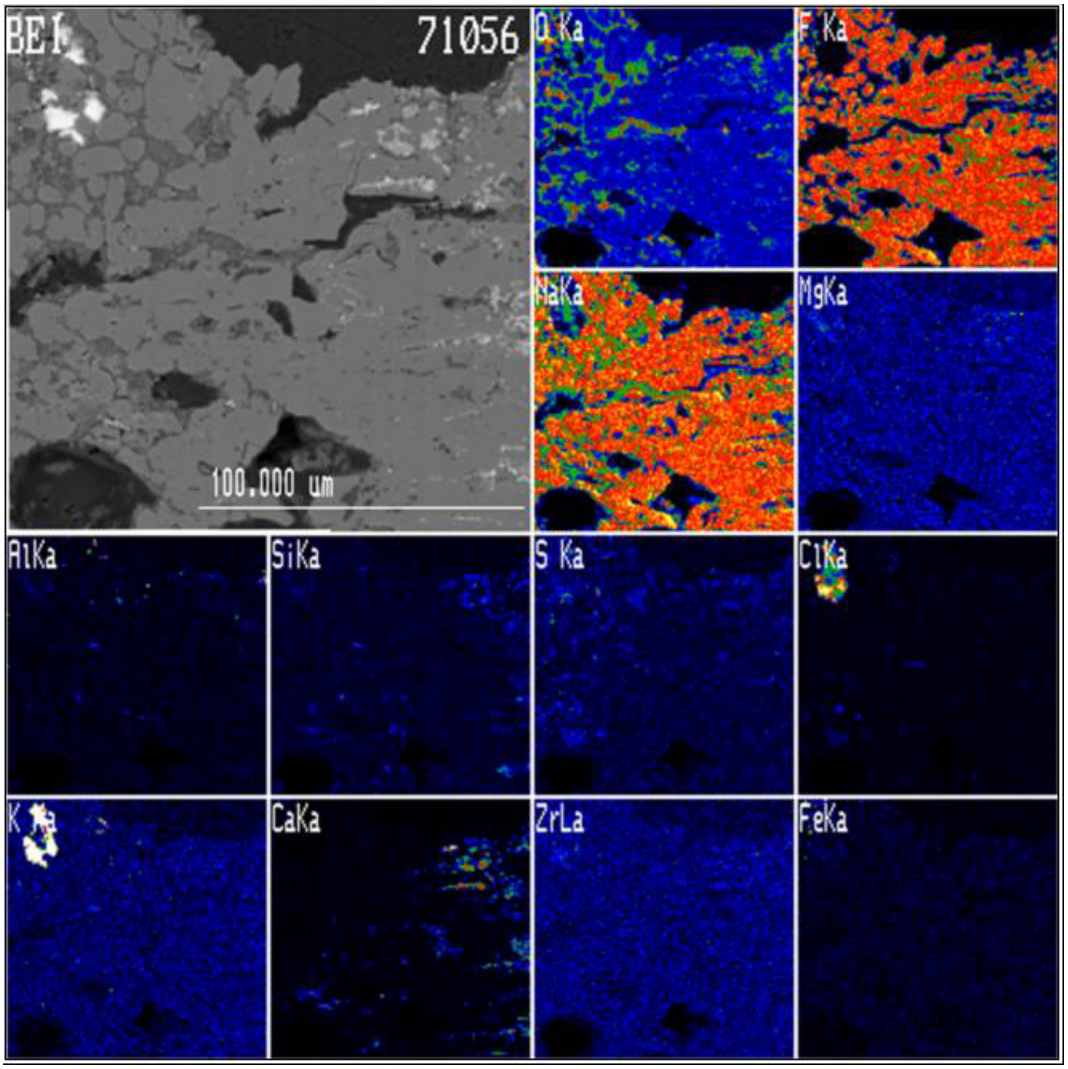

Figure a17. *A middle area of layer 4.*

APPENDIX 4

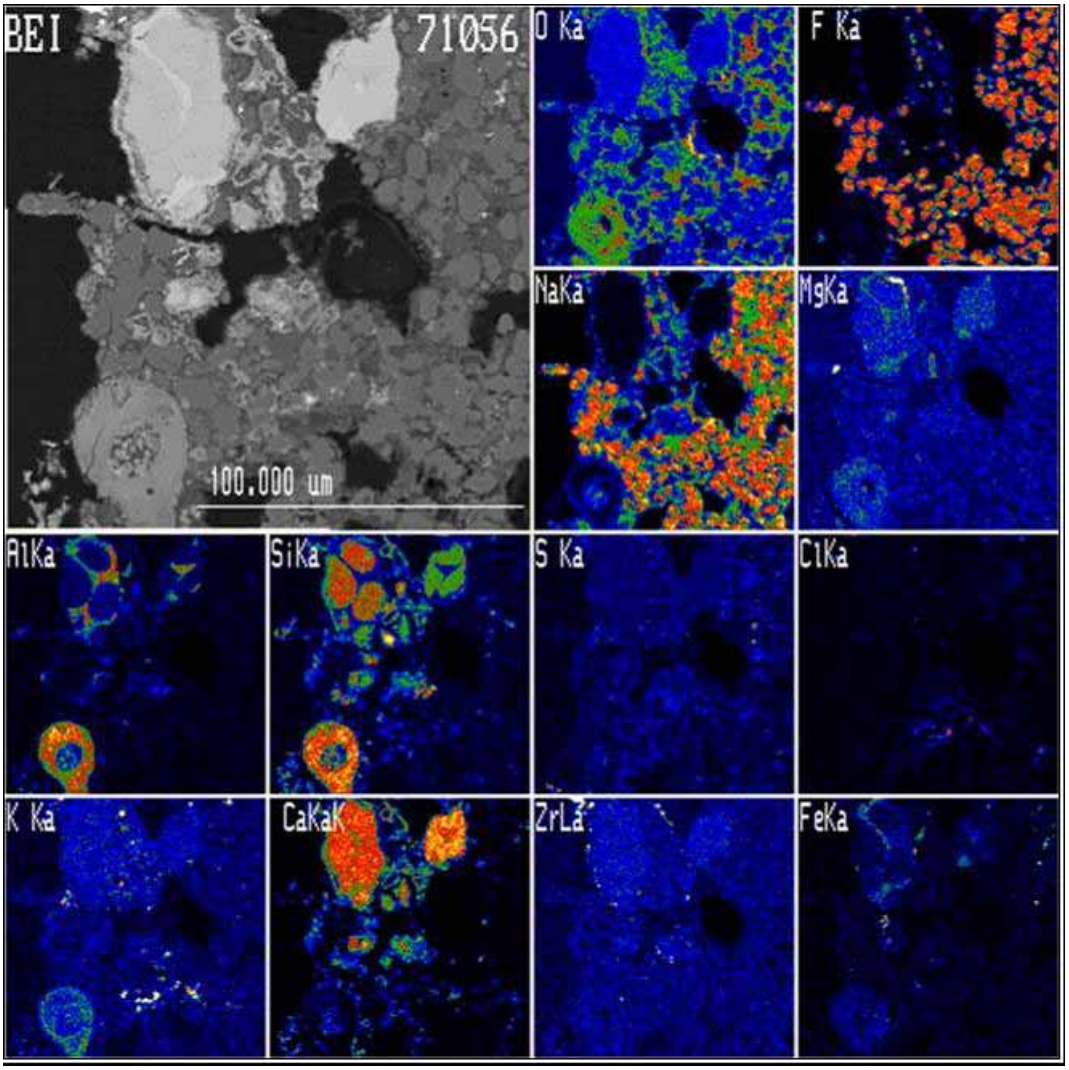

Figure a18. *The area of layer 4 next to the mould side.*

HELSINKI UNIVERSITY OF TECHNOLOGY PUBLICATIONS IN MATERIALS SCIENCE AND ENGINEERING

TKK-MT-181 Liukkonen, M., Friman, M., Hämäläinen, M., Holappa, L.
Kiinteiden alkuaineiden pintaenergia-arvojen kooste ja kriittinen tarkastelu. 2006

TKK-MT-182 Lundström, M., Selin, L., (eds.)
Thermodynamic and Kinetic Phenomena in Hydrometallurgical Processes. Graduate School Course, 25-27, Espoo, Finland. 2006

TKK-MT-183 Heiskanen, K.,
Virtaustekniikka materiaalitekniikassa. Luentomoniste kurssille MT-0.2211. 2006

TKK-MT-184 Kekkonen, M., (ed.),
Materials Production and Synthesis / 2006. MT-0.3201

TKK-MT-185 Bunjaku, A., Holappa, L.,
On Production of Ferronickel. 2006

TKK-MT-186 Miettinen, J., Kytönen, H.,
Calculation of Dendrite Arm Spacing in Soliedified Steels. 2006

TKK-MT-187 Miettinen, J., Kytönen, H.,
Calculation of Density in Liquid Steels. 2006

TKK-MT-188 Miettinen, J., Kytönen, H.,
Calculation of Viscosity in Liquid Steels. 2006

TKK-MT-189 Kankaanpää, T.,
Behaviour of Organic-Aqueous Dispersion in Solvent Extraction Mixer-Settler Processes. 2007

TKK-MT-190 Liukkonen, M., Friman. M., Hämäläinen, M., Holappa, L.,
Compilation and Critical Examination of Surface Energy Values of Solid Alloys and Inorganic Compounds. 2007

TKK-MT-191 Liukkonen, M., Friman, M., Nakamoto, M., Hämäläinen, M., Holappa, L.,
Assessment of Surface Energy Functions for Solid Elements. 2007

TKK-MT-192 Miettinen, J.,
Thermodynamic Substitutional Solution Descriptions of Fe-B-C, Fe-B-N and Fe-C-N Systems. 2007

TKK-MT-193 Miettinen, J.,
Thermodynamic Substitutional Solution Descriptions of Fe-Al-C and Fe-Al-N Systems. 2007

TKK-MT-194 Selin, L. (ed.),
Activity Report 2004 – 2006. Department of Materials Science and Engineering. 2007

ISBN 978-951-22-9030-7
ISBN 978-951-22-9031-4 (electronic)
ISSN 1455-2329